Entangled state stabilization by local couplings through reservoir-engineering methods

Vincent Martin

École doctorale de sciences mathématiques de Paris centre

Thèse de doctorat

Discipline : Mathématiques Appliquées

présentée par

Vincent Martin

Entangled state stabilization by local couplings through reservoir-engineering methods

---

dirigée par Alain Sarlette

Président du jury: Jean-Michel Coron

Membres du jury: Nina Amini, John Gough, Francesca Chittaro, Thomas Schulte-Herbrüggen, Alain Sarlette

Centre Inria de Paris
2 rue Simone Iff
CS 42112 – 75589 Paris Cedex 12

Université de Paris.
ED S386
4 place Jussieu Tour 15-25 - 1er étage Bureau 1.15
75252 PARIS CEDEX 05

Remerciements

Je souhaite avant tout remercier mon directeur de thèse, Alain, qui a été incroyablement gentil avec moi tout au long de la thèse dans mes moments difficiles, en plus d'avoir été un mentor dans ma vie scientifique.

Merci à mes camarades de thèse, Jéremie, Michiel, Christian et les autres, qui ont égayé mes journées au bureau de l'INRIA ou pendant les confinements.

Merci à tous mes amis qui m'ont soutenu pendant la thèse, de près ou de loin, tout particulièrement à Armand et Clément qui ont su me motiver à la finir, et Philippia qui m'a aidé dans les moments qui n'allaient pas durant le confinement.

Merci à mes parents de m'avoir soutenu, et d'avoir été compréhensifs pour mes périodes de silence.

Et enfin merci à Marie, qui a bien fait de ne pas attendre la fin de ma thèse pour que l'on sorte ensemble.

Merci à tous.

Abstract

This thesis aims to use techniques of reservoir engineering in order to stabilize systems of N qubits, with N potentially big, and to develop the tools for the performance analysis of such stabilization.

Quantum systems can be used to process information in ways not achievable by classical means. In classical computing, a system of N bits can be in 2^N states. For example, for a 2-bit system, there are 4 possible states 00, 01, 10, and 11. In a quantum system of N qubits, there are 2^N basis states and the system can be in any superposition of all these states. Those systems can be used to perform quantum computation, which is the current ultimate practical goal of quantum information technology, i.e. building a quantum computer. The promise of quantum technology hinges on the ability to precisely control and manipulate the values — both magnitudes and phases — in the superposition of basis states. The big challenge is that these values are very sensitive to any spurious signals and couplings to its environment, such that they naturally get progressively blurred; this process is called decoherence. One way to fight decoherence is measurement and feedback action, but the interaction that this constantly involves with the classical world involves design complications and delays. An alternative control approach for quantum state stabilization is quantum reservoir engineering: a dissipative ancilla system (reservoir) and its interaction with the system of interest are designed in such a way that they stabilize the system without any need for external interventions. The key problem in reservoir engineering is to design these items with the limitations inherent to a physical system: it is for example out of question to make all different parts of our system interact with one central part (all to one coupling), because it is unachievable physically. The present thesis thus seeks to develop basic building blocks of scalable procedures to design such stabilizing reservoirs, and to analyze their performance.

The first part of this thesis develops several proposals about an application of local reservoir engineering to stabilize an especially delocalized state, namely a GHZ state, which is an entangled state with the characteristic that the "quantum phase" information is lost as soon as one subsystem's phase is blurred. These entangled states have applications in fields ranging from quantum communication and quantum metrology to quantum computing, as entanglement is a key concept in speeding up computations (otherwise, local classical models could simulate it) and to secure private communication channels (thanks to information being delocalized). It has been proved that exact stabilization of an N qubits GHZ state is impossible without realizing couplings between at least $N/2$ qubits, which cannot be done in realistic settings. This is why we propose several set-ups to approximately stabilize GHZ states using only local interactions with well-designed fixed dissipative dynamics. The main idea is to combine a scheme periodically resetting the whole system to the particular state $|++...+>$ with an existing conditional stabilization scheme, where the system converges towards the GHZ state if each qubit is initialized in the particular state $|++...+>$. We examine several ways to implement the synchronization between these two stabilization procedures with local couplings, either by adding as auxiliary subsystem a chain of ancillas acting like a clock, or by using a third level on each data subsystem to control operations on the "qubit" part. We then perform a theoretical analysis of the different set-ups, backed up by simulations, to evaluate how the approximate stabilization fidelity and the protection rate depend on the parameters, deducing optimal adjustments for each of these set-ups. The main idea of the analysis is to avoid tackling a full Lindblad equation, and rather build a classical Markov chain. We associate a particular configuration of the Markov chain to a particular set of hypothetical output signal values associated to jump detections in the Lindblad equation. This association is

not exact, but we can bound how this approximates the true dynamics, in particular choosing systematically pessimistic apprximations to provide performance guarantees.

The second part of this thesis focuses on quantum error correction. The most popular error correcting codes involve centralized processing of so-called "syndrome measurements" in order to deduce the correction to be applied. However, slightly larger codes are compatible with local decision-making, and hence with an implementation through reservoir engineering methods with local couplings. In particular, with locality defined according to a 2D lattice, local error correction schemes can provide an efficient protection against one type of error (either bit flip or phase flip) on quantum information. The most standard such error correction scheme uses majority vote, where a read out of the entire redundant system is performed, then a correction occurs if some parts of the systems are different from the majority. This process uses a read out and non-local decision making, and is moreover a non local action as we need to read all the redundant part together. In the present thesis, we thus design and analyze two reservoir engineering set-ups, protecting against the same type of errors on the basis of local interactions only, yet by interlinking qubits in a 2-D network; the resulting setting should be applicable in realistic experiments. The first design builds upon an existing reservoir engineering protocol that implements bit flip protection by majority vote on three qubits. We show how this building block can be used in a polygon-induced network of physical qubits such as to scale up information protection to higher orders. The tuning of frequencies in the interlinked systems was the principal problem tackled in scaling up this building block.The second method uses a known lattice technique for classical error correction on the basis of a local cellular automaton, known as Toom's rule. It consists in a 2-D code where qubits are disposed on the vertices of a $N \times N$ square that corrects one type of error. Toom's rule prescribes a different treatment for each of the qubits of a local coupling operator, and we observe how the above building-block is able to implement this asymmetric treatment. We then show how to implement Toom's rule with a reservoir engineering perspective and we perform a mathematical analysis of the corresponding error protection performance.

Contents

Chapter 1

Introduction

1.1 Quantum mechanics

In this section, we will give a very brief overview of quantum mechanics fundamentals. We will only focus on the concepts we will use throughout this thesis. We will explain the different notions by increasing complexity in order to give a coherent understanding. Starting with the description of the simplest quantum object, the qubit, we will continue by explaining the more general concept of matrix density. We will then talk about the specificity inherent to quantum mechanics, entanglement and measurement, and will end with the time evolution of quantum systems without and with dissipation. This section is largely inspired by [2], [24] and [18].

1.1.1 The simplest quantum object: the qubit.

In quantum computing, a qubit, or quantum bit is a two-level quantum system. It is the basic and simplest unit of quantum information, the quantum version of the classic binary bit. Many examples of this theoretical system can be found, like the spin of the electron in which the two levels can be taken as spin up and spin down; or the polarization of a single photon in which the two states can be taken to be the vertical polarization and the horizontal one.

A classical bit is numerical and has a defined value, 0 or 1. A qubit however works differently: it possesses two basis states $|0\rangle$ and $|1\rangle$, and the state $|\psi\rangle$ of a qubit is a linear superposition of these two states. The states $|0\rangle$ and $|1\rangle$ can thus be seen as basis vectors for our qubit. It is written

$$|\psi\rangle = \alpha|0\rangle + \beta|1\rangle \tag{1.1}$$

where α and β are complex coefficients with the constraint $|\alpha|^2 + |\beta|^2 = 1$. In the quantum formalism, α and β represent the probability amplitudes to be in the state $|0\rangle$ or $|1\rangle$ respectively. This means that $|\alpha|^2$ (resp $|\beta|^2$) is the probability to measure the qubit in the state $|0\rangle$ ($|1\rangle$), this will be developed in paragraph 1.1.3. The description of this qubit is not changed is we multiply it by $e^{i\theta}$: it is called the global phase, and it does not matter as all results will be governed by the projector $|\psi\rangle\langle\psi|$, where $\langle\psi|$ is the adjoint vector of $|\psi\rangle$. We can thus choose the arbitrary phase of ψ such as α is always a positive real number, and the state of the qubit can thus be represented using the Bloch sphere: a classical bit could be either at the North Pole or the South Pole, in the locations of $|0\rangle$ and $|1\rangle$, and a qubit can be represented by any point on the surface. The surface of the Bloch sphere is a two-dimensional space, with two degrees of freedom that can be represented by two angles θ and ϕ, with the relations

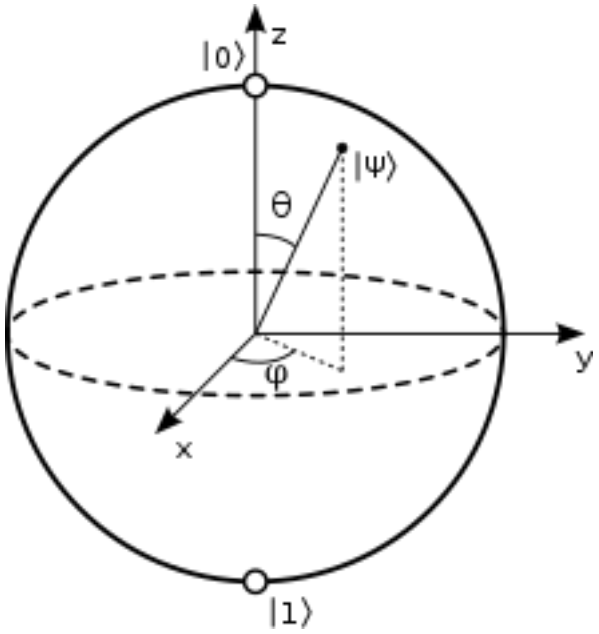

Figure 1.1: Representation of the Bloch sphere.

$$\alpha = cos(\frac{\theta}{2}) \tag{1.2}$$
$$\beta = e^{i\varphi} sin(\frac{\theta}{2})$$

During this thesis we will additionally speak of qutrits and qudits: these are only a generalization of the concept of qubits but with three (respectively d) levels. A qutrit will be described as

$$|\psi\rangle = \quad \alpha|0\rangle + \beta|1\rangle + \gamma|2\rangle \tag{1.3}$$

with $|\alpha|^2 + |\beta|^2 + |\gamma|^2 = 1$.

NB: qubits are usually a simplification of more complex quantum systems that have an infinity of levels, and proper mathematical restriction can be found in [2]. To give a rough idea it is possible to do a very good approximation where we isolate two energy levels that are not coupled to any other one. We will only work with finite dimension systems in this thesis, and qudits are thus the most complex base quantum systems we will use.

1.1.2 A more general representation of a qubit: the density matrix.

So far we have described the state of a qubit as a vector. This is because we assumed to have full knowledge of the state of our qubit: such states are called pure states. A pure state can be a superposition of multiple different basis states, which creates a quantum uncertainty for certain observables, as seen in the previous paragraph.

On the other hand, we can have different type of linear combination: statistical mixtures of state. A statistical mixture of states is a statistical ensemble of independent systems: they represent the degree of knowledge we have due to incomplete system knowledge, whereas the uncertainty within quantum mechanics is fundamental. Mathematically, a statistical mixture is not a combination using complex coefficients, but rather a combination using probabilities of different states (positive real valued numbers). If we consider a system where we have pure states ψ_i prepared with probability p_i, the state of the system will be represented by the density matrix ρ:

$$\rho = \quad \sum_i p_i |\psi_i\rangle\langle\psi_i| \tag{1.4}$$

where $\langle\psi_i|$ represents the adjoint of vector $|\psi_i\rangle$, such that $|\psi_i\rangle\langle\psi_i|$ is a rank-one matrix (in fact the orthogonal projection onto span($|\psi_i\rangle$)). Abstracting out which uncertainty on which pure states may be hiding behind it, a density operator in general is a positive semi-definite, Hermitian operator of trace one acting on the Hilbert space of the system.

1.1.3 Entanglement and measurement: the quantum specificity

A particular aspect of quantum mechanics is how two independent systems interact. If we consider two arbitrary quantum systems, A and B, with respective Hilbert spaces $\mathbb{H}_A$ and $\mathbb{H}_B$, the Hilbert space of the composite system is the tensor product $\mathbb{H}_A \otimes \mathbb{H}_B$. The simplest non trivial example is to take the tensor product of three qubits

$$\begin{aligned} |\psi_1\rangle &= \alpha_1|0\rangle_1 + \beta_1|1\rangle_1 \\ |\psi_2\rangle &= \alpha_2|0\rangle_2 + \beta_2|1\rangle_2 \\ |\psi_3\rangle &= \alpha_3|0\rangle_3 + \beta_3|1\rangle_3 \end{aligned} \tag{1.5}$$

When we take the system made of the three of them, we get

$$\begin{aligned} |\psi_1\psi_2\psi_3\rangle :=& |\psi_1\rangle \otimes |\psi_2\rangle \otimes |\psi_3\rangle \\ =& \alpha_1\alpha_2\alpha_3|000\rangle + \alpha_1\alpha_2\beta_3|001\rangle + \alpha_1\beta_2\alpha_3|010\rangle + \alpha_1\beta_2\beta_3|011\rangle \\ &+ \beta_1\alpha_2\alpha_3|100\rangle + \beta_1\alpha_2\beta_3|101\rangle + \beta_1\beta_2\alpha_3|110\rangle + \beta_1\beta_2\beta_3|111\rangle \end{aligned}$$

If the first system is in state $|\psi\rangle_A$ and the second in state $|\phi\rangle_B$, the state of the composite system is $|\psi\rangle_A \otimes |\phi\rangle_B$. States of the composite system that can be represented in this form are called separable states, like in the example we have given. But not all states are separable, and these other states are called entangled states. In particular, the Greenberger–Horne–Zeilinger state (GHZ) is an entangled, very non local state, which is

$$|GHZ_+\rangle = (|00..0\rangle + |11..1\rangle) / \sqrt{2}\,. \tag{1.6}$$

This thesis will focus a lot on how to stabilize such a state, as the entanglement of multiple subsystems is a major feature of quantum technology, with applications including metrology [10], secure communication [32], measurement-based computation schemes [7] and quantum error correction [4]. In line with the power of such states, the physical resources required for robustly generating or stabilizing them are not trivial.

Another particularity of quantum mechanics is the concept of measurement. In order to learn the state of a qubit, we need to measure it. A quantum measurement is fundamentally different than a classical one: as a classical bit of information is in the state 0 or 1, and with a perfect measurement of this bit we know the state of the system with probability one. But for a qubit with general form $\alpha|0\rangle + \beta|1\rangle$, we cannot directly have access to the parameters α and β, even with a perfect measurement. In quantum mechanics, we cannot measure directly the state of the qubit but the value of physical observables (which means some physical quantities that can be measured as position or momentum) corresponding to Hermitian operators acting on the state space. When the qubit is in the state $|\psi\rangle = \alpha|0\rangle + \beta|1\rangle$, the measurement of the operator produces a non-deterministic outcome: it gives 0 (respectively 1) with probability of the outcome $|\alpha|^2$ (respectively $|\beta|^2$). More importantly, such a measurement has a back-action on the quantum state of the system. If for example, the result of the measurement is 1, then the state of the qubit after the measurement is no longer ψ but $|1\rangle$, and another measurement following the first one would now give the result 1 with probability one. This phenomenon is known as the collapse of the wave function, and all the information contained in the complex numbers α and β is lost after the measurement. When one of two entangled systems is measured, the back action has an effect not only on the measured system, but also on the entangled one, hence the name. This concept will

be necessary to explain some of the work done in this thesis, for example the choice of reservoir engineering over more classic measurement and feedback to control control systems of interest, as the latter would damage the system it is supposed to control.

1.1.4 The time evolution of a simple quantum system: the Schrödinger's equation.

The Schrödinger equation is a linear differential equation that gives the evolution over time of a wave function $|\psi\rangle$ of an isolated physical system:

$$\frac{d}{dt}|\psi\rangle = -\frac{i}{\hbar}\,\mathbf{H}|\psi\rangle \tag{1.7}$$

where $\hbar$ is the reduced Planck constant, and $\mathbf{H}$ is a Hermitian operator, called a Hamiltonian, representing all the operators acting on the system, possibly time dependant. The density matrix version is

$$\frac{d}{dt}\rho = -\frac{i}{\hbar}\,[\mathbf{H},\rho] \tag{1.8}$$

where $[\mathbf{H},\rho] = \mathbf{H}\rho - \rho\mathbf{H}$.

The problem with the Schrödinger formulation of quantum mechanics is that the time evolution of the system is governed by unitary dynamics, which means there is no dissipation. There are two reasons to want to add dissipation in our analysis:

- for a realistic approach of the problem. Even with the best possible settings it is not possible to have a perfect isolated system from its environment (thermal noise, measure instruments,...), and taking into account the possible perturbation of the environment, and mitigate it, is one of the goal of this thesis. Such systems are called open systems.
- for a practical engineering design of control systems. When well controlled, dissipation can be used to stabilize systems of interests, and is the key concept in reservoir engineering that we will develop in next section. This is the focus of this thesis, and we thus need a more fitting representation of quantum' systems evolution through time.

NB: the Schrödinger equation for general quantum system (with infinite levels) is a partial differential equation. As we will only work on finite dimensions systems we will restrict ourselves to the version of the equation given in this paragraph, and will apply the same logic to next paragraph.

1.1.5 Time evolution of open quantum systems: the Lindblad's equation.

Certain mathematical techniques have been introduced to treat the interaction of a quantum system with its environment. We have seen one of these with the use of the density matrix, and its associated master equation. It allows more easily for the inclusion of incoherent processes, which represent environmental interactions and the progressive loss of knowledge about the quantum process that has been applied. Indeed, the density operator has the property that it can represent a classical mixture of quantum states, and is thus vital to accurately describe the dynamics of open quantum systems. We introduce the Lindblad superoperator, also called Lindbladian (a linear operator acting on a vector space of linear operators), expressing open quantum dynamics:

$$\mathcal{L}_{\mathbf{X}}(\rho) = \mathbf{X}\rho\mathbf{X}^\dagger - \frac{\mathbf{X}^\dagger\mathbf{X}\rho + \rho\mathbf{X}^\dagger\mathbf{X}}{2} \tag{1.9}$$

where $\mathbf{X}$ is an operator that is not necessarily Hermitian.

The Lindblad equation allows to give the evolution over time of such open quantum system:

$$\frac{d\rho}{dt} = -\frac{i}{\hbar}\,[\mathbf{H}(t),\rho] + \sum_{i=1}^{N}\kappa_i\mathcal{L}_{\mathbf{X}_i}(\rho) \tag{1.10}$$

where $\kappa_i \mathcal{L}_{X_i}(\rho)$ represents the dissipation caused by the operator X_i with a rate κ_i on the system.

The Lindblad equation describes the evolution of the quantum system on the Hilbert space spanned by ρ, in the approximation that all its interactions with its environment (other quantum systems, classical signals,...) is purely Markovian. It is similar to how classical dynamics, although ultimately stemming from a Hamiltonian universe, can be approximated as local systems with purely dissipative contributions. In physical terms, this typically assumes weak Hamiltonian coupling to a rapidly mixing environment. A proper derivation can be found in [6]. This Lindblad's equation will be used during all this thesis to describe the evolution of the different systems we will be studying.

1.2 Reservoir engineering

The usual way of controlling a system is by measurement and feedback: for a certain parameter we wish to control, we measure how it deviates from the value we want it to have. We then use this deviation signal to create a feedback in order to influence the system in such a way as to tend to reduce the deviation to zero.

Reservoir engineering takes a step back and changes the way of thinking the coupling between the system of interest and the measurement system. The goal is that the measurement system should not be measured anymore: it is just reset, and thus becomes a dissipative auxiliary system. The behavior of target system in this coupled system is controlled by smartly engineering the coupling between the target system and the measurement one, so as the modified system stabilizes itself in the desired steady state. Stabilization is based uniquely on physical coupling of the system of interest to an auxiliary system, acting as a continuous measurement system, which is called the "reservoir". There is no measurement involved, nor informatics intervention, nor feedback computation. The reservoir must be dissipative in order to allow stabilization and to be independent of the reservoir initial condition. The goals of reservoir engineering, as for regular control processes, are many and varied: stabilize a particular state, protect the system against perturbations, make it more robust to uncertainties, ... This method of control is particularly well adapted for quantum systems, as we have a large practical gain compared to control method based on measure and feedback: no need to know the exact precision of our measure instrument, no need to take into account delays in feedback loop, no need to protect fragile quantum signals going through this loop, ...

We will divide this section in three different parts: we will first give a classical example of what can be considered an early form of reservoir engineering, the centrifugal governor. This will gives a simple insight on basics principle of reservoir engineering. We will then give some theory principles of reservoir engineering when applied in quantum mechanics, and we will end with one classic example in this domain.

This section is largely inspired by the course "*Quantum Systems: Dynamics and Control*" given at Sorbonne Université, by Pierre Rouchon, Mazyar Mirrahimi and Alain Sarlette, and its lecture notes [22].

1.2.1 The centrifugal governor: an early example of reservoir engineering

Historically, this invention is attributed to James Watt for controlling steam engine, even if it can be traced to the 17th century to regulate the distance and pressure between millstones in windmills. The principle of this system is to control the speed of an engine by regulating the flow of fuel or working fluid, in order to stabilize its rotation speed.

The governor works as follows: power is supplied to the governor from the engine shaft by a chain connected to the lower belt wheel. The equilibrium angle of the pendulum of the flyballs depends on rotation speed: the faster the axis turns, the greater the kinetic energy of the flyballs and the closer to horizontal they are. If they are close enough, this motion causes the lever arms to pull down and to close the steam engine valve, which will slow down the rotation of the engine and

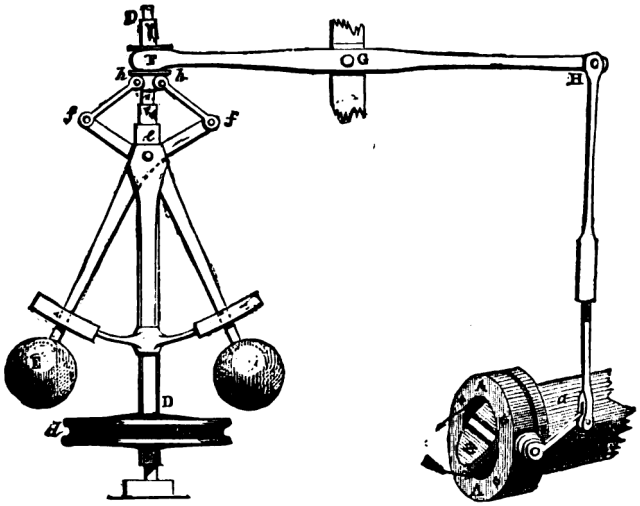

Figure 1.2: Diagram of a centrifugal governor. Image from "Discoveries & Inventions of the Nineteenth Century" by R. Routledge, 13th edition, published 1900.

thus of the flyballs. The flyballs movement is damped which provides dissipation. This prevents over speeding and should stabilize the rotation speed.

We can do a mathematical analysis of this system and see how we may see it as an early example of reservoir engineering. The target system to control is the engine, and if it were to be taken alone its linearized equation with perturbation would be

$$\frac{d}{dt}\delta\omega = \delta F_{steam} - \delta F_{load} - \Gamma_r \delta\omega \tag{1.11}$$

where $\delta\omega$ is the rotation speed of the engine, F_{steam} is the effect of the flow of steam feeding the engine and F_{load} the effects resisting the rotation of the engine excluding the friction along its rotation axis. The steady state of the rotation speed would thus depends on the parameter of friction Γ_r. In practice, we have a small Γ_r to minimize the energy lost by friction, but a big Γ_r would be necessary to stabilize the system fast. This causes the system to be very little robust and this is why we need to control the system.

The addition of the centrifugal governor acts as a damped (parameter Γ_p) harmonic oscillator. The linearization around equilibrium of rotation speed around the vertical axis $\delta\omega$ and flyball angle with the axis the $\delta\theta$ gives, without the perturbations:

$$\begin{aligned} \frac{d}{dt}\delta\omega &= -a\delta\theta - \Gamma_r\delta\omega \\ \frac{d^2}{dt^2}\delta\theta &= -\Gamma_p \frac{d}{dt}\delta\omega - \Omega^2(\delta\theta - b\delta\omega) \end{aligned} \tag{1.12}$$

where a, b are coupling parameters, Γ_r, Γ_p are friction parameters around the axis and of the flyballs movement respectively, and Ω is the frequency of the damped oscillator made by the flyballs, all positive constants, depending on the functioning point (ω_0, θ_0) with $\Gamma_r << \Gamma_p, a, b, \Omega$. If we take g the magnitude of the gravitational field and L the distance the flyballs are fro the central axis when at the horizontal, we have $a = \frac{g}{L}cos(\theta_0)$, $b = \sqrt{\frac{L}{g}}$, and $\Omega = \sqrt{\frac{g}{L}}cos(\theta_0)$ The linearized equations result from Euler's second law on the rotating central axis and the Newton's second law on the flyballs.

By deriving the second equation and injecting the first one in it, we obtain a third order linear system, stable if and only if $\Gamma_p(\Omega^2 + \Gamma_p\Gamma_r + \Gamma_r^2) > ab\Omega^2$. This is the Routh criteria to determine

if we have a Hurwitz polynomial of degree three, a polynomial whose roots are all in the left half-plane of the complex plane. With Γ_r very small compared to all other parameters, the condition reads $\Gamma_p > ab$. Once we know the system is stable, we see that the new steady state is

$$\delta\omega = \frac{\delta F_{steam} - \delta F_{load}}{ab + \Gamma_r} \tag{1.13}$$

We have a small dependence on $\delta F_{steam} - \delta F_{load}$ if $ab >> 1$ (strong coupling between the engine and the governor), which requires for stability a strong damping of the flyballs $\Gamma_p >> 1$, but nothing on Γ_r.

This study shows a remarkable example of reservoir engineering: a poorly robust, potentially unstable system is made robust and stable by coupling it to a dissipative auxiliary system. It is yet necessary to have a strong coupling between the two and a strong dissipation on the auxiliary system to guarantee this effect.

1.2.2 Reservoir engineering in quantum physics: the theory

The general principles for reservoir engineering in quantum physics mirror quite well the steps we went through in last paragraph.

We give ourselves:

- a system of interest that we want to control $\mathcal{H}_c$, possibly with perturbations, with a steady state $|\bar{\psi}\rangle$ we want to stabilize with a robust exponential convergence. (It is possible to extend this way of proceeding to subspaces of $\mathcal{H}_c$)
- an auxiliary system $\mathcal{H}_a$, the "reservoir", where an operator $\mathbf{A}$ causes dissipation towards a state $|0\rangle_a$ with a rate κ.

The steps to follow to design a reservoir engineering scheme are:

1. Construct an operator $\mathbf{R}$ on $\mathcal{H}_c$, acting non-trivially and such that it stabilizes the steady state of interest: $\mathbf{R}|\bar{\psi}\rangle = 0$. This is just a mathematical construction, but there are constraints to respect in order to make possible the next step, or because of the way we want to construct the system. For example a constraint can be that $\mathbf{R}$ is a local operator, only acting on systems "close" to each other.
2. Construct a coupling Hamiltonian between target and auxiliary systems $\mathbf{H}_{int} = \mathbf{R}^\dagger\mathbf{A} + \mathbf{R}\mathbf{A}^\dagger$ on $\mathcal{H}_c \otimes \mathcal{H}_a$. Building this with available components may generally only be done approximately, and in that case finding ways to manage these approximations in the systems while keeping the desired effects on the operator $\mathbf{R}$ is necessary.

   The resulting equation of the coupled system is thus :

$$\frac{d\rho}{dt} = -i[\mathbf{H}_{int}(t), \rho] + \kappa\mathbb{I}_c \otimes \mathcal{L}_{\mathbf{A}}(\rho) \tag{1.14}$$

3. Steps 1 and 2 ensure that $|\bar{\psi}\rangle \otimes |0\rangle_a$ is an invariant state of the joint system; and dynamics elsewhere should be nontrivial. Now, if necessary, we "add elements" to make sure that $|\bar{\psi}\rangle \otimes |0\rangle_a$ is globally attractive. This can involve Hamiltonians acting on $\mathcal{H}_a \backslash \{span(|0\rangle_a)\}$ and on $\mathcal{H}_c \backslash \{span(|\bar{\psi}\rangle)\}$, or also some dissipation operators.

The steps 1 and 2 are two different parts of reservoir-engineering, which can raise different difficulties. We will mostly focus on the first one during this thesis.

1.2.3 Reservoir engineering in quantum physics: an example

The term "*reservoir engineering*" results from its use in the paper [26]. It stems from the idea that they have a quantum harmonic oscillator coupled to a qubit linked to a "reservoir" of an infinite number of system (the environment) continuously dissipating information. In practice it is

as if our qubit is permanently being reset, and we control how this qubit is coupled to the system we want to control, the harmonic oscillator. The paper shows how to design different couplings between a single ion trapped in a harmonic potential and its environment. The coupling results from the absorption of a laser photon and then its spontaneous emission. Variations of the laser frequencies and intensities allow one to "engineer" the coupling and select the master equation in order to stabilize states of interest. We will analyze one of the design proposed in this article to give a working example of the last paragraph. The analysis will stay close to the course "Quantum Systems: Dynamics and Control", to stay more simple on a physical point of view than the paper. The mathematics involved are the same.

The system of interest $\mathcal{H}_a$ we want to stabilize is a quantum harmonic oscillator. A simple way to describe it without detailing the full system is to give a few key concepts. Its dynamic is

$$\frac{d}{dt}\rho_a = -\frac{i}{\hbar}\,\omega_m[\mathbf{a}^\dagger\mathbf{a} + \frac{\mathbb{I}}{2}, \rho_a] \tag{1.15}$$

where the operator $\mathbf{a}$ is the annihilation operator, its hermitian conjugate $\mathbf{a}^\dagger$ the creation operator, ω_m is the angular frequency of the oscillator. We can give a basis of $\mathcal{H}_a$ as eigenstates of the Hamiltonian of our system $|0\rangle, |1\rangle, |2\rangle, ...|n\rangle, ...$, the Fock states. They interact as follow with the two operators:

$$\begin{aligned} \mathbf{a}|n\rangle_a &= \sqrt{n}\ |n-1\rangle_a \\ \mathbf{a}^\dagger|n\rangle_a &= \sqrt{n+1}\ |n+1\rangle_a \end{aligned} \tag{1.16}$$

The auxiliary system $\mathcal{H}_c$ is a qubit with base states $|g\rangle_c$ (ground state) and $|e\rangle_c$ (excited state). We also introduce the Pauli matrices $\boldsymbol{\sigma}_x = |e\rangle\langle g| + |g\rangle\langle e|$, $\boldsymbol{\sigma}_y = -i|e\rangle\langle g| + i|g\rangle\langle e|$, $\boldsymbol{\sigma}_z = |e\rangle\langle g| - |g\rangle\langle e|$, $\boldsymbol{\sigma}_- = |g\rangle\langle e|$, and $\boldsymbol{\sigma}_+ = |e\rangle\langle g|$.

Its dynamic is given by the following equation:

$$\frac{d\rho_c}{dt} = -\frac{i}{\hbar}\frac{\omega_{eg}}{2}\ [\boldsymbol{\sigma}_z, \rho_c] + \kappa\mathcal{L}_{\boldsymbol{\sigma}_-}(\rho_c) \tag{1.17}$$

with ω_{eg} the difference of energies between the excited and ground state.

In this particular example, the Hamiltonian describing how these two subsystems interact is enabled by a control field. In general this depends on the physical setting, but often control fields (so-called "pumps") are used to make sure that some couplings become resonant and hence produce a significant effect; furthermore, varying these pumps is a handy way to turn on/off various components of the reservoir, if needed for quantum operations. In [26], the interaction Hamiltonian is the following:

$$\begin{aligned} H_{int} = &(ue^{i(\omega_{eg}t - \eta(\mathbf{a}+\mathbf{a}^\dagger))} + u^* e^{-i(\omega_{eg}t - \eta(\mathbf{a}+\mathbf{a}^\dagger))})\sigma_x \\ &+ (u_b e^{i((\omega_{eg}+\omega_m)t - \eta_b(\mathbf{a}+\mathbf{a}^\dagger))} + u_b^* e^{-i((\omega_{eg}+\omega_m)t - \eta_b(\mathbf{a}+\mathbf{a}^\dagger))})\sigma_x \\ &+ (u_r e^{i((\omega_{eg}-\omega_m)t - \eta_r(\mathbf{a}+\mathbf{a}^\dagger))} + u_r^* e^{-i((\omega_{eg}-\omega_m)t - \eta_r(\mathbf{a}+\mathbf{a}^\dagger))})\sigma_x \end{aligned} \tag{1.18}$$

where the control is the superposition of 3 mono-chromatic plane waves with the first of frequency ω_{eg} (ion transition frequency) and amplitude u; the second of frequency $\omega_{eg} - \omega_m$ (red shift by a vibration quantum) and amplitude u_r ; and the third of frequency $\omega_{eg} + \omega_m$ (blue shift by a vibration quantum) and amplitude u_b. We have the following scales $\omega_m << \omega_{eg}$, $|u| << \omega_{eg}$, $|\frac{du}{dt}| << \omega_{eg}|u|$, $\eta \approx \eta_r \approx \eta_b << 1$. Although all operators formally act on the full Hilbert space, we skip the part on which they are identity, thus writing $\mathbf{a}$ instead of $\mathbf{a} \otimes \mathbb{I}_c$, and similarly $\boldsymbol{\sigma}_x$ instead of $\mathbb{I}_a \otimes \boldsymbol{\sigma}_x$. The full system is thus the combination of the three parts 1.15, 1.17 and 1.18.

The idea now is to change the frame of our system: we put ourselves in the rotating frame with the change of variable $|\psi\rangle = e^{-i\omega_m t(\mathbf{a}^\dagger\mathbf{a} + \frac{\mathbb{I}_a}{2})} e^{-it\frac{\omega_{eg}}{2}\boldsymbol{\sigma}_z}|\phi\rangle$ where $|\psi\rangle$ is in our initial frame and

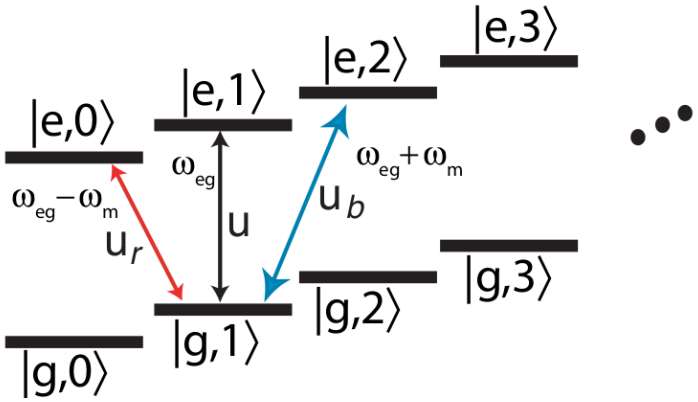

Figure 1.3: Resulting total Hamiltonian after RWA. We see the effects of first order transitions between the different states of definite energy of the system composed of the harmonic oscillator with infinite levels coupled to the qubit.

$|\phi\rangle$ in the rotating frame. Some calculations are necessary, notably non trivial commutations of exponentials of operators. We then make some approximation $z^{ix(\mathbf{a}^\dagger\mathbf{a})} = \mathbb{I}_a + ix(\mathbf{a}^\dagger\mathbf{a})$ for $x = \pm\eta, \eta_b, \eta_r$. This change of frame allows us to make apparent some approximations by averaging, which means neglecting highly oscillating terms of frequencies $2\omega_{eg}$, $2\omega_{eg} \pm \omega_m$ and $\pm\omega_m$. This is possible thanks to the difference of scale $|u|, |u_b|, |u_r| << \omega_m$.

This whole series of averaging and approximation is called the RWA method (rotating wave approximation), and in the first order we obtain an approximate resulting hamiltonian :

$$H_{rwa} = u|g\rangle\langle e| + u^*|e\rangle\langle g| + \bar{u}_b\mathbf{a}|g\rangle\langle e| + \bar{u^*}_b\mathbf{a}^\dagger|e\rangle\langle g| + \bar{u}_r\mathbf{a}^\dagger|g\rangle\langle e| + \bar{u^*}_r\mathbf{a}|e\rangle\langle g| \tag{1.19}$$

where $\bar{u}_b = -i\eta_b u_b$ and $\bar{u}_r = -i\eta_r u_r$. The effect of this Hamiltonian can be visualized in 1.3.

Now by choosing different u, u_b and u_r, we can stabilize different state of interest of our system. For example taking $\bar{u}_b = 0$, $\bar{u}_r$ constant different from 0 and u to get for $\alpha = -\frac{u}{\bar{u}_r}$, the system becomes

$$\frac{d}{dt}\rho = -\frac{i}{\hbar}\left[\bar{u}_r|g\rangle\langle e|(\mathbf{a}-\alpha)^\dagger + \bar{u^*}_r|e\rangle\langle g|(\mathbf{a}-\alpha), \rho\right] + \kappa\mathcal{L}_{\boldsymbol{\sigma}_-}(\rho) \tag{1.20}$$

where $\rho = \rho_a \otimes \rho_c$ in the rotating frame. Let's note that the Lindbladian does not change in the rotating frame.

A state such as $\mathbf{a}|\psi\rangle = \alpha|\psi\rangle$ is called a coherent state and noted $|\alpha\rangle$. We see that $|\bar{\psi}\rangle = |\alpha\rangle\otimes|g\rangle$ is invariant. This state is also attractive: a intermediary step is first to prove that the vacuum state $|0\rangle \otimes |g\rangle$ is attractive when $\bar{u} = 0$ thanks to the Lyapunov function $V(\rho) = Tr(|\bar{n}g\rangle\langle\bar{n}g| + \sum_{n=0}^{\bar{n}-1}|n\rangle\langle n|)$. Then for the case that concerns us where $\bar{u} \neq 0$, we just make the change of variable $\mathbf{D}_{-\alpha}\rho\mathbf{D}_\alpha$, where $\mathbf{D}_\alpha = e^{-\frac{|\alpha|^2}{2}}e^{\alpha\mathbf{a}^\dagger}e^{-\alpha^*\mathbf{a}}$ is the displacement operator.

Let us see how we followed the principles from last paragraph: we want a dissipation in $(\mathbf{a}-|\alpha\rangle)$ to stabilize the state $|\alpha\rangle$. Knowing that, we choose a certain way of coupling our systems such that, after some approximations, we obtain in the first order of the RWA the stabilization we are looking for. Let's note that these approximations are a key part of reservoir engineering, and that we usually cannot stabilize exactly the states of interest.

1.3 Quantum error correction

Since the development of Shor's algorithm for factoring integer numbers ([27]), quantum systems are viewed as a promising tool to process information faster than classical computers. However,

the uncontrolled effects of the environment on quantum systems cause so-called decoherence, degrading their quantum properties. Protecting information from such decoherence in order to build a memory for a quantum computer (see [24], from which this section is heavily inspired) is therefore a major challenge of quantum engineering. A redundant encoding of information allows, by repeating comparative measurements, to estimate the errors that occur and thereby protect logical information. Such Quantum Error Correction (QEC) has been proposed from the very beginning of the field. This thesis will use some concepts of this section to design two repetition codes in order to prevent some bit-flip errors from happening.

We will give a brief overview of QEC: starting by stating the differences between classical and quantum error correction, we will give a simple example of QEC and some of the most important concepts to evaluate the effectiveness of some QEC codes.

1.3.1 Classical and quantum error correction

We start by giving a brief overview of classical error correction, which tackles the same problems in classical system. The simplest but quite inefficient approach is the repetition code. The idea is to store the information multiple times, and if these copies disagree with each other after a certain amount of time, take a majority vote. To give an example, suppose we copy a bit in the 1 state three times. Then an error corrupts the three-bit state so that one of the copied bits is equal to 0 but the other two are still equal to 1. If errors are independent and occur with low probability p, it is most probable that only one bit have flipped after a certain amount of time when we perform a majority vote, e.g. we reset all the bits to the value of the majority of the bits, here 1. It is of course possible that a double-bit error occurs and the transmitted message is equal to three 0, but this outcome is less and less likely as p tends to zero. In this example, the logical information is the state of the majority of the bits, the physical information are the three copied bits, and determining what the logical state is from the physical state is called the decoding.

Similar to classical error correction, QEC codes do not always correctly decode logical qubits, but their use reduces the effect of noise. However, adapting already existing classical methods for quantum error correction is not immediate. Qubits are subject to the no-cloning theorem ([24]), meaning quantum information cannot be duplicated in the same way as classical one. Moreover, it is not possible to perform arbitrary measurements on a qubit due to the problem of the collapse of the wave-function. But it is possible to encode the information of one logical qubit onto a entangled state of multiple physical qubits. It can be done by expanding the Hilbert space in which the qubits are encoded [28].

To detect which error corrupts the encoded state, classical error correcting codes use syndrome measurements. If an error is found on a particular syndrome a correction process can be performed based on which syndrome detected the error.The same can be done in QEC: it performs a multi-qubit measurement that does not disturb the quantum information in the encoded state but retrieves the information about the error. In most QEC codes, the types of errors corrected are either a bit flip or a phase flip (sign of the phase), and thanks to the discretization of errors theorem [24], any error being a combination of the two will be corrected too. The syndrome measurement provides some information about the *error* that has happened, but not about the *information* stored inside the logical qubit. This is crucial, as otherwise the measurement would destroy any quantum superposition of this logical qubit, which would prevent it from being used to perform quantum operations.

1.3.2 Quantum redundancy and three-qubits code

We have mentioned that QEC is complicated by the no-cloning theorem, so let's see in practice how we can encode quantum information redundantly. We will begin by describing how to detect a single bit-flip error with a two qubit code.

We start by encoding the state ψ of the logical qubit on two different physical qubits:

$$|\psi\rangle = \alpha|0\rangle + \beta|1\rangle \rightarrow |\psi_L\rangle = \alpha|00\rangle + \beta|11\rangle = \alpha|0\rangle_L + \beta|1\rangle_L \tag{1.21}$$

Let's note that we do not clone our qubit, as $|\psi_L\rangle \neq |\psi\rangle \otimes |\psi\rangle$. The effect of this operation is to spread the quantum information ψ on the entangled state $|\psi_L\rangle$. This introduces redundancy to the encoding that can be exploited for error detection: before the encoding, the single qubit is parameterised within a two-dimensional Hilbert space $H_2 = span(|0\rangle, |1\rangle)$, but after the encoding the logical qubit occupies a four-dimensional Hilbert space $H_4 = span(|00\rangle, |01\rangle, |10\rangle, |11\rangle)$. However the logical qubit is only defined within a two-dimensional subspace of this expanded Hilbert space, called the code space C, where $C = span(|00\rangle, |11\rangle)$. Suppose that the logical qubit $|\psi_L\rangle$ is subject a bit-flip error on the first qubit, giving $|\psi_L\rangle = \alpha|10\rangle + \beta|01\rangle$. If the logical state $|\psi_L\rangle$ is uncorrupted, it is in the codespace C, but if it has been subject to a single bit-flip, it is in the error space $F = span(|01\rangle, |10\rangle)$. As C and F are orthogonal subspaces of H_4, it is possible to know which subspace our logical qubit is in with a projective measurement without compromising the encoded quantum information (the α and β parameters).

In order to differentiate the two subspaces C and F, a projective measurement of the form $\boldsymbol{\sigma}_{z1}\boldsymbol{\sigma}_{z2}$ (Pauli matrices on th two physical qubits) is performed. The $\boldsymbol{\sigma}_{z1}\boldsymbol{\sigma}_{z2}$ operator returns an eigenvalue equals to 1 if applied to the logical state $\boldsymbol{\sigma}_{z1}\boldsymbol{\sigma}_{z2}|\psi_L\rangle = \boldsymbol{\sigma}_{z1}\boldsymbol{\sigma}_{z2}(\alpha|00\rangle + \beta|11\rangle) = |\psi_L\rangle$. The $\boldsymbol{\sigma}_{z1}\boldsymbol{\sigma}_{z2}$ operator is said to stabilize the logical qubit. In the case $|\psi_L\rangle$ is on the F subspace, $\boldsymbol{\sigma}_{z1}\boldsymbol{\sigma}_{z2}$ projects the errored states onto the -1 eigenspace. Let's note that such a process cannot detect if the two physical qubits have flipped, as the logical qubit would be in the code space.

From here, creating a code protecting from one physical bit flip doesn't require much. The syndrome produced by this two-qubit encoding gives the information that an error occured, but it does not does not tell us on which physical qubit the error occurred. For this, we need to encode our information on a larger Hilbert space: the quantum information will be more spread on different physical qubits, allowing multiple stabilizer measurements need to be performed. We thus encode our logical state as $|\psi_L\rangle = \alpha|000\rangle + \beta|111\rangle$. This logical state lives in an Hilbert space of dimension eight, that we can partition as

$$C = span(|000\rangle, |111\rangle) \quad , \quad F_1 = span(|001\rangle, |110\rangle) \tag{1.22}$$

$$F_2 = span(|010\rangle, |101\rangle) \quad , \quad F_3 = span(|100\rangle, |011\rangle) \tag{1.23}$$

with C the logical code space, F_1, F_2 and F_3 the logical error spaces. If one physical qubit is subject to a bit-flip, we see that we can tell which one by analyzing in which error space the logical qubit is. To know that subspace, we just have to perform the measurements $\boldsymbol{\sigma}_{z1}\boldsymbol{\sigma}_{z2}$ and $\boldsymbol{\sigma}_{z2}\boldsymbol{\sigma}_{z3}$. By analyzing the result of these measurements, we can see that a $-1/1$ (resp $-1/-1$, $1/-1$) result would mean abit-flip error on the first physical qubit (resp second and third), while a $1/1$ result would mean that we are in the code space. We stress out the fact that a correct decoding is only possible if one or less bit flip happens. Once the decoding is done, we are able to choose a suitable recovery operation. We could reinforce the protection of the logical qubit against bit-flip by adding more physical qubits: for example a 5-qubit code would allow two errors on physical qubits to be detected.

This code only protects against bit flip errors and is very simple, but gives a good basis for what is QEC. An example of code correcting both bit flip and phase flip is the Shor code (which can be found in [24]), which needs 9 physical qubit to encode the informaiton of a logical qubit.

1.3.3 Important concepts for quantum error correction

Up to this point, we have described QEC codes in a theoretical setting. It is important to describe some of the practical issues that arise when considering when implementing QEC on actual hardware, as these concepts often define why some ones are preferred to others.

The first notion is the code threshold: as mentioned in previous section increasing from three to five qubits would allow to correct if two errors, instead of one, would happen on a physical qubit. But scaling this code is only interesting if the resultant larger code has a lower logical error rate. The threshold theorem for stabilizer codes states that increasing the distance (the minimum number of errors that will change one logical qubit to another in this way) of a code will result in a corresponding reduction in the logical error rate p_L , provided that the physical error rate p of the individual physical qubits is below a threshold $p < p_{th}$ [24]. This means that QEC codes can in

theory be used to arbitrarily suppress the logical error rate. Alternatively, if $p > p_{th}$, the process of quantum encoding actually causes harm to the protection of information. The threshold of a code thus provides a minimum experimental requirement that quantum computing experiments must reach before QEC becomes useful.

The other important notion is fault tolerance. One of the most important applications of QEC is not the protection of stored/transmitted quantum information, but the protection of quantum information that is undergoing dynamical computation, i.e. going through logical quantum gates. In that case, only performing error-correction periodically is not sufficient to prevent the accumulation of errors, even if it is applied after every logical quantum gate. Indeed, an error on one qubit (for example a bit flip) can propagate through quantum gates to other qubits and create several errors without any additional physical errors happening. This is why the concept of fault tolerance was introduced: a procedure is said to be fault tolerant if only one component in the procedure fails then the failure causes at most one error in each encoded block of qubits output from the procedure. Different methods exist to make QEC code fault tolerant, but the basic idea for all of them is to ensure that small errors do not spread uncontrollably through the circuit. Its is important to note that modifying a quantum error correction circuit for fault tolerance can require a considerable number of ancilla qubits, and even the most efficient schemes will result in an increased number of physicals qubits needed.

1.4 Presentation of the thesis

This thesis focuses on different uses of reservoir engineering in multi-partite quantum problems, as we are usually constrained to do local operations: many quantum devices are unable to perform high-fidelity long-range interactions between qubits. Chapters 2 and 3 are about the stabilization of GHZ state, while chapter 4 focuses on how to perform error correction.

1.4.1 Stabilizing GHZ state

The first part of this thesis, chapters 2 and 3, proposes a stabilization procedure for an approximate multi-partite GHZ state on n qubits, by using fixed dissipation operators acting each on few local subsystems. The basis is the work of Ticozzi and Viola (QIC 2014), [29], proving that exact stabilization of a multipartite GHZ state is impossible in this way, but also highlighting how a sequence of two quasi-local stabilization procedures does generate convergence towards the GHZ state. We work out how these two procedures can be applied in some appropriate probabilistic superposition. We examine several alternative ways to implement the classical synchronization of the two stabilization procedures with local couplings only, thanks to a chain of "clock" ancillas or to additional levels on the data subsystems. The practical value of these alternatives depends on experimental constraints. They all feature a design tradeoff between approximate stabilization fidelity and protection against perturbations. The methods and analysis are meant to illustrate how simple autonomous automata can be implemented in quantum reservoir engineering.

The high-fidelity production of multi-partite entangled states can be approached from several angles. A most direct way is to start from a well-known, typically separable state, and apply a sequence of gates to neighboring qubits [24]. For instance, starting from the separable state $|+\rangle|00..0\rangle$, where $|+\rangle = (|0\rangle + |1\rangle)/\sqrt{2}$ on the first qubit, and applying a chain of CNOT gates acting on qubits (1,2), then (2,3), ... generates the Greenberger-Horne-Zeilinger state (GHZ, [17]) on all qubits. Along similar lines, applying C-phase gates generates cluster states for instance [34]. These approaches require fast and robust gates to dominate decoherence effects during state preparation, after perfect initialization of the individual qubits. Another approach is to use an ancilla, which interacts consecutively with each subsystem or which could be emitted by any of several subsystems [11, 36], such that the system is projected onto the target multi-entangled state if the ancilla measurement gives a particular outcome. Such "heralded preparation" can be complemented with feedback actions. It could be used as an additional error correction procedure after preparation with a gate sequence, but most interestingly it allows entanglement between distant (i.e. not directly interacting) systems. Entanglement distillation enables to further improve

entanglement fidelity, by combining several lower-quality copies of the target state into one higher-quality instance [3]. All these approaches involve sequential procedures for generating an entangled state at a given time.

In contrast, reservoir engineering methods have also emerged to stabilize GHZ states: while building a more general toolset, the authors of [29] have initiated the investigation of such a thing, as they propose a method which allows to stabilize a GHZ state over $n \leq 3$ qubits. In more recent work, [8] describe another way to stabilize the state $|GHZ_{3+}\rangle = (|000\rangle + |111\rangle + |222\rangle)/\sqrt{3}$ on three *qutrits*. However, beyond $n = 3$, the first message is an impossibility result [29]. In particular, they have established the impossibility to stabilize a GHZ state on n qubits, if no quasi-local dissipation operator spans more than $n/2$ qubits. In follow-up work, they investigate the possibility to stabilize such states approximately, and provide a construction for the $n = 4$ particular case [20]. Importantly for the present work, [29] also proposes a conditional stabilization scheme, where the GHZ state is stabilized provided each qubit is initialized in the particular state $|+\rangle$; this approach is thus (slightly) sequential again, and if phase-flip perturbations act on a qubit after resetting into $|+ + ...+\rangle$, the system will not recover. Other engineered reservoirs have been proposed for stabilizing a sub-manifold of highly *correlated* states, while the non-local quantum phase "+" in $(|00..0\rangle + |11..1\rangle)/\sqrt{2}$ remains unprotected [35]; this is essentially a more concrete circuitQED (quantum electrodynamics) proposal of what the conditional stabilizer of [29] is doing. Given the impossibility result of [29], the best we can hope to achieve with quasi-local "fixed reservoir engineering" is global stabilization of *approximately* a GHZ state.

This thesis proposes concrete ways to globally stabilize an approximate GHZ state with reservoir engineering using quasi-local operators only. The main idea is to apply the two steps of the sequential stabilization proposed in [29] "alternatively": most of the time, the qubits apply the conditional GHZ stabilizers of [29]; but occasionally, they all jump back to $|+\rangle$. Applying these resets at random times, the reservoir "average" dynamics, which is all that matters for quantum predictions, involves an average between recently reset states (thus, far from target) and those which have evolved with the GHZ stabilizers for some time. If resets are scarce enough, then the average state should be close enough to the target one. The trade-off is of course that, with fewer resets, the system will recover more slowly from general perturbations. A first point of this work is thus to analyze the trade-off and its scaling with the number of qubits. A second point is to *synchronize* the resets of all the qubits, without which the scheme would not work. We propose two types of architectures to achieve this synchronization with *local interactions* only, by which we mean each subsystem interacting with a few neighbors only, and each interaction operator involving few (ideally two) subsystems.

Chapter 2 focuses on presenting the different architectures proposed to stabilize the GHZ state. Our first architecture, described in Section 2.2, uses a modified version of the clock ancilla used in the dissipative computing proposal of [33] and related papers. Their clock ancilla is directly coupled to all the data qubits and the desired outcome is heralded by a particular state of the unitarily evolving clock. We propose a more local and non-heralded scheme. Regarding locality, we associate one ancilla 'clock' subsystem to each data qubit, letting the 'clock' subsystems interact locally and with their respective data qubit, all with local operators only. Regarding non-heralding, we modify the Hamiltonian-based symmetric clock evolution of their proposal, into a cyclic clock evolution with jump operators, and adjust the jump rates to have a larger population on the target state. The clock synchronization only requires classical correlation of ancillas. Its efficiency depends on the time-scale separations that are achievable among various components of the dynamics. We present a few alternatives in this direction. In particular, one option triggers a wave propagating through the qubit chain, and we evaluate the possibility to use the produced GHZ state in the wave's space-time frame. Our second architecture, presented in Section 2.3, proposes to replace the data qubits by qutrits, using the additional level to operate the resets' synchronization. The target state is still specified by (1.6), with timescale separation ensuring that only a small fraction of the state has leaked to levels $|2\rangle$ of the qutrits. These constructions are meant to be in line with developing local Lindbladian automata whose dynamics protect valuable quantum information states.

Chapter 3 characterizes the performance of those schemes, both in simulations and through

approximate analysis methods. The aim is to compute the steady-state fidelity of the reservoir in presence of general perturbations. Our approximate analysis is based on timescale separations and classical Markov chain models. For this we develop some methods to translate our Lindbladian dissipative system into such classical Markov chains.

1.4.2 Error correction and Toom's rule

The second part of this thesis, chapter 4, examines how to perform error correction thanks to reservoir engineering. We propose two set-ups to protect errors from happening by interlinking qubits on a 2-D network, and only using local interactions to have a practical setting that can be applied for realistic experiments. The basis is work of Joachim Cohen ([9]), which gives an autonomous QEC scheme that protects a logical qubit encoded in the three-qubit code against bit-flip errors. We work on this premise to propose to set-ups scaling up this scheme by interlinking qubits on a 2-D network, while keeping the particularity of only using local interactions.

QEC schemes have evolved in different directions. The surface code is currently the most widely pursued quantum error correction scheme for experiment [23] [25]. This is due to its comparatively high threshold combined with the fact it requires only closest-neighbour interactions. However, there are some drawbacks, most notably the poor encoding density. Another problem relative to the surface code is that resource intensive methods are required to obtain a universal encoded gate set. Some alternatives to the surface code have been explored based on different layering of the qubit lattice [5]. These constructions typically have lower thresholds, but offer other advantages such as (potentially) easier access to universal encoded gate sets [70]. Efforts are also in progress to develop code constructions based on principles from high-performance classical codes [16] [30]. The main problem with these codes is that oftentimes it is necessary to perform arbitrary long range interactions between the code qubits.

This thesis proposes two QEC set-ups that counter bit-flip errors, and how to scale up the network encoding a logical quantum bit, towards stronger information protection. The challenge has been to devise a network architecture which allows to autonomously correct higher-order errors, while remaining realistic towards experimental realization by avoiding all-to-all or all-to-one coupling. This unusual approach, to protect from one type of error only, is justified as the research group in which this thesis was written focuses on the cat-qubits scheme [14]: instead of using many qubits to provide redundancy required to protect the encoded information, it is encoded in a harmonic oscillator and uses the vastness of the associated Hilbert space. Such a design suppresses (say) logical phase flips, leaving only bit-flip errors associated to parity jumps. The two set-ups proposed, once realized with cat-qubits, would thus provide a complete protection of the quantum information.

They both start from the work of [9], which aims to stabilize a logical qubit composed of 3 physical qubits in order to increase the memory fidelity under perturbations inducing physical bit flip errors. We first describe briefly the associated physical system and the resulting error correction protocol, before showing how it can be scaled up to increase the order of information protection. The first proposal works by coupling several of these systems into networks of progressively more physical qubits, inspired by regular polygons. The new method and pattern proposed here is modular and can be used to extend the code, providing protection of increasing orders, while each local operation involves three qubits treated in a symmetric way. A preliminary analysis is provided, showing how the scheme allows to correct an increasing number of initial errors located at arbitrary places in the network.

The second proposal uses the correction protocol imagined by Toom in [31]. It consists in a 2-D code where qubits are disposed on the vertices of a $N \times N$ square. In a discrete time approach, at each round of correction, the protocol is: if one qubit is different from both its bottom and right neighbour, then flip it. Error correction operations hence propagate through the network, while treating the three qubits of a single operation in an asymmetric way (only one of them is allowed to flip). Remarkably, this discrete algorithm can quite easily be mixed with the reservoir engineering operation developed in [9], where qubits are naturally paired three by three, but also the correction can naturally be made asymmetric among them. We further propose an analysis of

this scheme using the work of [1] section 5.2, which consists in giving a reduced model describing the slowest dynamics in a two timescale system and parameterizing the slow invariant eigenspace. Here the fast dynamics corresponds to the error-correcting reservoir, while the slow perturbation corresponds to the bit flips occurring. The reduced model describes the latter's effect both in terms of leakage (the "stationary regime", described by the slow invariant eigenspace, will not be composed of exactly zero errors) and of residual error rate (overall "logical" bit-flips at the code level will still appear, but at much lower rate than on the physical qubits). In particular, we adapt the techniques of [1] to classical Markov chains and we observe how conclusions can be drwan by working out only a targeted part of the reduced model.

Chapter 2

Construction and explanation of the GHZ state stabilizing set-up with quasi local couplings

In this chapter, we will first give a precise Lindbladian description of our base settings from which we will build upon our different set-ups, with the restrictions it will have to follow. The general idea is to combine two processes, whose succession stabilize the GHZ state, into a single time-invariant Lindbladian using only local couplings in order to obtain a steady state which would be close to the GHZ state.

We will then give the different set-ups we can build from this idea, which are divided into two families of architecture: if we want our data subsystem to be composed of qubits or qutrits. We will progressively explain how the two processes can coexist for both of them, and give some further possible refinements in the design of the set-ups.

2.1 Problem description

The original setting involves a chain of n (data) qubits which have to be stabilized in the entangled superposition (1.6). Our proposals rely on the novelty of enlarging the full Hilbert space, either by using additional levels on the data subsystems, or by adding ancillary subsystems to the setting. We introduce these novelties from the start in our system description. We keep the spatial arrangement of a chain and require local interactions along this chain.

Consider thus a chain of n (data) subsystems, each of finite dimension Q, to which we adjoin a chain of m ancillas, each of dimension D. The full Hilbert space $\mathcal{H}$ is thus of dimension $Q^n D^m$ and we want a procedure that works for arbitrary n.

- Our first type of proposal relies on data qubits ($Q = 2$) and associates typically one ancilla per data qubit ($m = n$) or per pair of neighboring data qubits ($m = n - 1$).
- Our second type of proposal relies on data qutrits ($Q = 3$) and requires no ancillas ($m = 0$).

In all cases, we denote by $|0\rangle, |1\rangle, |2\rangle$ the canonical states of the data subsystems, while we use letters $|g\rangle, |e\rangle, |m\rangle, |f\rangle, ...$ for canonical states of the ancillas. We use an index when appropriate to label which ancilla and/or data subsystem is meant.

We let this system evolve in an engineered reservoir, according to a time-independent Lindblad equation of the form:

$$\begin{aligned}\frac{d}{dt}\rho_t = -i[H,\ \rho_t] &+ \sum_{k=1}^{K_1} L_k\rho_t L_k^\dagger - \tfrac{1}{2}\left(L_k^\dagger L_k\rho_t + \rho_t L_k^\dagger L_k\right)\\ &+ \sum_{k=1}^{K_2} M_k\rho_t M_k^\dagger - \tfrac{1}{2}\left(M_k^\dagger M_k\rho_t + \rho_t M_k^\dagger M_k\right)\\ &+ \sum_{k=1}^{K_3} N_k\rho_t N_k^\dagger - \tfrac{1}{2}\left(N_k^\dagger N_k\rho_t + \rho_t N_k^\dagger N_k\right) \qquad (2.1)\end{aligned}$$

The distinction of operators L_k, M_k and N_k for the dissipation channels is to facilitate later discussion. The objective is to design constant operators H and L_k, M_k, N_k such that any initial state on $\mathcal{H}$ converges towards the so-called Greenberger-Horne-Zeilinger (GHZ) state

$$|GHZ_+\rangle \ = \ (|00..0\rangle + |11..1\rangle)\,/\,\sqrt{2}$$

It is important to insist on the objective followed throughout this chapter: the dynamics follows a *time-independent* Lindblad equation, with constant operators, and the state of interest is the *steady state* $\bar{\rho}$ reached with this Lindbladian when tracing over the ancilla degrees of freedom (global and unconditional asymptotic stabilization). In particular, if the steady state is not unique and there exist initial states from which stabilization of $|GHZ_+\rangle$ fails, then we consider that the scheme is not working. On the other hand, when an engineered reservoir does stabilize a unique steady state, we will use fidelity $\mathcal{F}(\bar{\rho}) = \langle GHZ_+|\,\bar{\rho}\,|GHZ_+\rangle$ as a measure of closeness to our objective. To evaluate the protective power of the engineered reservoir, we will consider the case where on top of (2.1) each subsystem is subject to perturbation channels.

The essential constraint for reservoir design is that each term in H and each of the operators L_k, M_k and N_k must be quasi-local, namely each one of them must act like the identity on all of the Hilbert space except a few subsystems; furthermore, we require that these subsystems are neighbors according to the physical layout of a chain. Thus each data or ancilla subsystem can only be coupled to a small and fixed number of neighbors, independent of n. The catch is that [29] has proved the impossibility in this context to globally asymptotically stabilize a GHZ state with a fixed Lindbladian reservoir on n qubits, thus with $m = 0$ and $Q = 2$. In fact, their general theorem also covers the case with $Q > 2$, and the impossibility result also remains true in presence of additional ancilla subsystems. Therefore, our objective is to stabilize a state $\bar{\rho}$ which is a good approximation of $|GHZ_+\rangle\langle GHZ_+|$. We provide the proofs of these generalisation.

For the case of quQits, i.e. subsystems of Q levels with $Q > 2$, the method is the same as in [29].

Proposition 1 *The dynamics (2.1) with only data subsystems of dimension $Q \geq 2$ cannot globally asymptotically stabilize the GHZ state $(|00...0\rangle + |11...1\rangle)/\sqrt{2}$ on n subsystems if each operator involves interaction of at most $< n/2$ subsystems.*

Proof We use two results reported in [29]. For a target state $|\psi_d\rangle$, denote ρ_k the associated reduced state on the neighborhood on which one of the dissipation operators L_k acts nontrivially. Denote $\mathcal{H}_{(k)} = \text{support}(\rho_k \otimes \text{Identity})$ and let $\mathcal{H}_0 = \cap_k \mathcal{H}_{(k)}$. Then:

- $|\psi_d\rangle$ can be globally asymptotically stabilized with only quasi-local dissipation operators L_k if and only if $\mathcal{H}_0 = \text{span}(|\psi_d\rangle)$ (Theorem 1 in [29]).
- if $\mathcal{H}_0 \supset \text{span}(|\psi_d\rangle)$, then $|\psi_d\rangle$ can be globally asymptotically stabilized by adding a quasi-local Hamiltonian H if the latter can satisfy (i) $H|\psi_d\rangle = 0$ and (ii) $e^{iHt}|\phi\rangle$ leaves $\mathcal{H}_0$ for all other $|\phi\rangle \in \mathcal{H}_0$. (Proposition 3 in [29])

Applying this to $|\psi_d\rangle = (|00...0\rangle + |11...1\rangle)/\sqrt{2}$ when the state space consists of $\text{span}\{|0\rangle, |1\rangle, ..., |Q-1\rangle\}^{\otimes n}$ involves the exact same reasoning as in [29] for $Q = 2$.

- With bipartite interactions, $\mathcal{H}_{(k)} = \text{span}(|00\rangle_{j,\ell}, |11\rangle_{j,\ell}) \otimes \text{span}\{|0\rangle, |1\rangle, ..., |Q-1\rangle\}^{\otimes(n-2)}$ where j, ℓ are the pair of quQits associated to decoherence operator L_k. Then $\mathcal{H}_0 = \text{span}\{|00...0\rangle, |11...1\rangle\}$ so there is no way to globally asymptotically stabilize this state with only quasi-local decoherence operators L_k.

- Having $H|\psi_d\rangle = 0$ requires
$$H|00...0\rangle = -H|11...1\rangle \; . \tag{2.2}$$
But if each term in H only acts on $< n/2$ subsystems, then each term on the left of (2.2) contains $> n/2$ subsystems on $|0\rangle$ while each term on the right contains $> n/2$ subsystems on $|1\rangle$; i.e. the left and right hand side of (2.2) are orthogonal, leaving as only possibility that $H|00...0\rangle = H|11...1\rangle = 0$. But in this case, the state $(|00...0\rangle - |11...1\rangle)/\sqrt{2} \in \mathcal{H}_0$ also remains invariant. □

The case with ancillas requires some adaptation, because we do not need to stabilize a pure state over the whole Hilbert space: only the data subsystems must converge towards $|\psi_d\rangle = (|00...0\rangle + |11...1\rangle)/\sqrt{2}$, while the ancillas need not converge. We here provide a more specific proof for the target state $|GHZ_+\rangle$.

Proposition 2 *The dynamics (2.1) with n data qubits ($Q = 2$) and auxiliary subsystems, cannot globally asymptotically stabilize the GHZ state $(|00...0\rangle + |11...1\rangle)/\sqrt{2}$ if each operator involves interaction of at most $< n/2$ data subsystems.*

Proof Note that the dynamics (2.1) must have at least one steady state, even if it is not globally attractive. Since we want $|GHZ_+\rangle$ to be globally attractive, we can write this steady state $\bar{\rho} = |GHZ_+\rangle\langle GHZ_+| \otimes \bar{\rho}_{aux}$, with thus $\bar{\rho}_{aux}$ the associated steady state of the ancilla subsystems.

We will use for the data Hilbert space the following specific basis:

$$\begin{aligned}
|0+\rangle &:= (\,|000...00\rangle + |111...11\rangle\,)/\sqrt{2} \qquad (2.3)\\
|0-\rangle &:= (\,|000...00\rangle - |111...11\rangle\,)/\sqrt{2}\\
|1+\rangle &:= (\,|000...01\rangle + |111...10\rangle\,)/\sqrt{2}\\
|1-\rangle &:= (\,|000...01\rangle - |111...10\rangle\,)/\sqrt{2}\\
&...\\
|S+\rangle &:= (\,|100...00\rangle + |011...11\rangle\,)/\sqrt{2} \qquad (2.4)\\
|S-\rangle &:= (\,|100...00\rangle - |011...11\rangle\,)/\sqrt{2}\,,
\end{aligned}$$

where $S = 2^{n-1} - 1$. Note that we order the two terms on each line such that the second term contains more qubits on $|1\rangle$. Thus, $|s-\rangle = Z_k|s+\rangle$ for all $s \in 0, 1, ..., S$ and a phase-flip operator Z_k on any *data qubit* $k \in 1, 2, ..., n$ *which equals* $|1\rangle$ *in the second term of* $|s\pm\rangle$. In particular, $|GHZ_+\rangle = |0+\rangle = Z_k|0-\rangle$ for any $k \in 1, 2, ..., n$ and for instance, $|3-\rangle := (|00011\rangle - |11100\rangle)/\sqrt{2} = Z_k|3+\rangle$ for $k \in 1, 2, 3$. By construction, for each $s \in 0, 1, .., S$, there are at least $n/2$ such qubits on which Z_k can be applied with this property.

Consider any quasi-local decoherence operator or any quasi-local term in the Hamiltonian of (2.1), and denote it D_ℓ. Each such D_ℓ acts non-trivially on strictly less than $n/2$ data qubits. Therefore:

- Take any $s \in 0, 1, ..., S$ and denote K_s the set of indices of data qubits which equal $|1\rangle$ in the second term of the basis as written in (2.3). For instance, with $n = 5$ and if $s = 3$ then $K_s = \{1, 2, 3\}$. The set K_s contains at least one qubit $\bar{k}$ on which D_ℓ acts *trivially*, thus for which $Z_{\bar{k}} D_\ell = D_\ell Z_{\bar{k}}$.

- Taking the phase flip operator on $\bar{k}$, we establish that for each ℓ and for any $s \in 0, 1, ..., S$:
$$\begin{aligned}
\langle s\pm|D_\ell|0-\rangle &= \langle s\mp|Z_{\bar{k}} D_\ell|0-\rangle = \langle s\mp|D_\ell Z_{\bar{k}}|0-\rangle = \langle s\mp|D_\ell|0+\rangle \; , \qquad (2.5)\\
\langle 0-|D_\ell|s\pm\rangle &= \langle 0+|Z_{\bar{k}} D_\ell|s\pm\rangle = \langle 0+|D_\ell Z_{\bar{k}}|s\pm\rangle = \langle 0+|D_\ell|s\mp\rangle \; .
\end{aligned}$$
Note that the result of these brackets are operators on the ancilla Hilbert space.

- Let D_ℓ a decoherence operator. Writing down (2.1) and checking the block-diagonal part *outside* $|GHZ_+\rangle\langle GHZ_+|$, a first condition for $\bar\rho$ to be invariant is that $\langle s\pm|D_\ell|0+\rangle\bar\rho_{aux}=0$ for each ℓ. From (2.5), this also implies $\langle s\pm|D_\ell|0-\rangle\bar\rho_{aux}=0$. In other words, this first condition holds for keeping $\tilde\rho:=|GHZ_-\rangle\langle GHZ_-|\otimes\bar\rho_{aux}$ invariant as well.

- For each decoherence operator D_ℓ, denote $A_\ell=\langle 0+|D_\ell|0+\rangle$ and $B_\ell=\langle 0+|D_\ell$. For each Hamiltonian term D_j, denote $P_j=\langle 0+|D_j|0+\rangle$ and $Q_j=\langle 0+|D_j$. Writing down (2.1) and checking the remainder of the components, the second condition for $\bar\rho$ to be invariant is that

$$\begin{aligned} 0 &= \sum_\ell A_\ell\bar\rho_{aux}A_\ell^\dagger-\tfrac{1}{2}A_\ell^\dagger A_\ell\bar\rho_{aux}-\tfrac{1}{2}\bar\rho_{aux}A_\ell^\dagger A_\ell-i\sum_j[P_j,\bar\rho_{aux}]\ , \qquad (2.6)\\ 0 &= -\tfrac{1}{2}\sum_\ell\bar\rho_{aux}A_\ell^\dagger B_\ell-i\sum_j\bar\rho_{aux}Q_j\ . \end{aligned}$$

  Now by (2.5), we also have $A_\ell=\langle 0-|D_\ell|0-\rangle$ and $P_j=\langle 0-|D_j|0-\rangle$, meaning that the first line holds for keeping $\tilde\rho$ invariant as well.

  Similarly, annihilating the second line of (2.6) multiplied by $|s\pm\rangle$, for any $s\neq 0$ or for $|s\pm\rangle=|0-\rangle$, implies by (2.5) that this line multiplied by $|s\mp\rangle$ is annihilated when redefining A,B,P,Q with $|0-\rangle$ instead of $|0+\rangle$. In other words, again the corresponding conditions for keeping $\bar\rho$ invariant and for keeping $\tilde\rho$ invariant are satisfied together.

- The conditions discussed in the last two items are all the ones for keeping a state invariant, as they are just obtained by annihilating each component of (2.1) applied to the steady state. Thus, from those two items, the conditions for keeping $\bar\rho$ invariant imply that we would also keep $\tilde\rho$ invariant. It is thus impossible to have $\bar\rho$ globally asymptotically stable. □

Note that in this result, we assume nothing about the ancillary subsystems: it may even be a single big subsystem connected individually to all the data subsystems. The same impossibility proof keeps holding when allowing both ancilla subsystems *and* $Q>2$ in the data subsystems.

In addition to the impossibility result, the authors in [29] also notice a simple procedure to generate the GHZ state. This would work by first stabilizing each qubit individually towards $|+\rangle=(|0\rangle+|1\rangle)/\sqrt{2}$, and then applying the dissipation channels

$$L_k=\sqrt{\kappa_c}(|11\rangle\langle 10|+|00\rangle\langle 01|)\text{ on qubits }(k,k+1)\ ,\qquad \text{for } k=1,2,...,n-1 \qquad (2.7)$$

by which (coherently) qubit $k+1$ is asymptotically set to the same bit-value as qubit k. The aim of the present paper is to investigate how to combine these two procedures into a single time-invariant Lindbladian, still with local interactions only, and whose steady state $\bar\rho$ would be close to the target GHZ state. Concretely, we propose several stabilization procedures based on the same simple idea: at each time step t the data subsystems are all reset to $|+\rangle$ with a small probability, and from there they have a high probability to keep applying just the dissipation operators L_k of (2.7), hence approaching $|GHZ_+\rangle$. The resulting average dynamics should induce a steady state $\bar\rho$ close to the target GHZ state. When resets are scarcer, the steady state would get closer to $|GHZ_+\rangle$, but recovery from a phase-flip error gets slower; at the limit of infinitesimal reset probability, the system would feature fast convergence towards a subspace infinitesimally close to span$\{|00..0\rangle, |11..1\rangle\}$, and infinitesimally slow convergence towards $|GHZ_+\rangle$ within this subspace.

It is essential though for this idea, that the reset to $|+\rangle$ takes place synchronously, and only synchronously, on all the data subsystems. The first reason is that a reset pulls the state away from $|GHZ_+\rangle$, so we want to minimize the fraction of time doing restes. In this sense, it is more efficient to correct potential phase errors on *all* qubits at every reset round. The second and more important reason is that even when starting on $|GHZ_+\rangle$, when a single data subsystem undergoes a reset to $|+\rangle$ and we let the system converge back with (2.7), the state will *not* converge to $|GHZ_+\rangle$. In other words, every reset round involving some but not all data subsystems, would not only be

useless but even deteriorate the fidelity *until the next all-data-subsystems reset round*. To make synchronous resets (significantly) more probable than partial ones, a dedicated synchronization procedure is needed. In our proposals, the enlarged Hilbert space serves the essential role of implementing this *synchronous* reset of all qubits to $|+\rangle$. In the following sections, we describe and analyze different ways to obtain engineered reservoirs from this principle, first with $Q = 2$ and a chain of ancillas (Section 2.2), then without ancillas but exploiting a third level on each data subsystem (Section 2.3).

Remark 1: The reader could notice that compared to [29], we target *approximate* stabilization *and* we enlarge the Hilbert space. In [20] the authors propose a way to approximately stabilize a GHZ state on $n = 4$ qubits. We had no particular ideas for efficiently stabilizing an *approximate* GHZ state of arbitrary n using the Hilbert space of the data qubits only, yet in fact this possibility remains open.

2.2 Architectures with a "clock" of ancilla quDits

In this type of architecture, the system consists of the chain of n data qubits (Q=2), to which we adjoin a chain of ancilla quDits, see Figure 2.1. In (2.1), the dissipation operators

- L_k will always be related to stabilizing the subspace span$\{|00...0\rangle, |11...1\rangle\}$ like in (2.7),
- M_k will govern the evolution of the ancillas, and
- N_k are used to reset data qubits to $|+\rangle$ conditional on ancillas.

Our proposals take Hamiltonian $H = 0$; future work may revise this choice, e.g. to combine some dissipation operators into a single coherent superposition while killing its dark states with H. In the most constraining setting, we only allow bipartite interactions: each L_k can act non-trivially only on two neighboring data qubits j and $j + 1$; each M_k on two neighboring ancilla quDits j and $j + 1$; and each N_k on data qubit j and ancilla quDit j. We will also discuss proposals with slightly different constraints, e.g. allowing tripartite interaction. The interactions will always be reduced to direct neighbors according to the double-chain topology (dotted ellipses on Figure 2.1).

2.2.1 Engineering the approximate GHZ reservoir through ancilla state conditioning

Step 0: assuming correlated ancilla evolution

As a preliminary discussion, let us start with relaxing the locality constraint on the M_k and assuming that we have an operator implementing synchronous jumps of all the ancilla's. To further simplify this preliminary discussion, we will assume that the ancillas are confined to the space span$\{|gg...g\rangle, |ee...e\rangle\}$ thanks to some (not further specified) mechanism, and hence we can reduce the ancilla dissipators to:

$$M_1 = \sqrt{\kappa_u}\, |ee...e\rangle\langle gg...g| \quad , \quad M_2 = \sqrt{\kappa_d}\, |gg...g\rangle\langle ee...e| \,.^{1} \tag{2.8}$$

To finalize this preliminary construction, each data qubit keeps applying fast local reset dynamics conditioned on its ancilla being in $|e\rangle$:

$$N_k = \sqrt{\kappa_r}|e,+\rangle\langle e,-|_{k,k} \qquad \text{for } k = 1, 2, ..., n \,. \tag{2.9}$$

The idea of this scheme is that the data qubits are continuously applying the L_k from (2.7); but occasionally the ancillas all jump to $|e\rangle$ for a short time, during which this triggers resets of each data qubit to $|+\rangle$ as dominating dynamics.

Several relevant observations can already be made with the preliminary system (2.7),(2.8),(2.9).

[1] In fact, thanks to both the departure and arrival states being orthogonal, we may in principle replace (2.8) by a single operator $M = M_1 + M_2$, although it is doubtful whether this would be easier to implement.

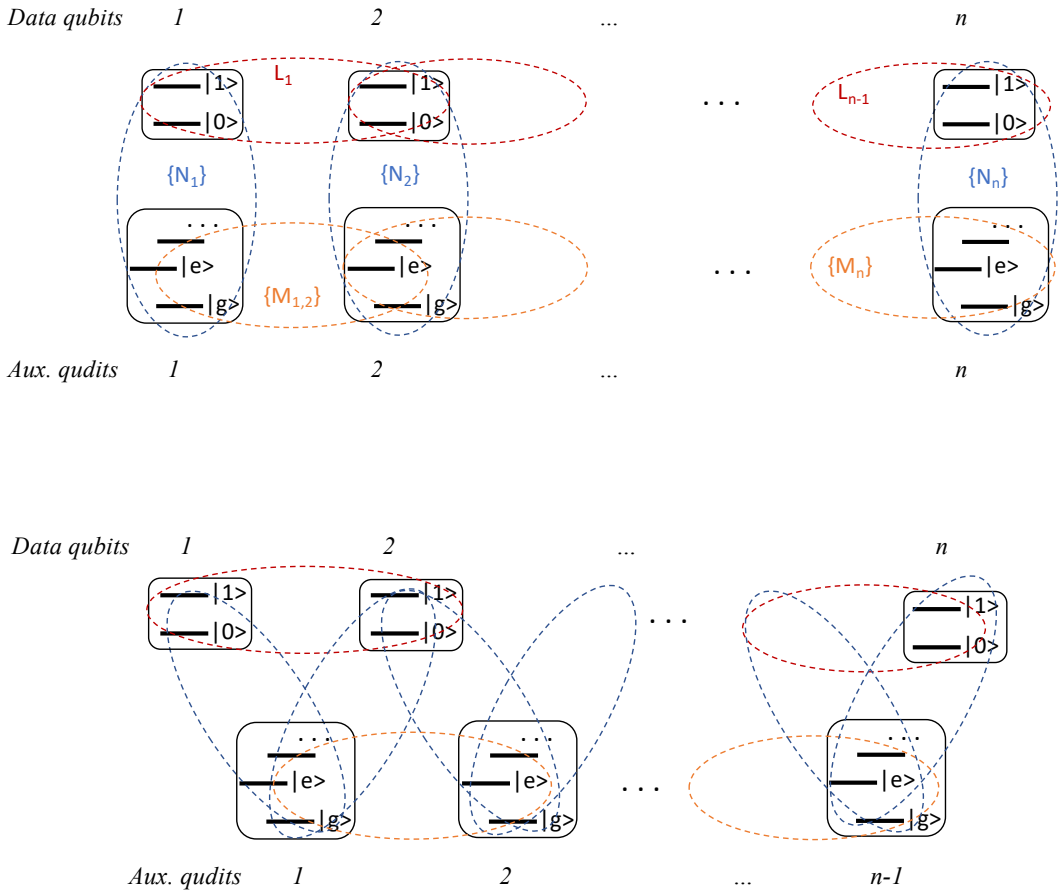

Figure 2.1: General architecture of our approximate GHZ reservoir with "clock-ancillas". An ancilla quDit is associated to each data qubit (top), or to each pair of adjacent data qubits (bottom). Only neighboring qubits or quDits can interact through dissipation operators, according to a double-chain topology (dotted ellipses, labeled with corresponding operators). The data qubits interact according to dissipation operators (2.7) proposed by [29]; taken alone, this would stabilize them in the manifold $\mathcal{H}_s := \text{span}\{ |00...0\rangle, |11...1\rangle \}$. The mechanism with auxiliary quDits is meant to softly reset the data into an initial state from which they converge towards the + superposition of the basis states in $\mathcal{H}_s$; see Figure 2.2 for more details.

- The scheme relies on selecting the time scales as follows. Since reset dynamics (2.9) has to overpower (2.7) (which is always left on, see third item), we need $\kappa_r \gg \kappa_c$. Since having ancillas on $|ee...e\rangle$ is meant to synchronize qubit resets, we also mean to take $\kappa_r \gg \kappa_d$. We nevertheless want to take κ_d rather large, to avoid spending unnecessary time doing resets to $|+\rangle$ which move the state away from $|GHZ_+\rangle$. Finally, we aim for $\kappa_c \gg \kappa_u$ to leave enough time for re-convergence towards $|GHZ_+\rangle$ after a reset. The rate of protection against general perturbations is then set by the slowest rate i.e. κ_u . At first sight there appears to be no clear scaling request between κ_d and κ_c, some optimal tuning should be sought. More analysis is provided in Section 3.1.

- Instead of applying data reset dynamics conditioned on its ancilla *being in* state $|e\rangle$, one could apply the data reset conditioned on the associated ancilla *jumping to* state $|e\rangle$. This option will be discussed in Section 2.2.2.

- The proposed construction switches on and off the single-qubit reset through (2.9), but it leaves the L_k always on. Instead of dominating the L_k by the N_k when ancillas are in $|e\rangle$, one could consider to switch off the L_k. Because each L_k already involves two data qubits, unlike the reset operator $|+\rangle\langle -|$, conditional switching of the L_k is somewhat harder and will be considered later in the paper.

- There is no need to protect the phase of the ancillas in the canonical basis: their only role is to establish a *classical correlation* between all qubits resetting. In this sense, the synchronous jump operators (2.8) are a slightly weaker resource than a coherent quantum channel; but more importantly, this insensitivity to ancilla phase errors will remain true for other reservoir constructions below. We consider the system (2.1) with the corresponding operators and assume that the density matrix ρ_t only has population on the diagonal in the canonical ancillas basis, i.e.:

$$|r\rangle\rho_t|s\rangle = 0 \quad \text{for all } r \neq s \in \{g, e, m\} \ .$$

  Our claim is that the Lindblad equation preserves this property. This is easy to check with any particular jump operator M_k or N_k, thanks to the fact that these operators map an ancillas canonical state to an orthogonal ancillas canonical state. A stronger claim would be that if any coherences are present initially, then they exponentially vanish over time. Although such property can be put in place, it is not at all essential for our analysis, so we leave this open for the interested reader.

  Thus, we do not really need ancilla quDits: we only need classical Dits, or quDits with heavily biased noise protection i.e. generalizing the qubits with biased noise where bit-flips are heavily suppressed while phase-flips remain rather common [21]. For this reason, we can consider that the ancilla populations remain stable at much longer timescales than the data qubits.

- Reasoning about this system is facilitated by the fact that ancilla dynamics is not influenced by the data states. The description of the system architecture quite speaks for itself. The formal property goes as follows.

  – Take the Lindblad equation (2.1) with the corresponding operators;

  – Plug in any state ρ_t of the joint system;

  – Compute the transition rates of the ancillas e.g. trace$(|e\rangle\langle g|_k \frac{d}{dt}\rho_t)$

  – Observe that those rates only depend on $\rho_t^{(A)}$, the partial trace of ρ_t over the data subsystems.

  The computations involve no originality and are left for the interested reader. Note that at this point we have said nothing more about the ancillas state, thus the "transition rates" are complex values in the Lindblad equation. We explained how the ancillas can rigorously be reduced to a purely classical system in the last point.

  We will make sure to keep this property in our other constructions.

The next step is to replace (2.8) by Lindblad dynamics with *quasi-local* operators, achieving essentially the same effect. In a different context, [33] has used a single "timer" ancilla, assuming that it is coupled individually to each data qubit. This would mean, in the setup just described, to use the same unique ancilla $|e\rangle$ in each of the N_k. Such operators would still be bipartite only, in fact tripartite in the context of [33]. However, it would require a single ancilla to be physically connected to all the n data qubits. With the following synchronization mechanism using n ancillas, each subsystem is connected only to a few neighbors in a double-chain layout.[2]

Step 1: constructing a correlated ancillas clock

Our proposal to replace (2.8) by dynamics involving local interactions on a chain needs the ancillas to be qutrits, with levels $|g\rangle, |e\rangle$ and $|m\rangle$. The idea (see Figure 2.2.a) is that each ancilla has a relatively small probability to change its state *spontaneously* towards the "next" state in a cyclic way $|g\rangle \to |e\rangle \to |m\rangle \to |g\rangle ...$, but a relatively large probability to get *stimulated* to the "next" state if a neighboring ancilla has this value. The qutrit structure is necessary to introduce directionality in this cycle. Indeed, if the mechanism was implemented with ancilla *qubits*, then an ancilla that has jumped spontaneously say from $|g\rangle$ to $|e\rangle$ would be attracted back towards $|g\rangle$ by its neighbors at the same time as attracting them towards $|e\rangle$; on a chain of ancillas, the boundary between ancillas in the $|g\rangle$ and $|e\rangle$ states could thus move either way at the same rate, suggesting that it would be hard to synchronize the whole chain. In contrast, with the *qutrit* structure, if all ancillas are in $|g\rangle$ and one of them jumps to $|e\rangle$, then this ancilla has only very low probability to spontaneously jump to the next state $|m\rangle$, while the neighbor ancillas have a high probability to join it on level $|e\rangle$, attracting in turn their own neighbors, and so on; thus, the ancillas would essentially follow the cycle

$$|gg...g\rangle \to |ee...e\rangle \to |mm...m\rangle \to |gg...g\rangle \to ... \tag{2.10}$$

with very little time spent on other states, if the stimulated jump is sufficiently dominating.

Assuming that the subsystems are arranged as a chain, the quasi-local jump operators could be:

$$\begin{aligned} M_{k,sp} &= \sqrt{\kappa_u}|e\rangle\langle g|_k + \sqrt{\kappa_d}|m\rangle\langle e|_k + \sqrt{\kappa_t}|g\rangle\langle m|_k \\ M_{k,st+} &= \sqrt{\kappa_{st}}\ (|ee\rangle\langle ge| + |mm\rangle\langle em| + |gg\rangle\langle mg|)_{k,k+1} \\ M_{k,st-} &= \sqrt{\kappa_{st}}\ (|ee\rangle\langle eg| + |mm\rangle\langle me| + |gg\rangle\langle gm|)_{k-1,k} \end{aligned} \tag{2.11}$$

for each $k = 2, 3, ..., n-1$, and one of the two last channels dropping for ancillas $k = 1$ and $k = n$. The indices $_{sp}$ or $_{st}$ distinguish spontaneous or neighbor-stimulated processes, while $_+$ or $_-$ indicate stimulation by the left or right neighbor. The structure (2.11) is just one proposal and admits several degrees of freedom which seem general for such clock-systems.

- Like for step 0, the coherences among canonical states of the ancillas play no role, as ancillas only need to preserve classical information. Therefore it is likely that they can be protected much more efficiently than the data qubits. This also underlies the following points.
- We have written each dissipation operator as a coherent sum of three terms; $M_{k,sp}$ has full rank and thus features no spurious dark states, similarly for the other operators. In principle one could also take e.g. $M_{k,st} = M_{k,st+} + M_{k+1,st-}$, with an additional Hamiltonian to avoid a dark state associated to e.g. $M_{k,st}(|ge\rangle - |eg\rangle)_{k,k+1} = 0$. This would yield a lower number of dissipation channels, but usually engineering a single coherent dissipator is harder than engineering them separately. Conversely, it is equally valid to split each jump operator e.g. $M_{k,sp}$ into three separate jump operators.
- It is not essential at all to have the same rates $\kappa_{...}$ for each k for instance. All that is needed for a synchronized working is that the various transitions summarized under κ_{st} happen at a very fast rate compared to the others. The average time to perform one cycle (2.10) is

[2] Note that even with a unique timer ancilla connected to each data qubit, *exact* GHZ stabilization for large n remains impossible. Indeed, since each dissipation operator would involve bi- or tripartite interactions only, our slightly generalized version of the [29] no-go still applies.

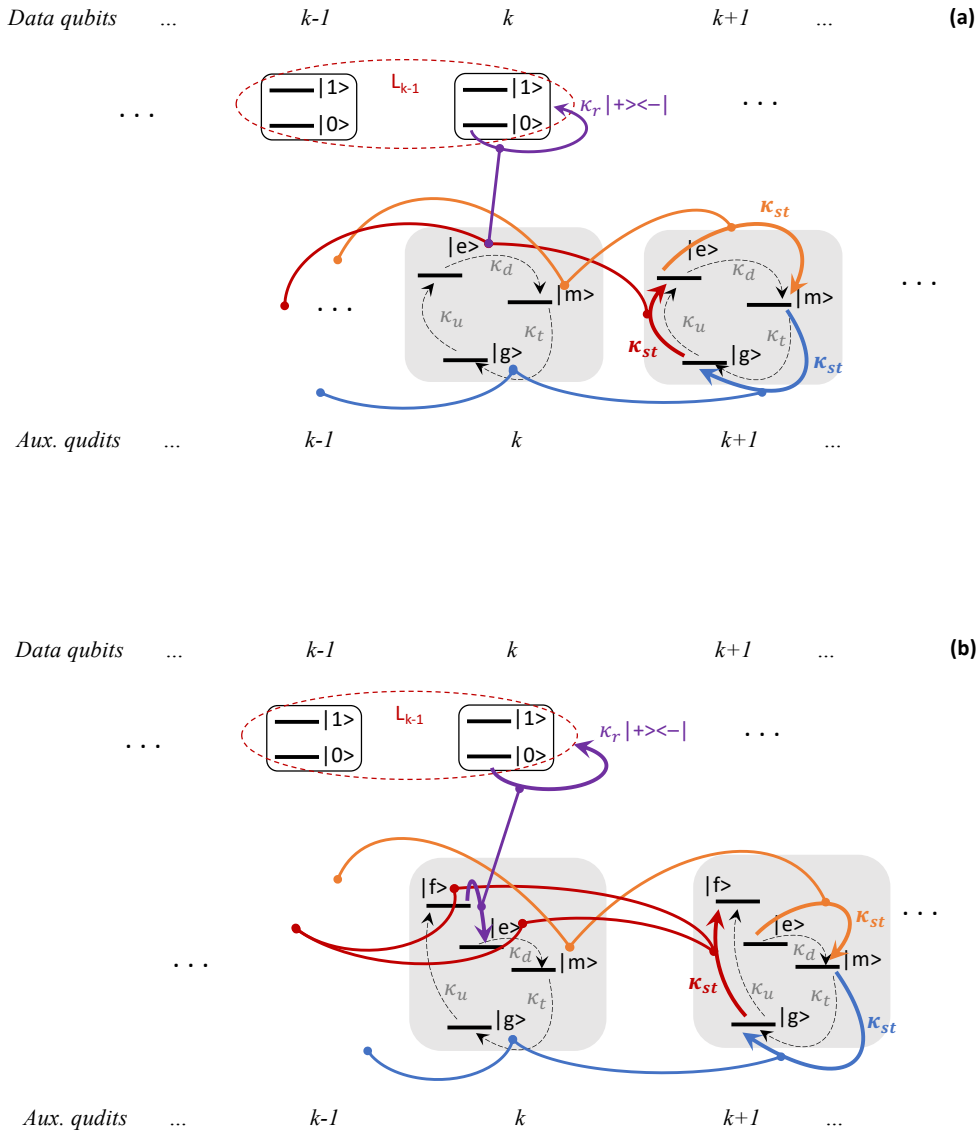

Figure 2.2: Architecture of the correlated ancillas clock inducing synchronized resets of the data qubits to $|+\rangle$. **(a)** Reset with state conditioning (Section 2.2.1): each data qubit applies a fast reset channel while its ancilla is in $|e\rangle$. The spontaneous and neighbor-stimulated ancilla jumps are meant to approximately induce a well-synchronized cycle $|gg...g\rangle \to |ee...e\rangle \to |mm...m\rangle \to |gg...g\rangle \to ...$, with random transition times but little time spent on $|ee...e\rangle$. Each channel only involves pairwise interactions between neighboring subsystems. To avoid clutter, interactions are shown only for a small part of the system. Big dots at arrow end indicate state-conditioning, as is usual in quantum circuits. **(b)** Reset with jump conditioning (Section 2.2.2): each data qubit applies a fast reset when its ancilla jumps to $|e\rangle$. In this architecture involving only pairwise interactions, the ancilla jumps are meant to approximately induce a well-synchronized cycle $|gg...g\rangle \to |\zeta_1\zeta_2...\zeta_N\rangle \to |mm...m\rangle \to |gg...g\rangle \to ...$ where each $\zeta_i \in \{e, f\}$. The additional level $|f\rangle$ could be dropped if tripartite interactions among neighbors were allowed.

then in first approximation given by $(\frac{1}{\sum_k \kappa_{u,k}} + \frac{1}{\sum_k \kappa_{d,k}} + \frac{1}{\sum_k \kappa_{t,k}})$, since each ancilla has a probability to spontaneously launch the transition to the next clock state.

- Note that the channels (2.11) ensure the target behavior for the whole ancilla Hilbert space, not assuming initialization in a suited subspace as was done in the sentence before (2.8).

The engineered reservoir would thus combine (2.11) with the conditional reset (2.9) and the subspace stabilization channels (2.7). The selection of the various rates must ensure, roughly:

1. ancillas behave as an almost synchronized clock: $\kappa_{st} \gg \kappa_d, \kappa_t, \kappa_u$
2. data qubits do a reset with high probability before ancillas leave $|e\rangle$: $\kappa_r \gg \kappa_d$
3. reset dynamics dominates (2.7) when both are applied together: $\kappa_r \gg \kappa_c$
4. resets stop at a well synchronized time with respect to the evolution (2.7) : $\kappa_{st} \gg \kappa_c$.
5. data qubits have ample time to converge with (2.7) after each reset round: $\frac{1}{\kappa_c} \ll (\frac{1}{\kappa_t} + \frac{1}{\kappa_u})$
6. reset periods take up a small fraction of cycle time: $\frac{1}{\kappa_d} \ll (\frac{1}{\kappa_t} + \frac{1}{\kappa_u})$.

Altogether, this suggests the rough timing guidelines:

$$\left\{\frac{1}{\kappa_t}\,,\,\frac{1}{\kappa_u}\right\} \sim T_1 \quad \gg \quad \left\{\frac{1}{\kappa_c}\,,\,\frac{1}{\kappa_d}\right\} \sim T_2 \quad \gg \quad \left\{\frac{1}{\kappa_r}\,,\,\frac{1}{\kappa_{st}}\right\} \sim T_3\,. \tag{2.12}$$

By construction, the scheme gives a limited fidelity even in absence of external perturbations. Fidelity lost due to resets pushing the state away from $|GHZ_+\rangle$ can be roughly estimated as the typical "away from GHZ" portion of a full cycle and should thus be of order $(\frac{1}{\kappa_d} + \frac{1}{\kappa_c})\ /\ (\frac{1}{\kappa_d} + \frac{1}{\kappa_t} + \frac{1}{\kappa_u}) \sim T_2/T_1$. Inaccuracy in resetting to $|+ + ...+\rangle$ should add errors of order $(\frac{\kappa_c}{\kappa_r} + \frac{\kappa_c}{\kappa_{st}} + \frac{\kappa_d}{\kappa_r}) \sim T_3/T_2$. In turn, arbitrary external perturbations with characteristic time T_p will, at worst, be rejected according to the slowest reservoir timescale and thus induce errors of order T_1/T_p. At fixed extremal values T_3 and T_p, the tradeoff between these error contributions will fix the optimal values of T_1 and T_2. Since an improvement by a factor C on T_3/T_p will have to be factored into three timescale separations, we may expect the error to only improve by $C^{1/3}$. A finer performance analysis, with the dependence on n for instance, is provided in Section 3.1.

Remark 2: It may be worth noting that the two fastest rates, involved in T_3, are of a very different nature: while κ_r involves a quantum jump conditioned on an ancilla value, κ_{st} only involves classical synchronization. In this sense, the constraint of fast κ_r can be considered as harder to achieve.

Step 2: possibility to switch the GHZ stabilizers

In the above setup, one might wonder if instead of dominating (2.7) with the reset dynamics when the ancilla is in $|e\rangle$, one could not switch (2.7) off conditioned on ancilla states. This would enable to drop the requirement $\kappa_r \gg \kappa_c$, and by Remark 2, it would possibly enable higher values of κ_c to push the state towards $|GHZ_+\rangle$. We just quickly mention two constructions with the present ancilla-clock architecture to highlight the associated issues. More efficient constructions are presented further below, in particular using data qutrits.

Tripartite: A first possibility would be to admit tripartite interactions, thus directly conditioning each L_k on the state of an associated ancilla. In this way, each ancilla k would be associated to a *pair of adjacent data qubits* $(k, k+1)$, unlike in the previous scheme. This choice also works for the N_k operators. Indeed, we can strictly exclude the possibility to apply L_k and N_k simultaneously on the same data qubit with the following tripartite interactions:

$$\begin{aligned}
\tilde{L}_k &= (|g\rangle\langle g| + |m\rangle\langle m|)_k \otimes L_k \quad \text{for } k = 1, 2, ..., n-1\,, \\
\tilde{N}_k &= \sqrt{\kappa_r}|ee\rangle\langle ee|_{k-1,k} \otimes |+\rangle\langle -|_k \quad \text{for } k = 2, 3, ..., n-1\,, \\
&\quad \tilde{N}_1 = \sqrt{\kappa_r}|e\rangle\langle e|_1 \otimes |+\rangle\langle -|_1\ ,\ \ \tilde{N}_n = \sqrt{\kappa_r}|e\rangle\langle e|_{n-1} \otimes |+\rangle\langle -|_n\,,
\end{aligned}$$

with M_k as in (2.11), L_k as in (2.7). The fidelity lost due to resets pushing the state away from $|GHZ_+\rangle$ is still of order $(\frac{1}{\kappa_c}+\frac{1}{\kappa_d})/T_1$. However, the advantage could be that, as we drop the constraint $\kappa_c \ll \kappa_r$, we can take larger κ_c such that the error is dominated by just $(\frac{1}{\kappa_d})$ / $(\frac{1}{\kappa_d}+\frac{1}{\kappa_t}+\frac{1}{\kappa_u})$. The κ_c which is allowed bigger now, as well as the new κ_r, involve tripartite interactions though.

Bipartite: The stricter requirement of bipartite interactions can be met at the cost of additional levels. An efficient solution using *data qutrits* is presented in Section 2.3. Sticking to data qubits and adding levels to the *ancillas*, we could imagine:

$$\begin{aligned} N_k\ , M_k &\quad \text{as in (2.9),(2.11)} \\ \tilde{L}_{1,k}/\sqrt{\kappa_{cr}} &= |m_1\rangle\langle m|_{k+1}|0\rangle\langle 0|_k + |m_2\rangle\langle m|_{k+1}|1\rangle\langle 1|_k + |g_1\rangle\langle g|_{k+1}|0\rangle\langle 0|_k + |g_2\rangle\langle g|_{k+1}|1\rangle\langle 1|_k \\ \tilde{L}_{2,k}/\sqrt{\kappa_{ch}} &= |m,0\rangle\langle m_1,1|_k + |m,1\rangle\langle m_2,0|_k + |g,0\rangle\langle g_1,1|_k + |g,1\rangle\langle g_2,0|_k \\ \tilde{L}_{3,k}/\sqrt{\kappa_{ch}} &= |m,0\rangle\langle m_1,0|_k + |m,1\rangle\langle m_2,1|_k + |g,0\rangle\langle g_1,0|_k + |g,1\rangle\langle g_2,1|_k\ . \end{aligned}$$

The only principle here is to have no action of L_k when the ancilla is on $|e\rangle$. The conditioning on $|g\rangle$ or $|m\rangle$ then requires to split the action of L_k into two parts. Therefore the new levels m_1, m_2 (or g_1, g_2) of the ancilla serve to transmit the levels $0, 1$ of data qubit k to its neighbor $k+1$. This transmission will induce an additional "downtime" of order $\frac{\kappa_{cr}}{\kappa_{ch}}$ during which the data are entangled with the ancilla. Moreover, the quantum coherence between those ancilla states must now be protected. Both effects are kept in check as the transition through those states is supposed to be fast. Nevertheless, this does not appear too practical.

The expected benefit of switching off the L_k was to allow taking larger κ_c, irrespective of κ_r. With the above construction, and assuming that κ_{st} acting on classical degrees of freedom of the ancillas constitutes no limitation, we can indeed take large κ_{ch}. However, we must now take κ_{cr} an order of magnitude lower, and the latter will dominate the convergence rate associated to the effective L_k dissipation channel.

In both the tripartite and bipartite schemes, adding more levels would enable to insert short timeouts between applying (2.7) and applying resets $|+\rangle\langle -|$. Such timeouts could for instance cover the limited synchronization of the ancillas, trading off increased accuracy for an additional downtime before converging back towards $|GHZ_+\rangle$. However, we want to stop adding further complexity into the reservoirs now and consider different architectures.

2.2.2 Engineering the approximate GHZ reservoir through ancilla jump conditioning

We now describe a setup where the data qubits undergo operations conditioned not on the ancilla *being in* a given state, but rather on the ancilla *jumping to* a state. We discuss how such resets appear to promise better performance than Section 2.2.1 for finite timescale separations.

In our first constructions, we assume like previously that (2.7) always remains on the conditioning thus just affects the $|+\rangle\langle -|$ resets. In Step 2 we mention issues with constructions where also (2.7) would involve jump-conditioning.

To ensure that ancillas keep jumping independently of the data state, we have to add in parallel to the "useful data jump operator", the same ancilla evolution but with "idle" data. This can probably be revised at places, but we prefer to make this choice systematically in order to simplify the system dynamics: like previously, the evolution of the ancillas in our schemes is not influenced by the data state.

Step 0: resets at ancilla jumps

The main idea is to make the data qubit reset instantaneously when the ancilla *jumps to* $|e\rangle$, with channels like:

$$\begin{aligned} M_k &= \sqrt{\kappa_d}|g\rangle\langle e|_k\ , \quad N_{k,1} = \sqrt{\kappa_u}|e,+\rangle\langle g,+|_k\ , \quad N_{k,2} = \sqrt{\kappa_u}|e,+\rangle\langle g,-|_k\ , \qquad (2.13) \\ L_k &\quad \text{as in (2.7)}\ . \end{aligned}$$

The separation of channels $N_{k,1}$ and $N_{k,2}$ is needed to avoid a dark state, or we could take $N_k = N_{k,1} + N_{k,2}$ plus a Hamiltonian breaking the dark state.

The remaining issue, like with the previous architecture, is to synchronize the jumps of all the ancillas. In fact this issue becomes even more essential with "jump-conditioning". Indeed, even in an approach like [33] where a single ancilla is assumed to be connected to all the data qubits, we cannot apply (2.13) verbatim: either, assuming n jump operators, the ancilla will reset just a single data qubit at random; or, assuming a single jump operator, it would now involve all the $n+1$ subsystems at once.

Associating again one ancilla per data qubit, a synchronized jumping can be implemented as follows.

Step 1: correlating the ancilla jumps

The idea is the same as in Section 2.2.1, namely to induce an ancilla clock cycling essentially through

$$|gg...g\rangle \to |ee...e\rangle \to |mm...m\rangle \to |gg...g\rangle \to ...$$

thanks to a large κ_{st}. However, as soon as an ancilla jumps to $|e\rangle$, the associated data qubit jumps to $|+\rangle$. Again various constructions are possible and we just list two, illustrated on Figure 2.2 (b), before commenting on their properties.

Tripartite: Correlating a *stimulated* ancilla jump with a data jump requires, a priori, tripartite interaction. Admitting such operators, we could propose a reservoir like:

$$\begin{aligned}
L_k \quad & \text{as in (2.7)} \\
N_{k,spr} &= \sqrt{\kappa_u}|e+\rangle\langle g-|_k \quad , \quad N_{k,spi} = \sqrt{\kappa_u}|e+\rangle\langle g+|_k \\
M_{k,sp} &= \sqrt{\kappa_d}|m\rangle\langle e|_k + \sqrt{\kappa_t}|g\rangle\langle m|_k \\
N_{k,st+r} &= \sqrt{\kappa_{st}}\,|e\rangle\langle e|_k\,|e+\rangle\langle g-|_{k+1} \quad , \quad N_{k,st+i} = \sqrt{\kappa_{st}}\,|e\rangle\langle e|_k\,|e+\rangle\langle g+|_{k+1} \\
M_{k,st+} &= \sqrt{\kappa_{st}}\,(|mm\rangle\langle em|_{k,k+1} + |gg\rangle\langle mg|_{k,k+1}) \\
N_{k,st-r} &= \sqrt{\kappa_{st}}\,|e+\rangle\langle g-|_k\,|e\rangle\langle e|_{k+1} \quad , \quad N_{k,st-i} = \sqrt{\kappa_{st}}\,|e+\rangle\langle g+|_k\,|e\rangle\langle e|_{k+1} \\
M_{k,st-} &= \sqrt{\kappa_{st}}\,(|mm\rangle\langle me|_{k,k+1} + |gg\rangle\langle gm|_{k,k+1})\ .
\end{aligned}$$

The indices $_r$ and $_i$ stand for reset and idle on data, $_+$ and $_-$ denote left or right neighbor conditioning, while $_{sp}$ and $_{st}$ distinguish spontaneous or neighbor-stimulated processes.

Bipartite: The above scheme can be adapted to bi-partite interactions by adding a fourth ancilla level $|f\rangle$, such that each ancilla would transition from $|g\rangle$ to $|f\rangle$ and then only to $|e\rangle$. The idea is that the reset of the associated data qubit happens during the very fast *spontaneous* ancilla jump from $|f\rangle$ towards $|e\rangle$, thus involving only a bipartite interaction. Meanwhile, to keep essentially the same clock behavior, an ancilla in $|g\rangle$ gets attracted to $|f\rangle$ as soon as one of its neighbors is *in* $|f\rangle$ *or in* $|e\rangle$.

Explicitly, the associated channels could be:

$$\begin{aligned}
L_k \quad & \text{as in (2.7)} \\
M_{k,sp} &= \sqrt{\kappa_u}|f\rangle\langle g|_k + \sqrt{\kappa_d}|m\rangle\langle e|_k + \sqrt{\kappa_t}|g\rangle\langle m|_k \\
N_{k,r} &= \sqrt{\kappa_f}|e,+\rangle\langle f,-|_k \quad , \quad N_{k,i} = \sqrt{\kappa_f}|e,+\rangle\langle f,+|_k \\
M_{k,st1+} &= \sqrt{\kappa_{st}}\,(|ff\rangle\langle gf| + |mm\rangle\langle em| + |gg\rangle\langle mg|)_{k,k+1} \quad , \quad M_{k,st2+} = \sqrt{\kappa_{st}}\,|fe\rangle\langle ge|_{k,k+1} \\
M_{k,st1-} &= \sqrt{\kappa_{st}}\,(|ff\rangle\langle fg| + |mm\rangle\langle me| + |gg\rangle\langle gm|)_{k-1,k} \quad , \quad M_{k,st2-} = \sqrt{\kappa_{st}}\,|ef\rangle\langle eg|_{k-1,k}\ ,
\end{aligned} \tag{2.14}$$

for each $k = 2, 3, ..., n-1$, and one of the last two channels dropping for $k = 1$ and $k = n$. Indices $_1$ and $_2$ distinguish stimulated excitation to $|f\rangle$ when a neighbor is in $|f\rangle$ or in $|e\rangle$.

Except for the rates, discussed below, the schemes' properties are similar to those of Section 2.2.1.

- No quantum coherence at all needs to be protected among ancilla levels: they only need to be correlated classical Dits.
- The dissipation channels are partly split into several channels to avoid dark states, but a linear combination of e.g. $M_{k,sp}, N_{k,r}, N_{k,i}$ associated to a Hamiltonian can have the same effect, if this appears less difficult for implementation.
- Conversely, coherences in the channel operators are not essential (except of course in L_k) and one might as well separate them into more channels. Dissipation rates need not be equal for every k, just their order of magnitude matters.
- The above constructions are meant to facilitate analysis, thanks to ancilla dynamics not being influenced by the data state.

Regarding the choice of dissipation rates, let us comment on the bi-partite scheme for a fairer comparison with Section 2.2.1. We must have, roughly (see finer analysis later):

1. ancillas behave as an almost synchronized clock: $\kappa_{st} \gg \kappa_d, \kappa_t, \kappa_u$
2. transition through $|f\rangle$ maintains clock synchronization on $|e\rangle$: $(\frac{1}{\kappa_{st}} + \frac{1}{\kappa_f}) \ll \frac{1}{\kappa_d}$
3. at a reset, (2.7) has little time to act until all qubits have reset: $(\frac{1}{\kappa_{st}} + \frac{1}{\kappa_f}) \ll \frac{1}{\kappa_c}$
4. data qubits have ample time to converge with (2.7) after each reset round: $\frac{1}{\kappa_c} \ll (\frac{1}{\kappa_d} + \frac{1}{\kappa_t} + \frac{1}{\kappa_u})$.

Altogether, this yields the rough timing guidelines:

$$\left\{\frac{1}{\kappa_d}\,,\ \frac{1}{\kappa_t}\,,\ \frac{1}{\kappa_u}\right\} \sim T_1 \quad \gg \quad \frac{1}{\kappa_c} \sim T_2 \quad \gg \quad \left\{\frac{1}{\kappa_f}\,,\ \frac{1}{\kappa_{st}}\right\} \sim T_3\,. \tag{2.15}$$

The fidelity lost due to resets pushing the state away from $|GHZ_+\rangle$ is now dominated by $\frac{1}{\kappa_c}/(\frac{1}{\kappa_d} + \frac{1}{\kappa_t} + \frac{1}{\kappa_u}) \sim T_2/T_1$, while the inaccuracy in resetting to $|{+}{+}...{+}\rangle$ adds an error of order $(\frac{\kappa_c}{\kappa_f} + \frac{\kappa_c}{\kappa_{st}}) \sim T_3/T_2$. Although we do not win an order of magnitude, these are still less error terms than in Section 2.2.1, at the cost of an additional ancilla level. In fact, compared to Section 2.2.1, here κ_f somewhat replaces κ_r, but with fewer constraints. Indeed here, no further data resets happen once every ancilla has jumped to $|e\rangle$. Therefore, tightly synchronizing this jump automatically implies a short reset period and a good reset effect despite the presence of κ_c.

Step 2: jumping with the GHZ stabilizers

Like in Section 2.2.1, we cannot take κ_c too large in the above scheme, because else the L_k would have significant (and deteriorating) effect before all qubits have been reset synchronously. To circumvent this limitation, it may be tempting to apply the L_k conditionally on ancilla states. In fact, in the present jump-conditioning context, it may even appear more natural to condition the application of L_k on ancilla *jumps*.

This warrants two points of attention.

1. Since the L_k preserve the GHZ state, it is a priori beneficial to apply them as often as possible. Indeed, while the lowest rate of protection will be dominated by the characteristic time T_1 for phase-flip corrections, the L_k alone are sufficient for correcting bit-flip errors on the data qubits. Having a faster bit-flip correction could be beneficial, in particular considering the existence of physical systems implementing biased noise qubits [21] where phase flips are much less likely than bit-flips. Since conditioning the application of L_k on e.g. an ancilla jump from $|e\rangle$ to $|m\rangle$ makes the bit-flip correction as slow as T_1, one should in turn identify a clear benefit before considering such operation.
2. When conditioning L_k on ancilla *jumps*, the parameter κ_c drops out. However, this does not mean that T_2 can be readily disposed of with respect to (2.15). Indeed, right after having applied a reset jump $N_{k,r}$, the qubit k has to wait, in order to ensure that all other qubits have likely reset too, before applying its L_k jump; this implies a waiting time of order

$T_2' \gg T_3$. In turn, this waiting time means that the system would spend a typical fraction T_2'/T_1 of its time waiting on "reset" states rather than on the GHZ target. With these two elements, T_2' plays a role very similar to T_2 and we still have the same number of timescales.

The attentive reader may find this analysis with waiting times too pessimistic. The next section will explain indeed how to circumvent this drawback.

2.2.3 Engineering a spatio-temporal GHZ wave reservoir

Until now, we have considered that the L_k, M_k, N_k for various k are applied in random succession. However, the chain topology suggests another, more organized possibility.

First, performance is wasted by letting the ancillas clock evolve independently of data qubit operations. Indeed, this requires the ancillas to wait until the required data operations have been performed very likely, before moving to the next clock step. If instead the data qubits could signal when their operations are done, then the clock could move forward without further waiting.

Second, it matters in which order a given operation is applied along the chain. Indeed, note that L_k assigns to data qubit $k+1$ the logical value of data qubit k. Hence, starting from $|++...+\rangle$ on the data and applying each jump operator L_k once, in a random order, would be insufficient for stabilizing the GHZ state. However, applying the L_k once in increasing order from $k = 1$ to $k = n - 1$, would result in the target GHZ state. We may thus want to favor such a "wave" process, both in the L_k and in the ancillas clock inducing resets.

These observations lead to proposing schemes with two specific adaptations. First, only the extremal ancilla 1 undergoes spontaneous jumps to trigger the clock evolution. The other ancillas will follow, through stimulated jumps, in the order of the chain. Note that in the proposals of Section 2.2.1 and Section 2.2.2, the clock transition to the next level was also propagating along the chain, but there was no particular place for the wave to start, so parts of it could propagate in a direction opposite to the natural direction implied by the L_k. Second, the reservoir will contain a mechanism to apply the L_k in increasing order of k, instead of in random order as in the previous schemes. Overall, this should allow a better coordination between the two processes and hence result in increased overall fidelity with $|GHZ_+\rangle$. The benefits of this spatio-temporal organization are expected to increase with chain length n.

Again, many variations are possible and we just propose a few.

Tripartite interaction with two timescales

When allowing tripartite interaction, it is possible to design relatively powerful wave-inspired reservoirs based on just two different timescales. This expressly hinges on the observation that both $|+\rangle\langle-|$ and L_k just have to be applied in order from lowest to highest data index k. We start with a scheme whose logic is very simple to follow. We then propose a second scheme which appears both more powerful and simpler in terms of resources. In both constructions, we assign one ancilla k to each *pair* of consecutive data qubits $(k, k+1)$.

Tripartite, jump-conditioning: Each operation on data is triggered by an ancilla jump. We use ancillas with 4 levels, like in the jump-conditioning process of Section 2.2.2. The idea is entirely sequential: wait for a long time on $|GHZ_+\rangle$ (in absence of perturbations), before launching the following jump sequence which should end up in $|GHZ_+\rangle$ as fast as possible:

$$\begin{array}{lll} \text{reset qubit 1 with } |+\rangle\langle-| \text{ ;} & \text{reset qubit 2 with } |+\rangle\langle-|; & \text{apply } L_1 \text{ ;} \\ & \text{reset qubit 3 with } |+\rangle\langle-| \text{ ;} & \text{apply } L_2 \text{ ;} \\ ...; & \text{reset qubit } k+1 \text{ with } |+\rangle\langle-| \text{ ;} & \text{apply } L_k \text{ ;...} \end{array} \tag{2.16}$$

Thanks to commutation of operators on distinct subsystems, this sequence is indeed strictly equivalent to applying first $|+\rangle\langle-|$ on each data qubit, then the L_k in the favorable order from $k = 1$ to $k = n - 1$. Yet it avoids waiting until all resets have been done, before launching the sequence

of L_k; this is both more efficient and easier to implement locally. This sequence of events could be implemented with an "ancilla automaton" using the following operators:

$$\begin{aligned}
N_{1,r12} &= \sqrt{\kappa_u}|e,+,+\rangle\langle g,-,-|_{1,1,2} \quad , \quad N_{1,r1} = \sqrt{\kappa_u}|e,+,+\rangle\langle g,-,+|_{1,1,2} \\
N_{1,r2} &= \sqrt{\kappa_u}|e,+,+\rangle\langle g,+,-|_{1,1,2} \quad , \quad N_{1,i} = \sqrt{\kappa_u}|e,+,+\rangle\langle g,+,+|_{1,1,2} \\
N_{k,r} &= \sqrt{\kappa_{st}}|e,+\rangle\langle f,-|_{k,k+1} \quad , \quad N_{k,i} = \sqrt{\kappa_{st}}|e,+\rangle\langle f,+|_{k,k+1} \quad \text{for } k = 2,3,...,n-1 \\
M_k &= \sqrt{\kappa_{st}}|g,f\rangle\langle m,g|_{k,k+1} \quad \text{for } k = 1,2,...,n-2 \\
\tilde{L}_{k,r} &= \sqrt{\kappa_c}|m\rangle\langle e|_k \otimes (|11\rangle\langle 10| + |00\rangle\langle 01|)_{k,k+1} \quad , \\
&\quad \tilde{L}_{k,i} = \sqrt{\kappa_c}|m\rangle\langle e|_k \otimes (|11\rangle\langle 11| + |00\rangle\langle 00|)_{k,k+1} \quad \text{for } k = 1,2,...,n-2 \\
\tilde{L}_{n-1,r} &= \sqrt{\kappa_c}|g\rangle\langle e|_{n-1} \otimes (|11\rangle\langle 10| + |00\rangle\langle 01|)_{n-1,n} \quad , \\
&\quad \tilde{L}_{n-1,i} = \sqrt{\kappa_c}|g\rangle\langle e|_{n-1} \otimes (|11\rangle\langle 11| + |00\rangle\langle 00|)_{n-1,n} \, .
\end{aligned} \tag{2.17}$$

Starting with ancillas in $|g,g,...,g\rangle$, the sequence is launched by one of the $N_{1,...}$: as ancilla 1 jumps to $|e\rangle$ it resets data qubits 1 and 2 towards $|{+}{+}\rangle$. Then the $\tilde{L}_{1,...}$ can act, so ancilla 1 jumps to $|m\rangle$ while applying L_1 on the data or, projecting onto the subspace on which L_1 had to act idle. Ancilla 1 finally jumps to $|g\rangle$ under the action of M_1, while kicking ancilla 2 towards level $|f\rangle$. This triggers the reset of data qubit 3 towards $|+\rangle$ while ancilla 2 jumps to $|e\rangle$, and so on. Remarks on some details:

- For each intended ancilla transition, several operators are needed in order to avoid dark states from the associated data evolution. This concerns in particular the presence of both $\tilde{L}_{k,r}$ and $\tilde{L}_{k,i}$. One easily checks that $\tilde{L}_{k,i}$ as well preserves the eigenstates of $\sigma_x^{\otimes n}$, as is required to stabilize a well-defined superposition of $|00...0\rangle$ and $|11...1\rangle$ whit this scheme.
- The ancilla level $|f\rangle$ is introduced just to avoid having ancilla $k-1$, ancilla k and data qubit $k+1$ in a single operator. Indeed, although each of the operators would remain just tripartite in absence of $|f\rangle$, together they would require ancilla $k-1$ to have connections to data qubits $k-1$, k, and $k+1$. This would possibly imply a significantly harder layout. If such a connection is available, then the level $|f\rangle$ could be skipped; in this case, the M_k and $N_{k+1,...}$ for $k \geq 1$ could be merged, so the $N_{k,...}$ would remain only for $k = 1$ to launch a clock cycle.
- The last ancilla $n-1$ needs to trigger no neighbor and thus skips the state $|m\rangle$ entirely.
- Like for the other constructions, the ancillas only encode classical information on their levels.

With this strategy, the next operation at site k is triggered as soon as site $k-1$ has finished, circumventing the inefficient waiting times. Hence, the reservoir just relies on taking

$$\kappa_c, \kappa_{st} \gg \kappa_u \, , \tag{2.18}$$

while κ_u should dominate the typical perturbation characteristic rate $1/T_p$. Thanks to the sequential construction, we need one less timescale separation compared to the previous sections.

Tripartite, ancilla qubits: While the "automaton" reservoir implementing (2.16) is easy to comprehend, it is not the most efficient one. In particular, the data qubits could keep applying the L_k as described in (2.7) more often, namely as soon as they are not resetting. Besides the potential benefits for bit-flip corrections, this allows significant simplification of the conditioning, reducing the ancillas to qubits ($D = 2$). The following reservoir works in this sense:

$$\begin{aligned}
N_{1,r} &= \sqrt{\kappa_u}|e,+,\rangle\langle g,-|_{1,1} \quad , \quad N_{1,i} = \sqrt{\kappa_u}|e,+\rangle\langle g,+|_{1,1} \\
N_{k,r} &= \sqrt{\kappa_{st}}|g,e,+\rangle\langle e,g,-|_{k-1,k,k} \quad , \quad N_{k,i} = \sqrt{\kappa_{st}}|g,e,+\rangle\langle e,g,+|_{k-1,k,k} \\
N_{k,v} &= \sqrt{\kappa_{st}}|g,e\rangle\langle e,e|_{k-1,k} \qquad \text{for } k = 2,3,...,n-1 \\
\tilde{L}_k &= \sqrt{\kappa_c}|g\rangle\langle g|_k \otimes (|11\rangle\langle 10| + |00\rangle\langle 01|)_{k,k+1} \, .
\end{aligned} \tag{2.19}$$

The key idea is to switch off L_k as soon as a reset is performed on data qubit k, and to switch it back on once the reset has been done on qubit $k+1$ too. Thus, when the $N_{1,...}$ launch a reset

cycle, they reset qubit 1 and switch off $\tilde{L}_1$ by putting the first ancilla into $|e\rangle$. Next, $N_{2,r}$ performs a reset on qubit 2, while at the same time the exchange $|g,e\rangle\langle e,g|_{1,2}$ switches back on $\tilde{L}_1$ and switches off $\tilde{L}_2$; and so on.

Compared to the previous scheme, (2.19) is thus (possibly) applying the L_k more frequently and repeatedly: (i) while the preceding data qubits are resetting, (ii) while the following data qubits are resetting and (iii) while other qubits are applying their L_j. Point (i) has no impact since at this time we are away from GHZ anyway, and the soon-to-happen reset on data qubits $\geq k$ makes their current state (with or without L_k applied) irrelevant. Point (ii) is not detrimental since L_k commutes with all the remaining resets, so all its actions can equivalently be seen as happening after all resets have been completed; with the preceding scheme we used the same argument, but mentioning a single jump with each L_k. Finally, point (iii) is fine because starting from $|+ + ...+\rangle$ (by the argument for point (ii)), convergence towards $|GHZ_+\rangle$ is ensured by applying the *subsequence* $L_1, L_2, ..., L_{n-1}$, irrespective of which other L_j the full sequence may contain.

We have the same remarks as for the other constructions:

- Several operators avoid dark states. In particular, the role of the $N_{k,v}$ is just to ensure global convergence of the ancilla reservoir, i.e. avoiding getting stuck if by chance several ancillas were in $|e\rangle$; we do not care about the associated data action since this situation should nominally never happen.
- The ancillas only encode classical information on their levels.

The rates still just have to satisfy

$$\kappa_c, \kappa_{st} \gg \kappa_u$$

for good performance. The construction (2.19) thus remains essentially as fast as (2.17), while using only two-level ancillas and applying the L_k more continuously.

Bipartite interaction

We now address the construction of a scheme with bipartite interactions only. Since conditioning L_k on an ancilla would necessarily imply tri-partite interaction, we face the same options as in the non-wave constructions:

(i) Either leave the L_k on all the time, like in e.g. Section 2.2.1, while applying the resets in a wave. This implies small fidelity losses associated to applying L_k while data qubit k has reset to $|+\rangle$ and data qubit $k+1$ still has to.

(ii) Or, separate the L_k operator in two steps, like in e.g. Section 2.2.1. This allows to switch off L_k, but between these two steps it adds a downtime, during which moreover the ancillas must maintain quantum coherences.

Since a scheme of type (ii) appears not too practical, we briefly describe a scheme of type (i). A more efficient scheme with L_k switch-off and bipartite interactions is proposed below when working with data qutrits ($Q = 3$).

Associating one ancilla qutrit to each data qubit ($Q = 2$, $D = 3$, $m = n$), we can propose the following reservoir where the resets to $|+\rangle$ follow a wave:

$$\begin{array}{rcl} L_k & & \text{as in (2.7)} \\ M_1 & = & \sqrt{\kappa_u}|e\rangle\langle g| \\ M_{k,r} & = & \sqrt{\kappa_{st}}|g,e\rangle\langle m,g|_{k-1,k} \quad , \quad M_{k,i} = \sqrt{\kappa_{st}}|g,e\rangle\langle m,m|_{k-1,k} \ , \\ & & M_{k,v} = \sqrt{\kappa_{st}}|g,e\rangle\langle m,e|_{k-1,k} \quad , \quad \text{for } k = 2,3,...,n \\ N_{k,r} & = & \sqrt{\kappa_{st}}|m,+\rangle\langle e,-|_{k,k} \quad , \quad N_{k,i} = \sqrt{\kappa_{st}}|m,+\rangle\langle e,+|_{k,k} \text{ for } k = 1,2,...,n \ . \end{array} \tag{2.20}$$

The nominal operator sequence for the resets would be M_1; $N_{1,r}$ or $N_{1,i}$; $M_{2,r}$; $N_{2,r}$ or $N_{2,i}$; ... , while the L_k have a (smaller) probability to act at any time. Details are similar to the other schemes, among others:

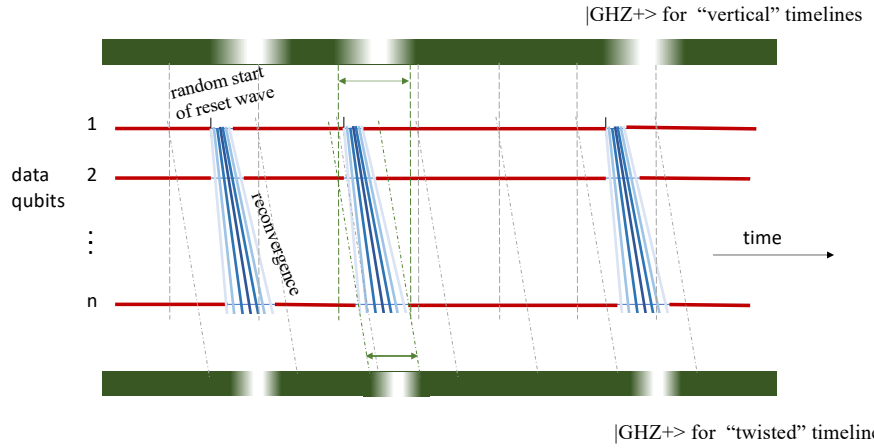

Figure 2.3: Arguing for a fidelity benefit when the wave-stabilized GHZ state is used in spatio-temporal order in an application. In an unraveling of our reservoir(s) with stochastic jump trajectories, an initial GHZ state $|GHZ_+\rangle$ remains unperturbed (100% fidelity, dark green) until a sequence of $|+\rangle\langle-|$ resets is triggered by ancilla 1. The fidelity to GHZ drops to a very low value (white) as soon as one of the data qubits has reset and until the last qubit has applied its $|+\rangle\langle-|$ and L_k. Taking fidelity of the state in standard "vertically synchronized" time for all qubits (top colorbar), we spend a significant time at low fidelity with just few qubits out of order. If one could rather use the state in sequential order from data qubit 1 to n, with "tilted time" (bottom axis), then this could *correlate* the times at which the qubits are out of order: ideally, they are either all out of order, or all good. This correlation reduces the portion of a cycle during which the GHZ state would be considered bad (green arrows).

- The two operators $N_{k,\dots}$ ensure a reset to $|+\rangle_k$ whatever the associated data qubit state. The $M_{k,\{i,v\}}$, not mentioned in the nominal sequence, are added to avoid getting stuck at non-nominal ancilla states. An exception to this is ancilla $k = n$, which would remain stuck in $|m\rangle$ as it excites no next neighbor, and thus nominally applies $M_{k,i}$; an alternative would be to reduce this last ancilla to a qubit.
- Ancillas only encode classical information.

Compared to the tripartite coupling schemes, fidelity is lost when an L_k jump occurs between applying $N_{k,\dots}$ and $N_{k+1,\dots}$ in this sequence. Making this event unlikely requires to re-instate a separation of timescales for good reservoir operation:

$$\kappa_{st} \gg \kappa_c \gg \kappa_u \ .$$

A benefit still of observing the wave property is that this intermediate timescale will involve no n-dependence: after $N_{k,\dots}$, we just have to wait for $N_{k+1,\dots}$ to happen, not for all resets to complete.

On evaluating GHZ fidelity as a wave too

It appears that the spatio-temporal wave might be beneficial not only for generating the GHZ state, but also possibly when using it. That is to say, if e.g. a quantum computing operation taking the GHZ state as input could also first act on the low-index qubits and proceed along the chain, then it may be possible to keep running the wave stabilizing the high-index GHZ qubits, while the low-index qubits are already used by the application. Given the wave-like stabilization procedure, one might hope that the *effective fidelity* for such use of the GHZ state could be higher than when just considering the state at a fixed time for all data qubits. See Figure 2.3 for a graphical explanation. Of course this opportunity heavily depends on the intended application of the GHZ state.

2.3 Architectures with data qutrits

We now turn towards a completely different way of enlarging the Hilbert space. Indeed, we will consider the *data* subsystems to be qutrits ($Q = 3$). Their logical space of interest is still the subspace span$\{|0\rangle, |1\rangle\}$ and we still target the same state $|GHZ_+\rangle = (|00...0\rangle + |11...1\rangle) \,/\, \sqrt{2}$, but the auxiliary levels $|2\rangle$ are now used for reservoir operation.

As a first approach, data qutrits could be combined with ancillas, and all the constructions of the previous section could be revised, trying to simplify the operation thanks to the auxiliary levels $|2\rangle_k$. However, the presence of level $|2\rangle$ even makes the ancillas unnecessary. We here describe two constructions which we deem particularly telling with this architecture, i.e. without using any ancillas. In both of them, level $|2\rangle$ serves both to switch between L_k and $|+\rangle\langle -|$ operators, and to synchronize those switchings. Although everything acts on data qutrits now, we keep using the decoherence operator letters L_k, M_k, N_k to suggest similar roles to those with ancillas.

2.3.1 Random order resets

Our first construction sticks to the viewpoint of Sections 2.2.1 and 2.2.2, where resets with $|+\rangle\langle -|$ can be launched at arbitrary places along the data chain. More precisely, we propose a construction with *bipartite* interactions, yet switching off the L_k during resets in the spirit of Sections 2.2.1 and 2.2.2.

Consider an engineered reservoir with the following operators:

$$\begin{aligned} L_k &\quad \text{as in (2.7)} \\ M_{k,spr} &= \sqrt{\kappa_u}|2\rangle\langle +| \quad , \quad M_{k,spi} = \sqrt{\kappa_u}|2\rangle\langle -| \\ M_{k,st+r} &= \sqrt{\kappa_{st}}|22\rangle\langle 2+|_{k,k+1} \quad , \quad M_{k,st+i} = \sqrt{\kappa_{st}}|22\rangle\langle 2-|_{k,k+1} \\ M_{k,st-r} &= \sqrt{\kappa_{st}}|22\rangle\langle +2|_{k-1,k} \quad , \quad M_{k,st-i} = \sqrt{\kappa_{st}}|22\rangle\langle -2|_{k-1,k} \\ N_k &= \sqrt{\kappa_d}|+\rangle\langle 2| \,. \end{aligned} \tag{2.21}$$

To understand its operation, assume a stochastic jump unraveling starting on $|GHZ_+\rangle$. The state stays there until, through $M_{k,sp...}$, some qutrit k gets excited to $|2\rangle$. This instantaneously switches off the L_k associated to this qutrit, since they only act on its subspace span$\{|0\rangle, |1\rangle\}$. Furthermore, taking κ_{st} large, qutrit k now quickly stimulates all other qutrits into their state $|2\rangle$ through the $M_{k,st...}$, thus switching off all the L_k. From there, the qutrits relax individually towards $|+\rangle$ with N_k at a rate κ_d. Note that an operator L_k will only start acting again once *both* associated qubits have reset from $|2\rangle$ to $|+\rangle$; the latter means that no further operation will be done on those qubits other than the L_k, until the next reset cycle is launched. This ensures efficient separation between the actions of L_k and of $|+\rangle\langle -|$, for proper choices of the rates (see below). The reader may want to note the following details similar to the ancilla-based reservoirs.

- The values of the rates could vary as a function of k, only their orders of magnitude matter.
- The $M_{k,...}$ operators are split in order to ensure possible excitation to $|2\rangle$ for any initial qutrit state, avoiding any dark states within the subspace span$\{|0\rangle, |1\rangle\}$.
- While there are no classical ancillas anymore, it remains true that the quantum phase associated to the auxiliary *level* $|2\rangle$ of any qutrit(s) is unimportant; indeed, now this level plays a role somehow equivalent to classical conditioning. In other words, a qutrit will never have to be in a coherent superposition of $|2\rangle$ with some other levels.

The selection of the various rates must ensure:

1. qutrits are stimulated to $|2\rangle$ before their neighbor resets down: $\kappa_{st} \gg \kappa_d$
2. qutrits have ample time to reset down to $|+\rangle$ and converge with the L_k of (2.7) before the next spontaneous excitation to $|2\rangle$ takes place: $(\frac{1}{\kappa_d} + \frac{1}{\kappa_c}) \ll \frac{1}{\kappa_u}$.

Thanks to the qutrit architecture, no other constraints seem necessary. In particular, as actions on different parts of the chain commute and the qutrit logic allows such strict separation, it is not

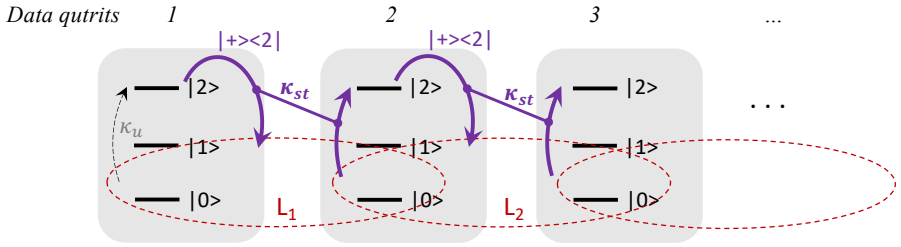

Figure 2.4: Illustration of the dynamics behind the scheme for stabilizing approximately $|GHZ_+\rangle$ using a chain of data qutrits, according to the Lindblad operators described by (2.23).

essential that all the resets have been done (likely) before the L_k start to act: the synchronization of resets must just be measured with respect to a full stabilization cycle, to avoid a too long time away from target. We thus have the rough timing guidelines:

$$\frac{1}{\kappa_u} \sim T_1 \quad \gg \frac{1}{\kappa_d} \sim T_2 \quad \gg \quad \left\{ \frac{1}{\kappa_c} \, , \, \frac{1}{\kappa_{st}} \right\} \sim T_3 \, . \tag{2.22}$$

This still involves three timescales. The advantage compared to e.g. Section 2.2.1 is that here κ_c can be taken large, independently of the other rates. Therefore, the fidelity loss due to resets pushing the state away from $|GHZ_+\rangle$ is dominated by just $(\frac{1}{\kappa_d})$ / $(\frac{1}{\kappa_d} + \frac{1}{\kappa_u})$, the contribution of κ_c being of a lower order. A better performance though can be obtained by combining the qutrit operation with a wave strategy.

2.3.2 A GHZ wave with data qutrits only

Our second construction uses qutrits in a GHZ-stabilizing wave, in the same spirit as Section 2.2.3. The idea, as illustrated on Figure 2.4 is just that the jump down from $|2\rangle$ on data qutrit k triggers the reset on data qutrit $k+1$. Explicitly, the following reservoir operators would do the job:

$$\begin{array}{rcl} L_k & & \text{as in (2.7)} \\ M_{0,r} & = & \sqrt{\kappa_u}|2\rangle\langle -| \quad , \quad M_{0,i} = \sqrt{\kappa_u}|2\rangle\langle +| \\ N_{k,r} & = & \sqrt{\kappa_{st}}|+,2\rangle\langle 2,-|_{k,k+1} \quad , \quad N_{k,i} = \sqrt{\kappa_{st}}|+,2\rangle\langle 2,+|_{k,k+1} \, , \\ & & N_{k,v} = \sqrt{\kappa_{st}}|+,2\rangle\langle 2,2|_{k,k+1} \quad , \quad \text{for } k = 1,2,...,n-1 \\ N_n & = & \sqrt{\kappa_{st}}|+\rangle\langle 2|_n \, . \end{array} \tag{2.23}$$

The intended evolution is to launch a wave by exciting qutrit 1 to $|2\rangle$, irrespective of its initial state (hence two operators $M_{0,...}$). This automatically switches off L_1. Then qutrit 1 resets from $|2\rangle$ to $|+\rangle$, while exciting qutrit 2 to $|2\rangle$ (operators $N_{1,...}$). This keeps L_1 off and switches off L_2 as well. Next, qutrit 2 resets to $|+\rangle$ while exciting qutrit 3 to $|2\rangle$ (operators $N_{2,...}$). This switches back on L_1 but not L_2; and so on. The last qubit of the chain just resets on its own with N_n.

This reservoir perfectly synchronizes all stabilizing operations without wasting time. It just has to assume that resets are triggered at a slow rate compared to the data-stabilizing operations, thus:

$$\kappa_c, \kappa_{st} \gg \kappa_u \, .$$

Thanks to this strategy, we hence recover just two timescales as in Section 2.2.3, but now with bipartite interactions only. For an improvement by a factor C on T_r/T_p, the ratio between fastest achievable reservoir rate T_r and expected rate of perturbations T_p, we may expect the error to improve by $C^{1/2}$. If the operators (2.23) associated with data qutrits are a realistic option, then this would probably be our most efficient GHZ reservoir.

We have seen two families of set-ups implementing the occasional synchronous reset of all qubits to $|+\rangle$, which allows stabilizing the GHZ state when put together with the process suggested by Ticozzi-Viloa in [29]. These two processes require different strength of application to have a steady state as close to GHZ as possible, which implies to have different time scale parameters. The first one consists of creating an auxiliary subsystem, a chain of ancilla acting as a clock, which periodically resets our data qubits based of either the ancilla chain *being* on a state or *jumping* on a state. The second one instead focuses on using a third level on each data subsystem, where the third level plays the role of the clock without an auxiliary chain being needed.

The main differences between the two, from a theoretical perspective, is we need one less time scale in the best setting for the set-up with qutrits compared to the one with qubits and an ancilla chain. We will analyze the theoretical performances of these two schemes after some model simplifications, and compare them with simulations of the full models in the next chapter.

Chapter 3

Performance analysis of the ancilla-clock and qutrits schemes

In this chapter, we will analyze more quantitatively the performance of the proposed reservoirs for GHZ state stabilization. In particular, we search for the optimal values of the various rates $\kappa_{...}$. We propose both approximate analytic results and numerical simulations. The full-system numerical results are limited to low values of n, the number of data qubits of our system, due to exponential growth of the Hilbert space dimension with n. The approximate analytic results thus serve to gain better insight into the scaling with larger n. In both sections we will focus on one prototypical case and, for the theoretical analysis, we will slightly adapt the setting in order to facilitate the analysis, involving a classical Markov chain.

3.1 Performance analysis: ancilla-clock based schemes

In the present section, we focus on the schemes based on the ancillas clock, more precisely the state-conditioning and jump-conditioning schemes of Section 2.2.1 and Section 2.2.2. We will analyze the wave-based scheme with data qutrits in Section 3.2.

Throughout the analysis sections, we use "configuration" to denote a possibility for the system, e.g. qubits being in $|+ + ...+\rangle$ or just having undergone the jump L_k. The term "state" will rather denote the distribution over configurations (quantum state ρ or probability distribution p associated to a Markov chain).

3.1.1 Behavior of the clock ancillas

As already mentioned in the system description and detailed in Step 0 of previous chapter, we have designed the ancillas' evolution to be not influenced by the data states. We can thus first analyze the subsystem composed of the ancillas only. Moreover, any quantum coherences between ancilla levels are irrelevant for the reservoir working, and when starting with a classical probability distribution over ancilla levels without quantum coherences, the system stays so (see step 0 of previous chapter). Therefore, we can treat the ancillas clock like a classical Markov chain, describing the evolution of a probability distribution p over all possible values of the ancillas.

Let us start with the state-conditioning scheme of Section 2.2.1. The vector p is thus a distribution over the 3^n possible elements constituting the set $\{|g\rangle, |e\rangle, |m\rangle\}^n$. We will use p_X to denote the population on the state $X \in \{|g\rangle, |e\rangle, |m\rangle\}^n$, for instance $p_{gg..g}$ denotes the population on the state "all the ancillas are in $|g\rangle$". The transitions among those elements are governed by the Lindblad equation

$$\frac{d}{dt}\rho_t^a = \sum_{\substack{k \\ j=sp,st+,st-}} M_{k,j}\rho_t^a {M_{k,j}}^\dagger - \frac{1}{2}\left({M_{k,j}}^\dagger M_{k,j}\rho_t^a + \rho_t^a {M_{k,j}}^\dagger M_{k,j}\right) \tag{3.1}$$

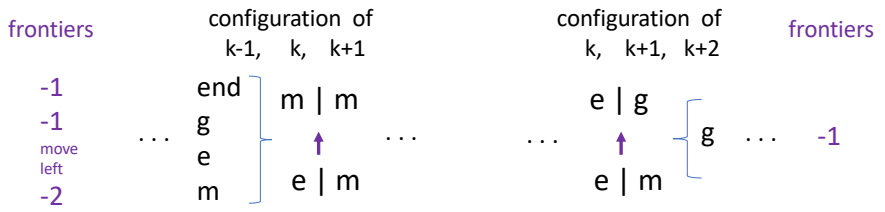

Figure 3.1: The possible evolution of "frontier" $F_{e,m}$ (from bottom to top) with only stimulated jump operators $\kappa_{st} \neq 0$, showing the associated evolution of the number of frontiers depending on the rest of the chain. The situation for other frontiers is obtained by symmetry.

on the ancillas' reduced density matrix ρ_t^a, with dissipation operators $M_{k,j}$ given by (2.11). Equivalently, assuming ρ_0^a diagonal in the canonical basis, this can be represented as the classical Markov chain

$$\frac{d}{dt}p_t = \sum_{\substack{k \\ j=sp,st+,st-}} A_{k,j}p_t \;=: A\,p_t \tag{3.2}$$

Each transition matrix $A_{k,j}$, and thus a fortiori the total transition matrix A, have non-negative off-diagonal elements and columns summing to zero. We keep using the quantum notation for basis vectors, e.g. $|e\rangle\langle g|_k - |g\rangle\langle g|_k$ denotes the $3^n \times 3^n$ matrix inducing (at a unit rate) transitions from $|e\rangle$ to $|g\rangle$ on ancilla k, while maintaining the other ancillas' values. Translating the effect of the operators $M_{k,j}$ given by (2.11), the transition matrices $A_{k,j}$ then write as follows:

$$\begin{aligned}
A_{k,sp} &= \kappa_u\left(|e\rangle\langle g| - |g\rangle\langle g|\right)_k + \kappa_d(|m\rangle\langle e| - |e\rangle\langle e|)_k + \kappa_t(|g\rangle\langle m| - |m\rangle\langle m|)_k \\
A_{k,st+} &= \kappa_{st}\left(|ee\rangle\langle ge| + |mm\rangle\langle em| + |gg\rangle\langle mg|\right)_{k,k+1} \\
&\quad -\kappa_{st}(|ge\rangle\langle ge| + |em\rangle\langle em| + |mg\rangle\langle mg|)_{k,k+1} \\
A_{k,st-} &= \kappa_{st}\left(|ee\rangle\langle eg| + |mm\rangle\langle me| + |gg\rangle\langle gm|\right)_{k-1,k} \\
&\quad -\kappa_{st}(|eg\rangle\langle eg| + |me\rangle\langle me| + |gm\rangle\langle gm|)_{k-1,k}
\end{aligned}$$

We will now focus on computing the steady state of this Markov chain (3.2), approximately, assuming $\kappa_{st} \gg \kappa_u, \kappa_d, \kappa_t$ as we have requested at the design stage.

With stimulated jumps only, the string of ancilla qubits exponentially converges to a distribution over $|gg..g\rangle$, $|mm..m\rangle$ and $|ee..e\rangle$.

We first prove that with only the interaction in κ_{st}, the distribution p over ancilla states converges, from any initial state, to span$\{|gg..g\rangle, |mm..m\rangle, |ee..e\rangle\}$.

With $\kappa_u = \kappa_d = \kappa_t = 0$, we are thus in the situation where the only interactions possible are an ancilla on g attracting a neighbour ancilla from level m to level g, an ancilla on e attracting a neighbour ancilla from level g to level e, and an ancilla on m attracting a neighbour ancilla from level e to level m, following the cycle $g \to e \to m \to g$....

The evolution of the ancillas can be seen as a sequence of steps where one ancilla changes at each step. We want to show, with only those interactions, that starting from any configuration, we converge in a finite number of steps towards a state where all the ancillas are either on $|gg..g\rangle$, or $|mm..m\rangle$, or $|ee..e\rangle$. For this, we define a frontier $F_{A,B}$ as a separation between two consecutive ancillas A and B in the chain, with $A, B \in \{g, e, m\}$ and $A \neq B$. We will demonstrate that the number of frontiers falls to zero in a finite number of steps.

- Consider two adjacent ancillas $k, k+1$ forming a frontier $F_{e,m}$ and let us list the implications of all the possible jumps involving those ancillas, see Figure 3.1

  The jump operator involving both ancillas can make them jump to $|m,m\rangle_{k,k+1}$. If ancilla $k = 1$ or ancilla $k-1$ was in $|g\rangle$, then this decreases the number of frontiers by 1. If ancilla

$k-1$ was in $|m\rangle$, then this decreases the number of frontiers by 2. If ancilla $k-1$ was in $|e\rangle$, then the frontier $F_{e,m}$ has moved down, to ancillas $k-1, k$.

Otherwise, a jump operator involving ancillas $k-1, k$ can switch ancilla k towards $|m\rangle$, iff ancilla $k-1$ was on m; this decreases the number of frontiers by 2.

Finally, a jump operator involving ancillas $k+1, k+2$ can switch ancilla $k+1$ towards $|g\rangle$, iff ancilla $k+1$ was on $|g\rangle$; this decreases the number of frontiers by 1.

Altogether: either the number of frontiers strictly decreases, or the frontier $F_{e,m}$ moves towards lower indices.

- By circular symmetry on the clock levels, the same is true for frontiers $F_{m,g}$ and $F_{g,e}$. By reversal of the index order, jumps involving the ancillas of a frontier $F_{m,e}$, $F_{g,m}$ or $F_{e,g}$ either strictly decrease the number of frontiers, or move this frontier towards higher indices.
- Consider two adjacent ancillas $k, k+1$ on the same level e.g. $|ee\rangle$. Ancilla $k+1$ can only jump towards m, iff ancilla $k+2$ was on m, thus moving towards lower indices the frontier $F_{e,m}$ which was present at ancillas $k+1, k+2$. Simlarly, ancilla k can only jump towards m by moving the frontier $F_{m,e}$ from indices $k-1, k$ towards $k, k+1$.

  Altogether, and by symmetry for $|gg\rangle$ and $|mm\rangle$: the frontiers move in the same way as for the previous items.

To summarize, at any jump, either the number of frontiers strictly decreases, or a frontier moves in a unique direction. This process can only go on for a finite number of steps, since frontiers can only move up to the end of the chain before at least one frontier has to disappear. We have thus demonstrated that, in a stochastic jump viewpoint, the number of frontiers must go to zero after a finite number of jumps. Since every jump is a Poisson point process of parameter κ_{st}, the convergence of the distribution p over ancilla states converges to span$\{|gg..g\rangle, |mm..m\rangle, |ee..e\rangle\}$ is exponential.

With stimulated jumps dominating spontaneous jumps, the string of ancilla qubits exponentially converges towards a unique steady state with little population outside $|gg..g\rangle$, $|mm..m\rangle$ and $|ee..e\rangle$.

We now consider the full ancillas clock, with $\kappa_{st} \gg \kappa_u, \kappa_d, \kappa_t > 0$. This situation can be seen as a perturbation of the previous case, with the perturbed transition matrix $A(\epsilon) = \kappa_{st}(A_0 + \epsilon A_1)$ where A_0 represents the stimulated jumps (Section 3.1.1) and A_1 represents the spontaneous jumps. Anticipating that we will take $\kappa_d > \kappa_u, \kappa_t$, we thus denote $\kappa_d/\kappa_{st} =: \epsilon$.

To quickly characterize the steady state of this perturbed transition matrix, we can use one of the results of Theorem S6.1, chapter S6 of [15]:

Proposition 3 *Take $A(\epsilon)$ a complex matrix-valued function analytic in a domain $\Omega \in \mathbb{C}$ with $r = max_{\epsilon\in\Omega}(rank(A(\epsilon)))$. There exist $y_{r+1}(\epsilon)$, ...$y_N(\epsilon)$, some analytic vector-valued functions which constitute a basis for the null space of $A(\epsilon)$, for all $\epsilon \geq 0$ except for a set of isolated points which consists exactly of those ϵ_0 for which $rank(A(\epsilon_0)) < r$. For such exceptional ϵ_0, we still have the inclusion $span\{y_{r+1}(\epsilon_0), ...y_N(\epsilon_0)\} \subset Ker(A(\epsilon_0))$.*

In our case, we have a rank $r = N-1$ for the perturbed matrix $A(\epsilon)$ for $\epsilon \neq 0$, since our Markov chain is irreducible: indeed, by using the spontaneous jumps of individual ancillas, we can go very simply from any combination of ancilla levels to any other combination of ancilla levels. The rank degenerates to $N-3$ for $\epsilon = 0$, as we have shown in Section 3.1.1 that Ker$(A(0)) =$ span$\{|gg..g\rangle, |mm..m\rangle, |ee..e\rangle\}$. Proposition 3 allows us to say that there exists $y_N(\epsilon)$, an analytic vector-valued function which constitutes a basis for the null space of $A(\epsilon)$, for all $\epsilon > 0$, and that $span\{y_N(0)\} \subset Ker(A(0))$.

When ϵ goes to zero, $y_N(\epsilon)$ thus analytically tends towards $y_N(0) \in$ span$\{|gg..g\rangle, |mm..m\rangle, |ee..e\rangle\}$. Concretely: only the configurations $|gg...g\rangle, |mm...m\rangle, |ee...e\rangle$ can have population of order 1 in steady state. We next use this insight to approximately compute the steady state.

The populations on $|gg...g\rangle$, $|mm...m\rangle$ and $|ee...e\rangle$ are each at least an order of magnitude larger than the ones of all other states.

We next show that the three "synchronized clock" configurations dominate all the other ones in steady state, as intended. We denote $\frac{\max(\kappa_t,\kappa_u)}{\kappa_d} = \epsilon_1 \ll 1$ and $\frac{\kappa_d}{\kappa_{st}} = \epsilon_2 \ll 1$.

Definition 1 We call *principal configurations* the three configurations $|gg...g\rangle$, $|mm...m\rangle$ and $|ee...e\rangle$. We call *main transition configurations* the configurations, with 1 or 2 frontiers, resulting from a single spontaneous jump of any ancilla of a principal configuration, followed by an arbitrary number of stimulated jumps.

For instance, $|emee...e\rangle$ is a main transition configuration resulting from a random jump on the second ancilla of $|eee...e\rangle$; and $|mmmee...e\rangle$ is also a main transition configuration, reached after this ancilla 2 has stimulated jumps of ancillas 1 and 3. As we will see, those are the main states enabling a flow from a principal configuration to another. We start with a preliminary result.

Proposition 4 *The distribution in steady state satisfies $p_{ee...e} \leq O(\epsilon_1)$.*

Proof The steady state condition on level $|me...e\rangle$ writes

$$(\kappa_{st} + (n-1)\kappa_d + \kappa_t)p_{me...e} = \kappa_d p_{ee...e} + P_1 \tag{3.3}$$

where P_1 represents all the other populations arriving in $|me...e\rangle$, so we have $P_1 > 0$. Dividing by $(\kappa_{st} + (n-1)\kappa_d + \kappa_t)$, we obtain that $p_{me...e}$ must be at least of order $\epsilon_2 p_{ee...e}$. We can repeat this reasoning on level $|mme...e\rangle$ of the steady state condition, yielding:

$$(\kappa_{st} + (n-2)\kappa_d + 2\kappa_t)p_{mme...e} = \kappa_{st} p_{me...e} + P_2 \tag{3.4}$$

where P_2 represents all the other populations arriving in $|mme...e\rangle$, so we have $P_2 > 0$. Dividing by $(\kappa_{st} + (n-2)\kappa_d + 2\kappa_t)$, we see that $p_{mme...e}$ must be at least of the same order as $p_{me...e}$. We can iterate this process until proving that $p_{m...me}$ must be at least of order $\epsilon_2 p_{ee...e}$. From there, the steady state equation on level $|mm...m\rangle$ gives

$$N\kappa_t p_{m...m} = \kappa_{st} p_{m...me} + P_3 \tag{3.5}$$

where $P_3 > 0$ represents all the other populations arriving in $|m...m\rangle$. Dividing by $N\kappa_t$ gives $p_{m...m}$ at least of order $\frac{1}{\epsilon_1\epsilon_2} \cdot \epsilon_2 p_{ee...e} = \frac{p_{ee...e}}{\epsilon_1}$. Since $p_{m...m}$ can be at most of order 1, we must indeed have $p_{ee...e}$ at most of order ϵ_1. □

Using this insight, we can compute the order of magnitude of steady state population on the principal configurations.

Proposition 5 *We have $p_{gg...g}$ and $p_{mm...m}$ of order one, and $p_{ee...e}$ is of order ϵ_1.*

Proof Using exactly the same method as in Proposition 4, we can prove that:

- $p_{mm...m}$ of order 1 $\implies$ $p_{gg...g} \geq O(1)$
- $p_{gg...g}$ of order 1 $\implies$ $p_{ee...e} \geq O(\epsilon_1)$
- $p_{ee...e} \geq O(\epsilon_1)$ $\implies$ $p_{mm...m} \geq O(1)$

Furthermore, since the populations must sum to 1, either $p_{mm...m}$ or $p_{gg...g}$ must be of order one at least. Combining these facts leads to the conclusion. □

Next, we can prove that the main transition configurations have a population an order of magnitude lower in steady state.

Proposition 6 *The main transition configurations have a population of order $\epsilon_1\epsilon_2$.*

PROOF We already know the steady-state populations of the configurations $|gg...g\rangle$, $|mm...m\rangle$ and $|ee...e\rangle$. Using the same reasoning as in Proposition 4, starting from the main transition configurations, we can prove that all main transition configurations are at most of order $\epsilon_1\epsilon_2$ (if bigger this would lead to the principal configurations being of an order bigger than what we already proved in Proposition 5). In the same way, starting from the principal configurations whose populations we know, we can prove that all transition configurations are at least of order $\epsilon_1\epsilon_2$. □

Finally, we prove with the two following propositions that any other configurations have a population of order $o(\epsilon_1\epsilon_2)$ in steady state.

Proposition 7 *Take X_k^0 a configuration with k frontiers, $k \geq 3$. Then $p_{X_k^0} = o(\epsilon_1\epsilon_2)$.*

PROOF First, note that the populations of those configurations must be at most of order $(\epsilon_1\epsilon_2)$: if bigger, then with the same reasoning as above this would lead to the principal configurations being of an order bigger than what we have already proved in Proposition 5.

We conduct a proof by induction for k going down from $n-1$ to 3, $n \geq 4$.

• Initialization: We look at a configuration X_{n-1}^0 with $n-1$ frontiers. No stimulated jump can ever lead to this configuration, so the only way to arrive there is with a spontaneous jump from configurations with $n-1$, $n-2$ or $n-3$ frontiers, denoted X_{n-1}^j, X_{n-2}^j and X_{n-3}^j with j spanning the different configurations. Moreover, the stimulated jumps draw X_{n-1}^0 onto other configurations, at a rate κ_{st} multiplied by the number $s_n \in [1, n-1]$ of ancillas which could undergo a synchronization jump, plus a small probability $s'_n\,\kappa_d$ to leave with spontaneous jumps. This gives the steady state equation for configuration X_{n-1}^0:

$$\begin{aligned}(s_n\kappa_{st} + s'_n\kappa_d)p_{X_{n-1}^0} =& \kappa_u \left[\sum_i p_{X_{n-1}^i} + \sum_j p_{X_{n-2}^j} + \sum_k p_{X_{n-3}^k}\right] \\ &+ \kappa_d \left[\sum_{i'} p_{X_{n-1}^{i'}} + \sum_{j'} p_{X_{n-2}^{j'}} + \sum_{k'} p_{X_{n-3}^{k'}}\right] \\ &+ \kappa_t \left[\sum_{i''} p_{X_{n-1}^{i''}} + \sum_{j''} p_{X_{n-2}^{j''}} + \sum_{k''} p_{X_{n-3}^{k''}}\right] \end{aligned} \tag{3.6}$$

All the populations on the right side of this equation are of order at most $\epsilon_1\epsilon_2$, as they are populations of states with at least 1 frontier. We can rewrite

$$(s_n\kappa_{st} + s'_n\kappa_d)p_{X_{n-1}^0} = \kappa_u O(\epsilon_1\epsilon_2) + \kappa_d O(\epsilon_1\epsilon_2) + \kappa_t O(\epsilon_1\epsilon_2) \tag{3.7}$$

and dividing by κ_{st}, we get

$$p_{X_{n-1}^0} = o(\epsilon_1\epsilon_2) \tag{3.8}$$

• Induction: We assume the property true for $k+1, k+2, ...n-1$ and show that it is true for k, provided $k \geq 3$.

Once again, the stimulated jumps draw the configuration X_k^0 onto other ones, at a rate $\kappa_{st}s_n < n$, as do some spontaneous jumps at a much smaller rate $s'_n\kappa_d$. Configurations that can directly jump to X_k^0 are either with k, $k+1$ or $k+2$ frontiers at a rate κ_{st}(as synchronization jumps can only lower the number of frontiers, and can lower it by at most 2), or configurations with at least $k-2$ frontiers at a smaller rate κ_u, κ_d or κ_t; since $k \geq 3$, those configurations with at least $k-2 \geq 1$ frontiers have a population of order $O(\epsilon_1\epsilon_2)$ or smaller. Thus the steady state equation for configuration X_k^0 would look like the following equation.

$$\begin{aligned}(s_n\kappa_{st} + s'_n\kappa_d)p_{X_k^0} = \kappa_{st}\sum_{i\neq 0} p_{X_k^i} + \kappa_{st}&\left[\sum_j p_{X_{k+1}^j} + \sum_l p_{X_{k+2}^l}\right] \\ &+ \kappa_u O(\epsilon_1\epsilon_2) + \kappa_d O(\epsilon_1\epsilon_2) + \kappa_t O(\epsilon_1\epsilon_2)\end{aligned} \tag{3.9}$$

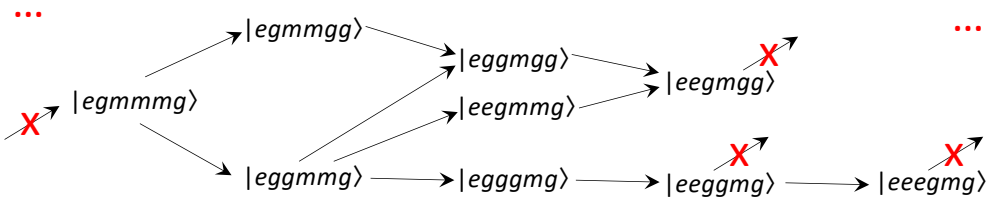

Figure 3.2: Part of the directed graph of possible frontier evolutions maintaining the number of frontiers k, illustrated for $k = 3$ and $n = 6$. Crossed arrows indicate that there is no further incoming or outgoing edge.

The $k+1$ or $k+2$ frontier states are of order $o(\epsilon_1\epsilon_2)$ and thus division by κ_{st} gives:

$$(s_n + s'_n\epsilon_1)\, p_{X_k^0} = \sum_{i\neq 0} p_{X_k^i} + o(\epsilon_1\epsilon_2)\ . \tag{3.10}$$

There remains to efficiently characterize the connections between various configurations X_k^0 and X_k^i in the above equation.

- Since the incoming $p_{X_k^i}$ in (3.10) result from evolutions with κ_{st} only, we resort again to the analysis of frontiers evolution as described in Section 3.1.1. Thus, for jumps with κ_{st} and maintaining the number of frontiers, a frontier $F_{e,m}$ for instance can only move towards lower indices, with unique directions of motions for other frontiers determined by symmetry. Conversely, the incoming states to a configuration X_k^0 are thus obtained by "moving back" one frontier, e.g. $F_{e,m}$ towards one higher index.

- We can build a graph $\mathcal{G}$ whose nodes are the configurations with k frontiers and whose directed edges represent valid frontier motions with κ_{st}, see Figure 3.2. Thanks to the unique direction of frontier motion, this graph contains no directed cycles. In particular, it features states with no incoming edges (respectively, no outgoing edges), i.e. where none of the k frontiers can be moved back (respectively, further) anymore.

- Consider X_k^0 any node of $\mathcal{G}$ with no incoming edges. Thus (3.10) reduces to $(s_n+s'_n\epsilon_1)\, p_{X_k^0} = o(\epsilon_1\epsilon_2)$ or equivalently $p_{X_k^0} = o(\epsilon_1\epsilon_2)$.

  Now when we move to X_k^0 a different node of $\mathcal{G}$, we can remove the nodes just treated from the sum over X_k^i in the right-hand side, since these nodes are thus captured by the term $o(\epsilon_1\epsilon_2)$. Therefore, we remove those nodes (with no incoming edges) from $\mathcal{G}$.

- The modified graph $\mathcal{G}$ now features new nodes with no incoming edges, for which (3.10) reduces to $(s_n+s'_n\epsilon_1)\, p_{X_k^0} = o(\epsilon_1\epsilon_2)$. We can thus repeat the above reasoning, until all nodes have been treated, proving that $p_{X_k^0} = o(\epsilon_1\epsilon_2)$ for any configuration X_k^0 with k frontiers.

The induction concludes the proof down to $k = 3$. □

The main transition configurations include all states with $k = 1$ frontier, e.g. $|ee...emm...m\rangle$ obtained from $|ee.ee\rangle$ by spontaneous jump $|e\rangle \to |m\rangle$ at the frontier, then stimulated jumps to $|m\rangle$ propagating along higher and higher indices only. They also include configurations with two frontiers and involving two level types, provided the "inner" level attract the outer one. For instance, $|eeemmmee\rangle$ can be obtained from $|ee...e\rangle$ with spontaneous jump $|e\rangle \to |m\rangle$ somewhere in the middle, then stimulated jumps to $|m\rangle$ of the neighbors. However, the converse configuration $|mmmeeemm\rangle$ is not a main transition configuration, since a single spontaneous jump followed by stimulated jumps cannot lead to this situation when starting from a synchronized configuration $|gg...g\rangle, |mm...m\rangle$, or $|ee...e\rangle$. Likewise, configurations with 2 frontiers but involving the 3 different levels $|g\rangle, |e\rangle$ and $|m\rangle$ are not main transition configurations. We thus conclude our claims by treating the configurations with 2 frontiers which are no main transition configurations.

Proposition 8 *Take X_2^1 a state with 2 frontiers and all three levels $|g\rangle, |e\rangle$ and $|m\rangle$ present in the configuration (for example $|egmm...\rangle$), and X_2^2 a state with 2 frontiers, involving only two levels and with the outer ancilla levels attracting the inner ones (for example $|...eeg...gee...\rangle$). Then $p_{X_2^1} = o(\epsilon_1\epsilon_2)$ and $p_{X_2^2} = o(\epsilon_1\epsilon_2)$.*

PROOF We can apply the same reasoning as in the proof of Proposition 7 for both cases $X_k^0 = X_2^1$ or $X_k^0 = X_2^2$. Configurations jumping towards X_k^0 at a rate κ_u, κ_d or κ_t cannot come from a configuration with 0 frontier, so their contribution in the steady state equation is at most of order $\epsilon_1 O(\epsilon_1\epsilon_2) = o(\epsilon_1\epsilon_2)$. We then obtain the same steady state equation (3.10), and we can repeat the proof with the graph $\mathcal{G}$ involving moving frontiers. The nodes now are the configurations of the same type as X_2^1 or as X_2^2 respectively, as one easily checks that stimulated jumps preserving the number of frontiers must also preserve this type of configuration. □

Final approximate steady state computation

The preceding propositions lead us to the following approximate computation of the steady state for the ancillas clock in the state-conditioning architecture. We first characterize the population on each of the three main configurations at first order. We then establish the n-dependence of the dominant population on other configurations.

Proposition 9 *In the limit $\epsilon_2 \to 0$, we have the steady-state populations:*

$$p_{gg..g} = \frac{1}{1 + \frac{\kappa_u}{\kappa_d} + \frac{\kappa_u}{\kappa_t}} \quad , \quad p_{mm..m} = \frac{1}{1 + \frac{\kappa_t}{\kappa_u} + \frac{\kappa_t}{\kappa_d}} \quad , \quad p_{ee..e} = \frac{1}{1 + \frac{\kappa_d}{\kappa_t} + \frac{\kappa_d}{\kappa_u}} \tag{3.11}$$

PROOF The limit $\epsilon_2 \to 0$ is the one where all the population is on the principal configurations $|gg...g\rangle$ $|mm...m\rangle$ and $|ee...e\rangle$. In other words, when being on the configuration $|gg...g\rangle$, a spontaneous jump of any of the ancillas to $|e\rangle$ will almost immediately lead to the configuration $|ee...e\rangle$, and similarly on the other principal configurations. We thus have the following steady state equations:

$$\begin{aligned} N\kappa_d p_{ee..e} &= N\kappa_u p_{gg...g} \quad , \quad p_{ee..e} + p_{mm...m} + p_{gg...g} = 1 \\ N\kappa_t p_{mm...m} &= N\kappa_d p_{ee..e} \quad , \quad N\kappa_u p_{gg...g} = N\kappa_t p_{mm...m} \end{aligned} \tag{3.12}$$

which immediately leads to the result. □

Proposition 10 *Consider a fixed number of ancillas n and small ϵ_1, ϵ_2 such that $n\epsilon_1 \ll 1$, $n\epsilon_2 \ll 1$. Then*

$$p_{gg..g} + p_{mm..m} + p_{ee..e} > 1 - \frac{3}{4}(n-1)(\tfrac{3n}{2} + 1)\,\epsilon_1\epsilon_2 + o(\epsilon_1\epsilon_2) \; . \tag{3.13}$$

Using the time scales of (2.22), this corresponds to a scaling in $\frac{T_3}{T_1}n^2$.

PROOF We have shown that $p_{gg..g}$, $p_{mm..m}$ and $p_{ee..e}$ are the only populations of order bigger than $O(\epsilon_1\epsilon_2)$, and main transition configurations are the only ones featuring populations of order $O(\epsilon_1\epsilon_2)$. We have to evaluate the latter, for example the main transition configurations between $|g...g\rangle$ and $|e...e\rangle$. The corresponding part of the ancillas clock Markov chain is represented on Figure 3.3.

- For the first line, the main transition configurations X_t^1 with a single ancilla on $|e\rangle$, we have the following steady state equation, with d being 1 or 2 depending on if we have a configuration with 1 or 2 frontiers:

$$(D\kappa_{st} + (n-1)\kappa_u + \kappa_t) p_{X_t^1} = \kappa_u p_{gg..g} + \kappa_{st} o(\epsilon_1\epsilon_2) \; . \tag{3.14}$$

  Indeed, configurations that can jump onto X_t^1 are either $|g...g\rangle$ under application of the corresponding spontaneous jump to $|e\rangle$; or configurations involving $n-2$ times $|g\rangle$, one $|e\rangle$, and one ancilla on $|m\rangle$, whose population is thus $o(\epsilon_1\epsilon_2)$ by our preceding results. On the other side, X_t^1 can be left through any corresponding spontaneous jump, or by stimulated attraction of a neighboring $|g\rangle$ towards $|e\rangle$ by the single $|e\rangle$ ancilla. Dividing by $(D\kappa_{st} + (n-1)\kappa_u + \kappa_t)$, we get

$$p_{X_t^1} = \frac{\kappa_u}{D\kappa_{st}} p_{gg..g} + o(\epsilon_1\epsilon_2) \; . \tag{3.15}$$

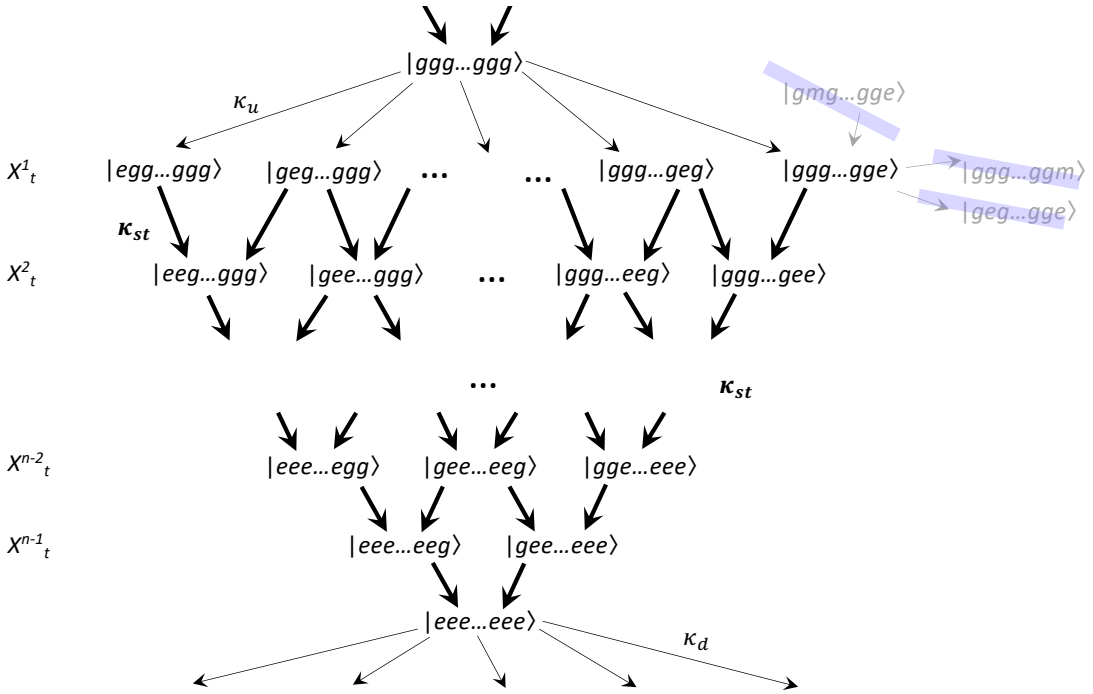

Figure 3.3: Representation of part of the ancillas clock Markov chain, used in the proof of Proposition 10. The main transition configurations are represented in full black, along with the relevant transitions towards the proof's result. A few other configurations and transitions are represented for illustration, shaded and crossed; indeed, those configurations play a negligible role in the computation and are thus discarded.

- Now consider the second line, the main transition configurations X_t^2 with two ancillas on $|e\rangle$. We can arrive on X_t^2 either with one of the $n-2$ ancillas jumping from $|m\rangle$ to $|g\rangle$, thus coming from a state with population $o(\epsilon_1\epsilon_2)$; or with (predominantly stimulated) jump from $|g\rangle$ onto $|e\rangle$ of one of the other 2 ancillas. Leaving X_t^2 follows the same scheme as for X_t^1. Thus, if X_t^2 has two frontiers, then its steady state equation writes:

$$(2\kappa_{st} + (n-2)\kappa_u + 2\kappa_t)p_{X_t^2} = \kappa_{st}p_{X_i^1} + \kappa_{st}p_{X_j^1} + \kappa_{st}o(\epsilon_1\epsilon_2) \ , \tag{3.16}$$

where both $p_{X_i^1}$ and $p_{X_j^1}$ satisfy (3.15) with $D=2$. This leads to

$$p_{X_t^2} = \frac{\kappa_u}{2\kappa_{st}}p_{gg..g} + o(\epsilon_1\epsilon_2) \tag{3.17}$$

for configurations X_t^2 with 2 frontiers.

If X_t^2 has a single frontier, then its steady state equation writes:

$$(\kappa_{st} + (n-2)\kappa_u + 2\kappa_t)p_{X_t^2} = \kappa_{st}p_{X_1^1} + \kappa_{st}p_{X_2^1} + \kappa_{st}o(\epsilon_1\epsilon_2) \ , \tag{3.18}$$

where $p_{X_1^1}$ and $p_{X_2^1}$ satisfy (3.15) with $D=1$ and $D=2$ respectively. This leads to

$$p_{X_t^2} = \frac{3\kappa_u}{2\kappa_{st}}p_{gg..g} + o(\epsilon_1\epsilon_2) \tag{3.19}$$

for configurations X_t^2 with 1 frontier.

- We can pursue a similar reasoning to show that the main transition configurations with 2 frontiers all have a population $\frac{\kappa_u}{2\kappa_{st}}p_{gg..g} + o(\epsilon_1\epsilon_2)$ in steady state, while the main transition configurations with 1 frontier have a population $\frac{(k+1)\kappa_u}{2\kappa_{st}}p_{gg..g} + o(\epsilon_1\epsilon_2)$ when k ancillas are on $|e\rangle$.
- Summing up the populations of the main transition configurations from $|g...g\rangle$ to $|e...e\rangle$ on all those lines then yields:

$$p_{t_{ge}} = \frac{\kappa_u}{2\kappa_{st}}(n-1)(\tfrac{3n}{2}+1)p_{gg..g} + o(\epsilon_1\epsilon_2) \tag{3.20}$$

- Similar properties hold, by circular symmetry, for the other pairs of levels, yielding:

$$\begin{aligned} p_{t_{em}} &= \frac{\kappa_d}{2\kappa_{st}}(n-1)(\tfrac{3n}{2}+1)p_{ee..e} + o(\epsilon_1\epsilon_2) \\ p_{t_{mg}} &= \frac{\kappa_t}{2\kappa_{st}}(n-1)(\tfrac{3n}{2}+1)p_{mm..m} + o(\epsilon_1\epsilon_2) \ . \end{aligned} \tag{3.21}$$

By summing up all these contributions and using Proposition 9, we obtain

$$p_{t_{ge}} + p_{t_{em}} + p_{t_{mg}} = (n-1)(\tfrac{3n}{2}+1)\,\frac{3\kappa_u\kappa_t}{2\kappa_{st}(\kappa_t+\kappa_u)} \ .$$

The result follows by definition of ϵ_1 and ϵ_2. □

Conclusion on state-conditioning ancillas clock: We have thus computed how the ancillas clock synchronizes in the regime $\epsilon_1, \epsilon_2 \ll 1$, allowing us to approximate it for our further analysis, as a clock jumping from $|gg...g\rangle$, to $|ee...e\rangle$, then $|mm...m\rangle$, and so on, with transition rates and a steady state distribution characterized by Proposition 9. The main timescale separation for this is $\epsilon_2 \ll 1$. The possibility for this to achieve very large κ_{st} is further encouraged by the fact that the corresponding transitions involve no operations on the truly quantum part of the system, namely the data qubits; having to treat purely classical degrees of freedom may facilitate achieving faster transition rates.

The scaling in n^2 in Proposition 10 can be seen as the consequence of two phenomena. First, the propagation of the synchronization over the ancillas chain takes a typical time n/κ_{st}.

Second, the fact that any of the n ancillas can spontaneously trigger a transition means that the expected time between two such perturbations of the synchronization procedure scales like $1/(n\kappa_d), 1/(n\kappa_u), 1/(n\kappa_t)$. For an optimal working point, it may be wise to decrease the κ_d, κ_u, κ_t with increasing n, in order to moderate this $1/n$ scaling of the expected time between clock transitions.

Similar results hold for the jump-conditioning ancillas clock

Until now our analysis has been restricted to the ancillas clock associated to the state-conditioning scheme of Section 2.2.1. We now consider the jump-conditioning scheme of Section 2.2.2. The associated ancillas clock features an additional level $|f\rangle$ on each ancilla. This level spontaneously jumps down to $|e\rangle$ at a rate κ_f, *irrespective of the associated data state*. More explanation on the latter property is given in Section 3.1.2. Stimulated jumps from $|g\rangle$ onto $|e\rangle$ occur if a neighboring ancilla is on $|e\rangle$ or $|f\rangle$. Furthermore, the rates now satisfy the timescale separation $\kappa_f,\ \kappa_{st} \gg \kappa_d, \kappa_t, \kappa_u$.

The idea is that this ancillas clock would behave very similarly to the one with state-conditioning, with each ancilla just quickly transitioning through $|f\rangle$ on its way from $|g\rangle$ to $|e\rangle$. The analysis confirming this can be carried out as follows.

In Section 3.1.1, we were keeping only the transitions associated to fastest timescales, which here would be κ_f and κ_{st}. Exponential convergence towards $\mathrm{span}\{|gg...g\rangle, |ee...e\rangle, |mm...m\rangle\}$ was proved using an argument on deleting all "frontiers" in a finite number of steps. A similar reasoning can be applied with the addition of level $|f\rangle$, and by considering that $|fe\rangle$ or $|ef\rangle$ is *not* a frontier. The essential idea is that any $|f\rangle$ jumps to $|e\rangle$ irrespectively of the other ancillas, in this way the $|f\rangle$ level does not really play a role in the synchronization mechanism.

In Section 3.1.1, we were analyzing the perturbation of the fast dynamics by the slower one. We have established that only the configurations $|gg...g\rangle, |mm...m\rangle, |ee...e\rangle$ can have population of order 1 in steady state. This result remains true as well. The parameter $\epsilon \ll 1$ now corresponds to T_3/T_1 according to (2.15).

In Section 3.1.1, we were distinguishing the "main transition configurations" with population of order $\epsilon_1\epsilon_2$, the three principal configurations with higher population (either $O(1)$ or $O(\epsilon_1)$), and all other configurations with population an order lower. A similar analysis can be carried out in presence of level $|f\rangle$, with the following modifications.

- There are only two timescales: a rapid one κ_{st}, κ_f, while all the slower rates $\kappa_u, \kappa_d, \kappa_t$ are of the same order. We thus denote $\epsilon = \min(\kappa_u, \kappa_d, \kappa_t) \ / \ \max(\kappa_{st}, \kappa_f)$.
- Consequently, the populations $p_{gg...g},\ p_{mm...m},\ p_{ee...e}$ will each be of order 1. In fact, this is already valid in Section 3.1.1 if one assumes $\kappa_u, \kappa_d, \kappa_t$ of the same order, thus taking $\epsilon_1 = O(1)$.
- To prove this result in presence of level $|f\rangle$, we can follow a similar reasoning with "main transition configurations", where we enlarge the set of such configurations for the transition from $|gg...g\rangle$ to $|ee...e\rangle$: they now include all the "main transition configurations" identified in Section 3.1.1, plus all configurations obtained from those where an arbitrary number of $|e\rangle$ levels is replaced by $|f\rangle$, plus all configurations consisting entirely of $k \geq 1$ levels $|f\rangle$ and $n-k$ levels $|e\rangle$.

  This just mirrors the quick transition $|g\rangle \to |f\rangle \to |e\rangle$ for each ancilla. The rest of the proof then follows similar lines.

As a result, we then obtain that $p_{gg...g},\ p_{mm...m},\ p_{ee...e}$ are all of order 1, the "main transition configurations" have population of order ϵ, and all other configurations have population $o(\epsilon)$.

In Section 3.1.1, we were providing the approximate distribution over $|gg...g\rangle, |ee...e\rangle, |mm...m\rangle$, and the n-dependence of the population outside those three configurations.

- In the present case, the distribution result of Proposition 9 remains unchanged, with thus $\epsilon_2 = \epsilon$ and just κ_d of the same order as κ_u, κ_t.

- Regarding the n-dependence of the population on "main transition configurations", we can take the following viewpoint to treat the now different transition from $|gg...g\rangle$ to $|ee...e\rangle$.

  First, consider as irrelevant whether an ancilla is on $|e\rangle$ or $|f\rangle$, grouping those two levels as some super-level $|\zeta\rangle$ = "$|e\rangle$ or $|f\rangle$". With this, we can repeat verbatim the proof of Section 3.1.1 and we obtain the same evaluations for the total population on each super-level configuration, e.g. for $p_{g\zeta gg...g}$. In particular, $p_{\zeta\zeta...\zeta}$ gets the population of order 1 which (3.11) attributes to $|ee...e\rangle$. More precisely, according to Proposition 10, the population not on $|gg...g\rangle, |\zeta\zeta...\zeta\rangle, |mm...m\rangle$ is of order $O(\epsilon\, n^2)$.

  Next, there remains to single out the configuration $|ee...e\rangle$ out of the super-level configuration $|\zeta\zeta...\zeta\rangle$. For this, let us denote X_k^j the configurations with k ancilla on $|f\rangle$ and the other ancillas on $|e\rangle$, and denote by p_k the sum of all the populations on configurations of type X_k^j.

  – The steady-state equation for $p_{ee...e}$ writes:

  $$n\kappa_d p_{ee...e} = \kappa_r \sum_j p_{X_1^j} = \kappa_r p_1$$

  or equivalently $p_1 = O(n\epsilon)$.

  – Consider the steady-state equation for $p_{X_k^j}$, with $k = 1, 2, ..., n-1$. The outgoing rate is $(k\kappa_r + (n-k)\kappa_d)\; p_{X_k^j}$, namely any of the k ancillas on $|f\rangle$ spontaneously jumping towards $|e\rangle$ or any of the $n-k$ ancillas on $|e\rangle$ spontaneously jumping towards $|m\rangle$. The incoming rate is the sum of possible transitions from configurations involving one ancilla on $|g\rangle$, and transitions from states of type X_{k+1}^ℓ. Dropping the former from the equation, we get

  $$(k\kappa_r + (n-k)\kappa_d)\; p_{X_k^j} \;>\; \kappa_r \sum_{\ell \in \mathcal{N}_k^j} p_{X_{k+1}^\ell}$$

  with the set $\mathcal{N}_k^j$ containing $(n-k)$ elements. Since $p_{X_k^j}$ is already of order ϵ, we will neglect the term in $\kappa_d p_{X_k^j}$ here. Then summing the equation over j, we obtain

  $$k\, p_k > (k+1)\, p_{k+1}$$

  The factor $(k+1)$ on the right comes from the fact that each of the $(k+1)$ ancillas on $|f\rangle$ in a given configuration X_{k+1}^ℓ can once play the role of the incoming path to some X_k^j.

  – Thus iteratively, we have that $p_k = \frac{1}{k} p_1$ for $k = 1, 2, ..., n$. Thus

  $$\sum_{k=1}^{n} p_k = O\left(\log(n)\right) p_1 = O\left(n \log(n)\epsilon\right)$$

  This proves that the population not on $|gg...g\rangle, |ee...e\rangle, |mm...m\rangle$ is still of order $O(\epsilon\, n^2)$.

3.1.2 Data qubits evolution

We now turn towards analyzing the data qubits. In order to obtain quantitative results, this analysis will involve several model simplifications.

- First, we will consider that the ancillas clock transitions only through $|gg...g\rangle, |ee...e\rangle, |mm...m\rangle$. Its remaining dynamics will be summarized by multiplying the obtained fidelity by $1 - O(\epsilon\, n^2)$ i.e. the proportion of cycle actually on those configurations.
- Second, we will introduce (small) model modifications such that we can treat the data qubits evolution like a *classical Markov chain* as well. While the quantum state evolves through non-orthogonal states $\rho(t)$, the Markov chain will model the (hypothetical) output signal

associated to the dissipation operators, which is a classical variable. The model modification ensures that the associated dynamics does not further depend on ρ, and thus indeed evolves autonomously.

- Related to the previous point, we will measure the fidelity to GHZ as the proportion of state on a particular configuration of the Markov chain. This is a pessimistic bound, since not all other configurations of the Markov chain are orthogonal to $|GHZ_+\rangle$. However, since it is trivial to achieve 50% fidelity with $|GHZ_+\rangle$ (e.g. just take the configuration $|00...0\rangle$), it seems legitimate to discard as "bad" all the configurations which are not doing better than this.
- Finally, we will make several approximations in the analysis of the classical Markov chain in order to evaluate its steady state.

The second point requires more precise information, which we provide next.

Markov chain definition

The idea is to build a classical Markov chain, over a finite number of configurations, related to the transitions that the dissipation channels would induce in a "jump"-type unraveling. More precisely, we will associate a particular configuration of the Markov chain to a particular set of (hypothetical) output signal values associated to jump detections. The main issue is to ensure an evolution of this Markov chain which does not further depend on the quantum state.

Concretely, let Q_k denote a generic Lindblad operator like the L_k, M_k, N_k introduced previously. The Lindbladian decoherence associated to Q_k can be viewed as the average over different purity-preserving evolutions, which would be distinguished by a hypothetical output associated to Q_k. In particular, in the so-called "jump stochastic master equation unraveling" of Lindbladian decoherence [13], the channel Q_k is associated to a Poisson process $q_k(t)$ reporting detections of "quantum jumps". The Poisson process is determined by

$$\mathbb{E}(dq_k(t)) = \mathrm{trace}(Q_k\,\rho(t)\,Q_k^\dagger)\;dt\;,$$

with associated state evolutions:

$$\begin{array}{lcl}
\text{for } q_k(t+dt)-q_k(t)=1 \;:\; \rho_{t+dt} &=& (Q_k\,\rho(t)\,Q_k^\dagger)\;/\;\mathrm{trace}(Q_k\,\rho(t)\,Q_k^\dagger)\\
\text{for } q_k(t+dt)-q_k(t)=0 \;:\; \rho_{t+dt} &=& (V_0\,\rho(t)\,V_0^\dagger)\;/\;\mathrm{trace}(V_0\,\rho(t)\,V_0^\dagger)\\
& & \text{with } V_0 = I + \tfrac{dt}{2}(\mathrm{trace}(Q_k\,\rho(t)\,Q_k^\dagger)\,I - Q_k^\dagger Q_k)\;.
\end{array}$$

Here I denotes the identity operator. In the following, we will also consider the case where a single detection signal q_μ does not distinguish from which operators Q_{μ_k} a jump is coming. This situation is governed by the following equations:

$$\mathbb{E}(dq_\mu(t)) = \textstyle\sum_k \mathrm{trace}(Q_{\mu_k}\,\rho(t)\,Q_{\mu_k}^\dagger)\;dt\;, \tag{3.22}$$

$$\begin{array}{lcl}
\text{for } q_\mu(t+dt)-q_\mu(t)=1 \;:\; \rho_{t+dt} &=& \dfrac{\sum_k Q_{\mu_k}\,\rho(t)\,Q_{\mu_k}^\dagger}{\sum_k \mathrm{trace}(Q_{\mu_k}\,\rho(t)\,Q_{\mu_k}^\dagger)}\\
\text{for } q_\mu(t+dt)-q_\mu(t)=0 \;:\; \rho_{t+dt} &=& (V_0\,\rho(t)\,V_0^\dagger)\;/\;\mathrm{trace}(V_0\,\rho(t)\,V_0^\dagger)\\
& & \text{with } V_0 = I + \tfrac{dt}{2}\textstyle\sum_k(\mathrm{trace}(Q_{\mu_k}\,\rho(t)\,Q_{\mu_k}^\dagger)\,I - Q_{\mu_k}^\dagger Q_{\mu_k})\;.
\end{array}$$

The deterministic evolution described by the Lindblad equation can be viewed as the average evolution, when such detectors are present but their output signal is not recorded. The principle of "unraveling" is to view this in converse: while there are no detectors actually present, we may find it easier to reason in terms of hypothetical detection results and consider their expectation as describing the engineered reservoir evolution. Here, we push this one step further, by setting up a specific system architecture which can be studied as a Markov chain on the (hypothetical) signals $q_\mu(t)$ alone. More precisely, *we will consider a signal $q(t)$ listing the various detections that have happened*, e.g.

$$q(t) = \mu_1,\,\mu_2,\,\mu_1,\,\mu_3\;.$$

if up to time t we have seen first a detection on μ_1, then on μ_2, then on μ_1 again, and finally on μ_3 and nothing more. Our aim is to describe the evolution of $q(t)$ like a classical Markov chain.

In order to set up a classical Markov chain based on $q(t)$ alone, the statistics $\mathbb{E}(dq_\mu(t))$ for the future evolution of the $q_\mu(t)$ should only depend on $q(t)$. Furthermore, to be useful, knowing $q(t)$ should give us valuable information on $\rho(t)$. We will ensure these by imposing a model with the two following, somewhat stronger properties:

(i) The $\mathbb{E}(dq_\mu(t))$ are independent of $\rho(t)$.

(ii) V_0 is proportional to identity, such that in absence of any detection the state $\rho(t)$ does not change.

These properties are not trivial, and we now show how to apply them for the three types of Lindblad operators acting on the data qubits: error channels, resets to $|+\rangle$, and two-qubit correlation operators L_k.

Error channels: With no particular implementation in mind, the error channels are somewhat arbitrary. In line with usual quantum computing assumptions, we will consider bit-flip and phase-flip errors on each qubit individually, associated respectively to decoherence operators:

$$E_{k,1} = \sqrt{\kappa_x}(|0\rangle\langle 1| + |1\rangle\langle 0|)_k \quad , \quad E_{k,2} = \sqrt{\kappa_z}(|0\rangle\langle 0| - |1\rangle\langle 1|)_k \ , \quad k = 1, 2, ..., n \ . \tag{3.23}$$

These error channels naturally satisfy the properties (i) and (ii) mentioned above, with a detector q_μ associated to each individual operator. Indeed, since $E_{k,s}^\dagger E_{k,s} = \kappa_s \, I$ proportional to the identity for $s \in \{x, z\}$, we have

$$\mathbb{E}(dq_{k,s}(t)) = \kappa_s \mathrm{trace}(\rho(t)) = \kappa_s \quad \text{and} \quad V_0 = I \ .$$

Note that with a loss operator $E_k = |0\rangle\langle 1|_k$ this would not have been as trivial and some adaptation would be required. This situation is in fact strictly analogous to the qubit reset channels, which we discuss next.

Reset channels: Consider a reset operator $N_k = \sqrt{\kappa_r}|+\rangle\langle -|_k$. The associated jump detection signal is associated to $\mathbb{E}(dq_{N_k}(t)) = \kappa_r \langle -|\rho(t)|-\rangle_k$ which does not satisfy condition (i). However, this issue can be solved by adding a no-reset operator, as we already did in the jump-conditioning architecture. Indeed, consider

$$q_{k,+} \text{ associated to } N_{k,r} = \sqrt{\kappa_r}|+\rangle\langle -|_k \quad \text{and} \quad N_{k,i} = \sqrt{\kappa_r}|+\rangle\langle +|_k \ . \tag{3.24}$$

Then $N_{k,r}^\dagger N_{k,r} + N_{k,i}^\dagger N_{k,i} = \kappa_r \, I$ is proportional to identity, such that properties (i) and (ii) again hold.

As a parenthesis, when discarding the other qubits, the Lindblad equation with $N_{k,r}$ and $N_{k,i}$ writes

$$\tfrac{d}{dt}\rho(t) = \kappa_r(\, |+\rangle\langle +| - \rho(t) \,) \ ,$$

while with $N_{k,r}$ alone the off-diagonal components $\langle +|\rho|-\rangle$ and $|-\rangle\rho\langle +|$ decay twice more slowly. Even after discarding the "hypothetical jump detections", there is thus a true difference between those two models.

Two-qubit correlation channels: The "jump" operator L_k is conceptually similar to a reset operator. Hence, with no surprise, properties (i) and (ii) can be satisfied only if we modify the setting. Namely, instead of just applying L_k, we will assume that we have

$$q_{k,L} \text{ associated to } L_k = \sqrt{\kappa_c}(|00\rangle\langle 01| + |11\rangle\langle 10|)_{k,k+1} \quad \text{and} \quad \tilde{L}_k = \sqrt{\kappa_c}(|00\rangle\langle 00| + |11\rangle\langle 11|)_{k,k+1} \ . \tag{3.25}$$

Like for the reset channel, this ensures properties (i) and (ii) thanks to $L_k^\dagger L_k + \tilde{L}_k^\dagger \tilde{L}_k = \kappa_c \, I$ proportional to identity, and this *does* (somewhat) modify the model proposed in Section 2.2. In terms of system operation, the $\tilde{L}_k$ appears unnecessary. However, it simplifies the analysis by allowing us to treat the whole system as a classical Markov chain on jump detection signals.

Markov chain: Having defined the output signals $q_{k,x}$, $q_{k,z}$, $q_{k,+}$, $q_{k,L}$ with associated Lindblad operators in (3.23),(3.24),(3.25), we are all set for describing our classical Markov chain. We make this explicit description for the case of state-conditioning; the same approach holds for jump-conditioning.

We recall that a configuration of the classical Markov chain would be described by a value of $q(t)$, i.e. an ordered list of jump detections like e.g.

$$q(t) = \{1L\}, \{2x\}, \{5+\}$$

if up to time t we have observed first a jump on $q_{1,L}$ from (3.25), then a jump on $q_{2,x}$ from (3.23), then a jump on q_{5+} from (3.24), and nothing more. Thus, $q(t)$ can take a countable infinity of configurations. However, we can reduce the Markov chain to a finite number of configurations by grouping the values of $q(t)$ as follows:

- Configurations R_ℓ, for $\ell = 1, 2, ..., n$: all $q(t)$ ending with a sequence composed of ≥ 1 times $\{k_1+\}$, $\{k_2+\}$,..., and $\{k_\ell+\}$, for some fixed and differing qubit indices $k_1, ..., k_\ell$, preceded by detections different from $\{\cdot+\}$.

  In particular, configuration R_1: all $q(t)$ ending with any number ≥ 1 of times $\{k+\}$ for some fixed k, preceded by detections different from $\{\cdot+\}$.

  In particular, configuration R_{n-1}: all $q(t)$ ending with a sequence composed of ≥ 1 times $\{1+\}$, $\{2+\}$,..., and $\{n+\}$, except one of the indices missing (and preceded by detections different from $\{\cdot+\}$).

  In particular, configuration R_n: all $q(t)$ ending with a sequence composed of ≥ 1 times $\{1+\}$, $\{2+\}$,..., and $\{n+\}$.

  Examples: $q(t) = ..., \{1L\}, \{3+\}$ belongs to R_1 ; $q(t) = ..., \{2\,x\}, \{3+\}, \{1+\}, \{3+\}$ belongs to R_2; $q(t) = ...\{3+\}, \{1+\}, \{4+\}, \{3+\}, \{2+\}\{1+\}, \{1+\}$ belongs to R_n for $n = 4$.

- Configuration G_0: all $q(t)$ ending with a sequence composed of ≥ 1 times $\{1+\}$, $\{2+\}$,..., and $\{n+\}$, followed by any number of detections $\{k\ L\}$ with $k \neq 1$.

  Examples: $q(t) = ...\{3+\}, \{1+\}, \{4+\}, \{3+\}, \{2+\}\{1+\}, \{1+\}, \{2L\}, \{3L\}, \{3L\}$ belongs to G_0 for $n = 4$.

- Configurations G_ℓ, for $\ell = 1, 2, ..., n-2$: all $q(t)$ ending with a sequence composed of ≥ 1 times $\{1+\}$, $\{2+\}$,..., and $\{n+\}$, followed by a sequence of $\{k\ L\}$ containing the ordered sub-sequence $\{1L\}, \{2L\}, ..., \{\ell L\}$ but not the ordered sub-sequence $\{1L\}, \{2L\}, ..., \{(\ell+1)L\}$.

  In particular, configuration G_1: all $q(t)$ ending with a sequence composed of ≥ 1 times $\{1+\}$, $\{2+\}$,..., $\{n+\}$, followed by a sequence of $\{k\ L\}$ containing $\{1\ L\}$ but no $\{2\ L\}$ after $\{1\ L\}$.

  Examples: $q(t) = ...\{3+\}, \{1+\}, \{4+\}, \{3+\}, \{2+\}\{1+\}, \{1+\}, \{2L\}, \{1L\}, \{3L\}, \{2L\}$ belongs to G_2 for $n = 4$; $q(t) = ...\{3+\}, \{1+\}, \{4+\}, \{3+\}, \{2+\}\{1+\}, \{1+\}, \{2L\}, \{1L\}, \{3L\}, \{3L\}$ belongs to G_1 for $n = 4$.

- Configuration G_{HZ}: all $q(t)$ ending with a sequence composed of ≥ 1 times $\{1+\}$, $\{2+\}$,..., $\{n+\}$, followed by a sequence of $\{k\ L\}$ containing the ordered sub-sequence $\{1\ L\}, \{2\ L\}, ..., \{(n-1)\ L\}$.

  Examples: $q(t) = ...\{3+\}, \{1+\}, \{4+\}, \{3+\}, \{2+\}\{1+\}, \{1+\}, \{2L\}, \{1L\}, \{3L\}, \{2L\}, \{3L\}$ belongs to G_{HZ} for $n = 4$.

- Configuration E: any $q(t)$ of a different form.

  Examples: $q(t) = ...\{3\,x\}$ or $q(t) = ...\{2\,z\}$; $q(t) = ...\{2\,x\}, \{2L\}, \{1L\}, \{3L\}$; $q(t) = ...\{3\,z\}, \{2+\}, \{1L\}$.

- Ancillas clock: finally, each of the above configurations will be split in two, depending if the ancillas clock is on $|ee...e\rangle$ or on $\{|gg...g\rangle, |mm...m\rangle\}$.

  Examples: $q(t) = ...\{3\,z\}, \{2+\}, \{1L\}$ belongs to E^e or to E^{mg}.

An example of these configurations for $n = 3$ is shown on Figure 3.4. The rationale behind this grouping is to follow the "main path" by which an arbitrary state ρ_0 is brought towards $|GHZ_+\rangle\langle GHZ_+|$: first all the qubits are reset to $|+\rangle$, then the operators L_k (or $\tilde{L}_k$) are applied, with the process completing once they have been applied in order from 1 to $n-1$. This completion corresponds to the configuration G_{HZ}, or in fact to the configurations G^e_{HZ} and G^{mg}_{HZ}. The configurations involving R_n and G_n are the steps towards completing this sequence. In particular, we have distinguished R_n from G_0 because detecting $\{k+\}$ has a different effect from these two configurations. Finally, the configurations E^e and E^{mg} contain many cases which we consider "have to be completely reset".

Note that this grouping, in particular in E^e and E^{mg}, involves pessimistic simplifications. Indeed, if e.g. a bit-flip $\{3\,x\}$ is detected when being in G^{mg}_{HZ}, then the single jump $\{2L\}$ would in fact correct back the value of qubit 3 towards $|GHZ_+\rangle$; instead, the Markov chain of Figure 3.4 would imply that a whole sequence of events has to be traversed, starting from E^{mg}. Similarly, the sequence e.g. $q(t) = ...\{2+\}, \{1+\}, \{2+\}, \{1L\}$ would only need to be completed by $\{3+\}, \{2L\}$ in order to obtain $|GHZ_+\rangle$, while the Markov chain of Figure 3.4 models a start in E^{mg} or E^e. However, following all the possible "partial corruptions of the state" would make the analysis more complicated, so we here go for a conservative bound on what has to be done to recover $|GHZ_+\rangle$.

We also recall that, while most of the states $\rho(t)$ obtained at configurations different from G_{HZ} are not orthogonal to $|GHZ_+\rangle$, anything less than 50% fidelity is kind of useless, since this is no better than just putting all qubits in the ground state $|00...0\rangle$. This supports our choice to measure success by the population on configurations G^e_{HZ} and G^{mg}_{HZ} of this Markov chain.

Once these configurations have been defined, the possible Markov transitions between them are not difficult to set up. As proved in the previous paragraphs, the transition rates on $q(t)$ are independent of the configuration (up to resets being allowed only when ancillas are in $|ee...e\rangle$). The transition rates between our "grouped outputs" configurations thus come down to a counting argument. For the transition between ancilla states, since we do not distinguish $|mm...m\rangle$ and $|gg...g\rangle$ anymore, we define summarized rates $\tilde{\kappa}_d = \kappa_d$ and $\tilde{\kappa}_u = (\frac{1}{\kappa_u} + \frac{1}{\kappa_t})^{-1}$, which are supposed to preserve the same population on $p_{ee...e}$ as in Proposition 9 and the same mean time to go around one cycle $|gg...g\rangle \to |ee...e\rangle \to |mm...m\rangle \to |gg...g\rangle$. The corresponding transitions are represented for $n = 3$ on Figure 3.4.

Markov chain analysis

The final step to evaluate the performance of the scheme is to compute the steady state of the Markov chain described in Section 3.1.2. For simplicity, we assume at this point an equal bit-flip and phase-flip rate $\kappa_x = \kappa_z =: \kappa_p/2$. In addition to the three timescales $T_1 \gg T_2 \gg T_3$ as described in (2.22), we thus have a fourth one $\frac{1}{\kappa_p} = T_0 \gg T_1$ corresponding to perturbations being slower than the reservoir stabilization rate.

Looking at the dominating terms, the steady state analysis goes roughly as follows. The total population p_e on $\cdot^e$, irrespective of the data qubits situation, is of order $O(T_2/T_1)$. Moreover, any state of type $\cdot^e$ receives at most $O(n\kappa_u)$ population from states of type $\cdot^{mg}$. Therefore, a majority of the population p_e is concentrated on R^e_n, the only configuration from which one cannot leave at the fastest rate κ_r (see Figure 3.4). All other configurations have a population at least $O(T_3/T_2)$ smaller, and thus of order at most $O(T_3/T_1)$. This includes in particular the state G^e_{HZ} and all the reset states R^e_k with $k < n$. Next, we observe that each R^{mg}_k, with arrivals $n\kappa_d p_{R^e_k}$ and departure at a rate $O((n-1)\kappa_c) = O(n\kappa_d)$, must have steady state population of the same order as R^e_k. In particular, $p_{R^{mg}_k} = O(T_3/T_1)$ for $k < n$ and $p_{R^{mg}_n} = O(T_2/T_1)$. With a similar argument, and knowing that the G^e_k have population at most $O(T_3/T_1)$, we observe that the G^{mg}_k all have population of the same order as R^{mg}_n, thus of order $O(T_2/T_1)$. The target configuration G^{mg}_{HZ} then features arrivals $\kappa_c O(T_2/T_1) = O(1/T_1)$ and leaks at a rate $\tilde{\kappa}_u = O(1/T_1)$, meaning that its population is $O(1)$. There remains to observe that E^{mg} cannot have population of order 1 if $\kappa_p \ll \kappa_u$, to conclude that G^{mg}_{HZ} is the only state with population of order 1, and thus necessarily close to 1.

To obtain an estimate of the infidelity, an exact steady state analysis can be carried out with

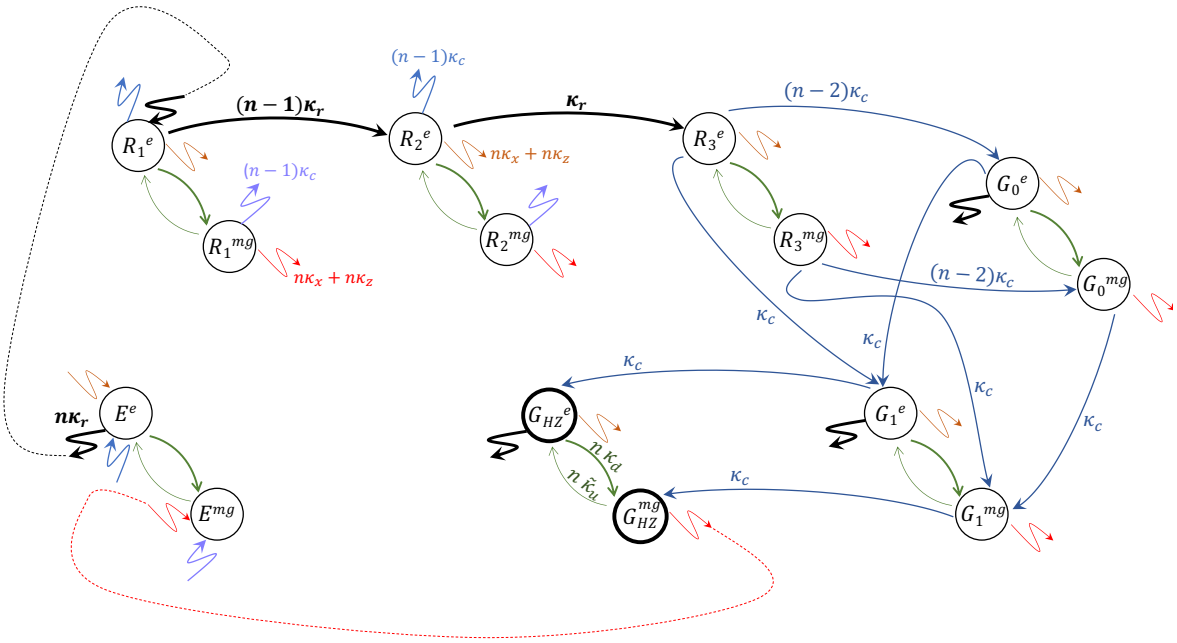

Figure 3.4: Representation of the Markov chain based on hypothetical jump detection outputs for $n = 3$ data qubits in the ancilla-state-conditioning architecture. To avoid clutter, wiggly output arrows indicate a connection of all these transitions to the input arrow of the same shape and color; a few dotted lines illustrate these connections. For instance, the six outgoing red arrows all indicate a transition towards configuration (E, mg); its rate is the sum of the bit-flip and phase-flip rates of the n qubits. Green arrows indicate the summarized transitions of the ancillas clock. Thick black arrows indicate reset detections, associated to $\{k+\}$, and are possible only with ancillas in $|ee...e\rangle$. All other detections occur irrespectively of the Markov chain configuration, the respective transitions are only a consequence of the grouping of output signals. For instance, the blue arrows are associated to detections $\{k\,L\}$. From configurations R_1 and R_2, i.e. when only part of the qubits have reset, this leads to the error configuration E. On configuration G_{HZ}, such detection induces no transition. On R_3, detecting $\{1L\}$ leads to G_1, while detecting $\{k\,L\}$ with $k \neq 1$ (thus here there is only $\{2L\}$) would lead to G_0. For $n > 3$, the Markov chain would look similar with just additional states R_k^e and R_k^{mg} before R_n^e and R_n^{mg} on the top row, and additional states G_k^e and G_k^{mg} before G_{HZ}^e and G_{HZ}^{mg} on the lower row.

simple algebraic means. The full expressions are provided in the proof below, while the (more readable) result to leading orders in T_k/T_{k-1} is summarized in the following statement.

Proposition 11 *The Markov chain defined in Section 3.1.2 has all its steady-state population on G^{mg}_{HZ}, up to terms of order T_k/T_{k-1}. More precisely, assuming nT_k/T_{k-1} to remain small, we have:*

$$p_{G^{mg}_{HZ}} + p_{G^{e}_{HZ}} \;\approx\; 1 - \tfrac{\kappa_p}{\tilde\kappa_u} - n(n-1)\tfrac{\tilde\kappa_u}{\kappa_c} - \tfrac{\tilde\kappa_u}{\kappa_d} - n\ln(n)\tfrac{\kappa_c+\kappa_d}{\kappa_r} + O\left((\tfrac{T_k}{T_{k-1}})^2\right). \tag{3.26}$$

The terms in $n\ln(n)$ can be computed more precisely for given n, e.g. for $n=3$ replace $n\ln(n)\kappa_d$ by $4.5\kappa_d$ and $n\ln(n)\kappa_c$ by $3\kappa_c$.

Proof The steady state equation for R^{mg}_k readily yields

$$p_{R^{mg}_k} = \frac{\kappa_d}{\kappa_p + \tilde\kappa_u + \frac{n-1}{n}\kappa_c}\, p_{R^e_k} \quad , \quad \text{for } k = 1, 2, ..., n\,. \tag{3.27}$$

Next, the steady state equations for R^e_k write

$$\begin{aligned}
(n\kappa_p + n\kappa_d + (n-1)\kappa_c + (n-1)\kappa_r)p_{R^e_1} &= n\tilde\kappa_u p_{R^{mg}_1} + n\kappa_r\left(p_e - \textstyle\sum_{k=1}^n p_{R^e_k}\right) \quad , \\
(n\kappa_p + n\kappa_d + (n-1)\kappa_c + (n-k)\kappa_r)p_{R^e_k} &= n\tilde\kappa_u p_{R^{mg}_k} + (n-k+1)\kappa_r p_{R^e_{k-1}} \quad \text{for } k = 2, 3, ..., n\,,
\end{aligned} \tag{3.28}$$

where p_e is the total population on $\cdot^e$, irrespective of the data qubits situation. Using (3.27) and recalling that $p_e = \frac{\tilde\kappa_u}{\tilde\kappa_u + \kappa_d}$, this solves to:

$$\begin{aligned}
p_{R^e_n} &= \frac{p_e}{1 + \frac{a_0}{\kappa_r} + \frac{a_0(a_0+\kappa_r)}{2!\,\kappa_r^2} + ... + \frac{a_0(a_0+\kappa_r)...(a_0+(n-1)\kappa_r)}{n!\,\kappa_r^n}}\,, \\
p_{R^e_k} &= \frac{a_0(a_0+\kappa_r)...(a_0+(n-1-k)\kappa_r)}{(n-k)!\,\kappa_r^{n-k}}\, p_{R^e_n} \quad \text{for } k = 1, 2, ..., n-1\,, \\
\text{with} \qquad a_0 &= n\kappa_p + (n-1)\kappa_c + n\kappa_d \frac{\kappa_p + \frac{n-1}{n}\kappa_c}{\kappa_p + \frac{n-1}{n}\kappa_c + \tilde\kappa_u}\,.
\end{aligned} \tag{3.29}$$

Next, writing the steady state conditions for the pair of configurations G^{mg}_k, G^e_k leads to the explicit recursion:

$$\begin{aligned}
b_1\, p_{G^{mg}_k} &= \kappa_c\, p_{G^{mg}_{k-1}} + \tfrac{n\kappa_d}{b_0+n\kappa_d}\,\kappa_c\, p_{G^e_{k-1}}\,, \\
(b_0 + n\kappa_d)p_{G^e_k} &= \tfrac{n\tilde\kappa_u}{b_1}\,\kappa_c\, p_{G^{mg}_{k-1}} + \left(1 + \tfrac{n\kappa_d}{b_0+n\kappa_d}\tfrac{n\tilde\kappa_u}{b_1}\right)\kappa_c\, p_{G^e_{k-1}} \\
\text{with} \qquad b_0 &= n\kappa_p + \kappa_c + n\kappa_r \\
b_1 &= \left(n\kappa_p + n\tilde\kappa_u \tfrac{b_0}{b_0+n\kappa_d}\right)\,,
\end{aligned} \tag{3.30}$$

for $k = 2, 3, ..., n-2$. For $k = 1$, the expressions (3.30) hold but replacing $p_{G^{mg}_{k-1}}$ and $p_{G^e_{k-1}}$ on the right hand side respectively by $(p_{G^{mg}_0} + p_{R^{mg}_n})$ and $(p_{G^e_0} + p_{R^e_n})$. For $k = 0$, the expressions (3.30) hold but replacing $p_{G^{mg}_{k-1}}$ and $p_{G^e_{k-1}}$ respectively by $(n-2)p_{R^{mg}_n}$ and $(n-2)p_{R^e_n}$. This allows, at least in principle, to explicitly compute through to G^{mg}_{n-2} and G^e_{n-2}. Finally, the steady-state equations for G^{mg}_{HZ} and G^e_{HZ} lead to

$$\left(n\kappa_p + n\tilde\kappa_u \tfrac{\kappa_r+\kappa_p}{\kappa_r+\kappa_p+\kappa_d}\right)\, p_{G^{mg}_{HZ}} = \kappa_c\, p_{G^{mg}_{n-2}} + \tfrac{\kappa_d}{\kappa_d+\kappa_r+\kappa_p}\,\kappa_c\, p_{G^e_{n-2}}\,. \tag{3.31}$$

Note that, while we provide these exact expressions here for completeness, all the terms in G^e_k in fact have no impact on the leading-order computation.

The statement of the Proposition is obtained by concatenating these explicit expressions, keeping only the leading order terms in T_k/T_{k-1} to obtain a more readable result. For low values of n the sums in (3.29) can be computed explicitly, as we do for $n = 3$. For large values of n, we keep in this sum the first-order term in a_0/κ_r and then approximate like $\sum_{k=1}^n 1/k \approx \int_0^n 1/x\, dx = O(\ln(n))$. □

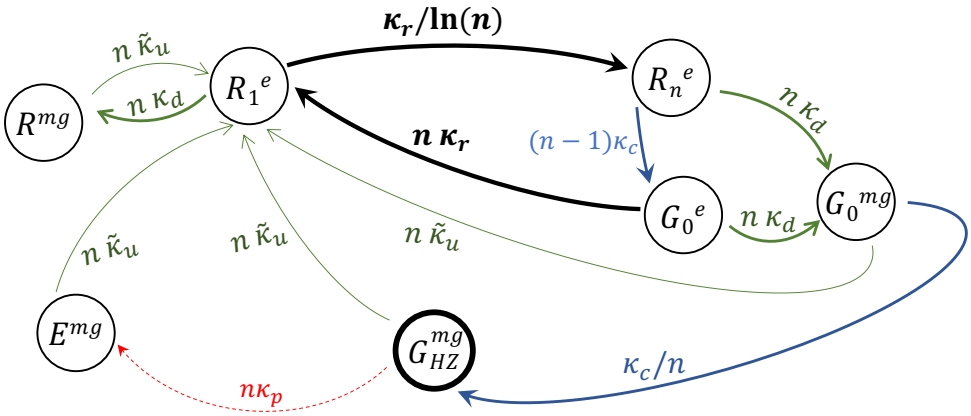

Figure 3.5: Further reduced Markov chain, with effective transition rates covering most relevant transitions, and yielding the same steady-state population on G_{HZ} as reported in Proposition 11.

The leading-order result reported in Proposition 11 is in fact the same as with the further reduced Markov chain represented on Figure 3.5.

We next argue why the ancilla configurations outside $|gg...g\rangle, |ee...e\rangle, |mm...m\rangle$ do not significantly modify this result.

In the context of Figure 3.4, the transition configurations model situations in which only part of the data qubits can undergo resets to $|+\rangle$. We only consider the main transition configurations (see definition above), which have population $O(T_3/T_1)$, since other configurations will have even lower impact. The argument goes as follows.

- A compact way to represent the limited synchronization at first order is to split each data qubit configuration into not 2 but 4 sub-levels, as represented on Figure 3.5. The sub-levels $|e_{\text{all}}\rangle$ and $|mg_{\text{all}}\rangle$ denote synchronized ancillas as before, while $|e_1\rangle$ and $|mg_1\rangle$ indicate that a single ancilla has jumped to the corresponding value. A transition of characteristic time $O(n/\kappa_{st})$ connects the single-ancilla to the all-ancillas sub-level.
- The distinction of one or all synchronization is sufficient for obtaining a pessimistic error bound, by modeling the data qubit transition rates as follows.
  - For data configuration E, i.e. when a first reset is needed, we take a lower bound on its likely occurrence by considering transition from E^{e_1} to $R_1^{e_1}$ at rate κ_r and from $E^{e_{\text{all}}}$ to $R_1^{e_{\text{all}}}$ at rate $n\kappa_r$.
  - For data configuration R_k, $k = 1, 2, ..., n-1$, i.e. when further resets are needed, we again take a lower bound and only allow them once the ancillas are on $|e_{\text{all}}\rangle$.
  - For all other data configurations, i.e. when resets would interrupt the intended GHZ-stabilizing cycle, we take an upper bound on this danger by considering transitions to $R_1^{e_1}$ and $R_1^{mg_1}$ at rates $(n-1)\kappa_r$, and transitions to $R_1^{e_{\text{all}}}$ at rate $n\kappa_r$.

More precisely, the main effect of imperfect ancilla synchronization is to smear out when data qubits enter the "reset" part of the cycle (top row on Figure 3.4).

The final estimate of the performance of our GHZ-stabilizing reservoir with ancillas clock state-conditioning, as described in Section 2.2.1, should further take into account the ancilla population outside the subspace spanned by $|gg...g\rangle, |ee...e\rangle, |mm...m\rangle$. However, as shown in Section 3.1.1, this is of second order (namely T_3/T_1), so the dominant contributions to the overall error are captured in Proposition 11.

Proposition 11 states the errors ordered according to T_1/T_0, T_2/T_1, T_3/T_2. All these ratios must be small to ensure a good fidelity to $|GHZ_+\rangle$. The reservoir engineering will usually be constrained by the observed error rate $1/T_0$ and the maximally achievable engineered reservoir rate $1/T_3$. The timescales T_1 and T_2 should be chosen between these two extremes to optimize the performance. The expression confirms that a gain by a factor C on T_0/T_3 shall be split up into gains of a factor $C^{1/3}$ on each of the error terms. Concretely, by taking the expression (3.26) as true, the best setting would take

$$\begin{aligned}
\tilde{\kappa}_u &\simeq \kappa_p \left(\frac{\kappa_r}{\kappa_p}\right)^{\frac{1}{3}} \frac{1}{n^{\frac{2}{3}} \ln(n)^{\frac{1}{3}}} \\
\kappa_d &\simeq \kappa_p \left(\frac{\kappa_r}{\kappa_p}\right)^{\frac{2}{3}} \frac{1}{n^{\frac{5}{6}} \ln(n)^{\frac{2}{3}}} \\
\kappa_c &\simeq \kappa_p \left(\frac{\kappa_r}{\kappa_p}\right)^{\frac{2}{3}} \frac{n^{\frac{1}{6}}}{\ln(n)^{\frac{2}{3}}} ,
\end{aligned}$$

for an error scaling roughly like $\left(n^{7/2} \ln(n)\, \kappa_p/\kappa_r\right)^{1/3}$. The scaling with n is of course quite approximate, given all the approximations made on the way. In the next section, we analyze the scheme based on the qutrits wave, which should improve the scaling towards $(\kappa_p/\kappa_r)^{1/2}$.

3.1.3 Simulations of the state-conditioning scheme

The simulation results consider the reservoir model (2.11) and (2.9) with $\kappa_r = \kappa_{st}$; we choose this setting despite the remark in 2.2.1 as we have already a lot of parameters to analyze. As an error model, we take back the one used in the theoretical analysis with bit-flip and phase-flip errors, with similar rate, on each qubit individually, associated respectively to decoherence operators:

$$E_{k,1} = \sqrt{\kappa_p}(|0\rangle\langle 1| + |1\rangle\langle 0|)_k \quad , \quad E_{k,2} = \sqrt{\kappa_p}(|0\rangle\langle 0| - |1\rangle\langle 1|)_k \ , \quad k = 1, 2, ..., n \ . \tag{3.32}$$

We then set up the full Lindblad equation and compute its steady-state, evaluating its fidelity to $|GHZ_+\rangle$ in presence of the perturbation.

We have performed simulations varying the parameter κ_r/κ_p and exploring values of the intermediate rate $\tilde{\kappa}_u$, κ_d and κ_c, for $n = 3, 4, 5, 6$. Those intermediate rates where taken around their theoretical best settings as seen in the previous sections; we only give the simulation for each n with the best results with the local optimum that was found on each parameter. Figure 3.6 shows the comparison between the the simulation values (colored full lines) and the theoretical value of the analysis (dotted black line). It confirms that our analytical formulas are close to the true error scaling, overestimating it by a fixed factor for higher value of κ_r/κ_p, which can be explained by the several approximations made along the analysis. The difference gets bigger for lower values of κ_r/κ_p. This tends to validate our analysis performed in Section 3.1.2 for high values of κ_r/κ_p.

3.2 Performance analysis: scheme based on data qutrits

In this section, we analyze the performance of the approximate-GHZ state stabilization schemes based on local bipartite interactions of data qutrits, as presented in Section 2.3. This also illustrates the analysis in the framework of a "reset wave" propagating along the data chain.

Like in Section 3.1.2, we focus on one prototypical case, namely the scheme of Section 2.3.2. For easing the theoretical analysis, again we slightly adapt the model in order to involve classical Markov chains based on hypothetical output detections. We have performed an approximate analysis in two ways. The first one checks how a reset wave (going through level $|2\rangle$) propagates

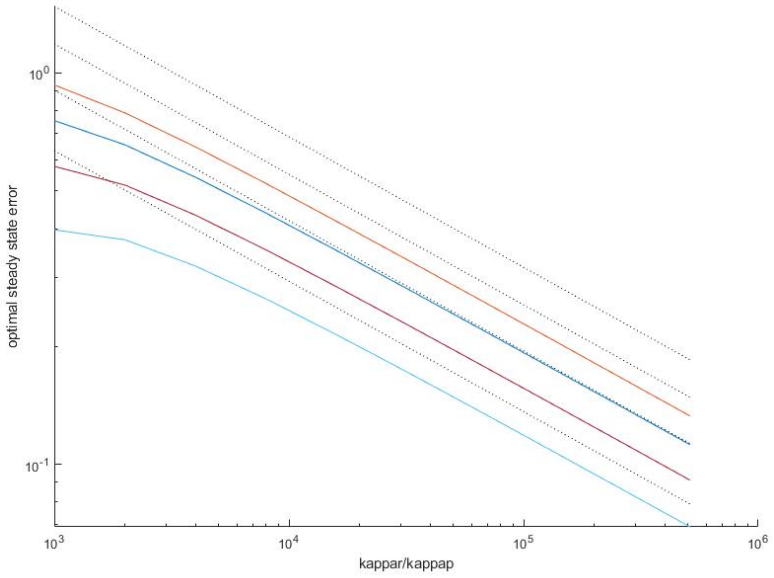

Figure 3.6: Steady state error corresponding to the setting of Figure 3.12. The number of qutrits is $n = 3, 4, 5, 6$ from bottom (lowest error) to top (largest error).

along the whole chain unperturbed by L_k events, then an L_k sub-sequence leads to $|GHZ_+\rangle$. This is easier to follow, and pessimistic by a small factor. Indeed, reset wave and GHZ-stabilizing wave can in principle propagate in parallel. A second analysis hence considers the characteristic time for those two waves in parallel; it involves estimating how to cross a 2-dimensional lattice.

3.2.1 Qutrit wave description with classical Markov chains

The qutrit level $|2\rangle$ plays a role analogous to the classical ancillas of Section 2.2. Each qutrit only jumps to and from this level $|2\rangle$ by involving states which are orthogonal to it. In particular:

- Consider an initial state $\rho(0)$ of the full system where $\langle 1|\rho(0)|2\rangle_k = \langle 0|\rho(0)|2\rangle_k = 0$ for all qutrits k, i.e. there are no quantum coherences involving level $|2\rangle$. Then this property remains true for $\rho(t)$ for all $t \geq 0$. The proof is trivial, just by inspecting the Lindblad equation for those components.

- Consider a model where for each qubit we only differentiate whether it is in level $|2\rangle$ or in the "logical" subspace span$\{|0\rangle, |1\rangle\}$, with populations thus denoted $p_{x_1,x_2,...}$ and each x_i taking the value either 2 or ℓ ("logical"); in other words, the levels $|0\rangle, |1\rangle$ are considered as a refined subdivision of the level $|\ell\rangle$, and we currently discard this refinement. Then the model of Section 2.3.2, aggregated in this way on $\{|\ell\rangle, |2\rangle\}^n$, does follow an autonomous classical Markov chain $\frac{d}{dt}p = A\,p$ with:

$$\begin{aligned} \langle 2|_1 A|\ell\rangle_1 &= \kappa_u \,\text{Identity}_{2^{n-1}} \,, \\ \langle \ell|_n A|2\rangle_n &= \kappa_{st} \,\text{Identity}_{2^{n-1}} \,, \\ \langle \ell, 2|_{k-1,k} A|2, \ell\rangle &= \kappa_{st} \,\text{Identity}_{2^{n-2}} \quad \text{for } k = 2, 3, ..., n \,, \end{aligned} \tag{3.33}$$

  zero for the other off-diagonal elements of A, and the diagonal fixed to ensure zero column sums. This property holds thanks to the internal state $|0\rangle$ or $|1\rangle$ of $|\ell\rangle$ having (by design) no effect on the aggregated jump probabilities involving $M_{...}$ and $N_{...}$ in (2.23), while the L_k only change the internal state of $|\ell, \ell\rangle_{k,k+1}$, and hence have no effect at this point.

This observation means that, in order to model the full process with a classical Markov chain, we need a particular approximate procedure only when treating the effect of the L_k, and possibly of

the perturbation. The procedure is similar to Section 3.1.2, to which we refer the reader for more details and justifications.

The basic idea is to associate a (virtual) detector monitoring when jump operators are applied, in a Poissonian unraveling of the Lindblad master equation. We gather in an output signal $q(t)$ the sequence of detection events. Then, we associate a configuration of the Markov chain to a set of signals $q(t)$ ending with a particular property, for instance:

> Configuration E: any $q(t)$ ending with an application of an error channel on a qutrit.
>
> Configuration G_{n-1}: any $q(t)$ whose ending comprises a sequence of jumps which we have identified (see later) as bringing $\rho(t)$ exactly onto the target GHZ state.

This construction involves both an exact Markov property, and an approximation.

- The exact Markov property is that we want the jumps between these configurations to follow, exactly, an autonomous Markov chain. In other words, the probability rate for jumping say from configuration μ_{n-1} to configuration E should at most depend on the fact that we are on μ_{n-1}, and on nothing else in the original system. For detection of jumps involving level $|2\rangle$, this is trivial thanks to the above observations. For the other jumps, we need some conditions.
  - Regarding error channels: we will assume, to get this Markov property, that each qutrit in the original system is independently undergoing the possibility of an "error" jump at a rate κ_p, from any state $\rho(t)$. This would not be true for instance for a decay channel, where the error rate would typically depend on the energy in $\rho(t)$; but assuming a uniform rate is a reasonable way to get a pessimistic bound.
  - Regarding the L_k operators: With the L_k operators of Section 2.3.2, the probability of detecting a jump depends not only on whether we are on $|2\rangle$ or $|\ell\rangle$, which a classical Markov chain can model (see above), but also on where $\rho(t)$ is inside the logical subspace. Indeed, L_k only acts on the subspace where qutrits k and $k+1$ take different values. Unfortunately, this is where quantum Lindblad appears as richer than a classical Markov chain: a reset jump will map $\rho(t)$ to a quantum superposition involving this subspace on which L_k acts, and its complement. To avoid modeling this process with a Lindblad equation, we can simply like in Section 3.1.2 modify the setting by assuming that we have two operators L_k and $\tilde{L}_k$ whose jumps we do not distinguish in the outputs, see (3.25). The probability of detecting a jump with L_k or $\tilde{L}_k$ indistinguishably is now the same for any state of type $|\ell,\ell\rangle_{k,k+1}$, allowing us to discard the exact evolution of $\rho(t)$.

  Importantly, with this, we do not need to model $\rho(t)$ and backaction of no-detection events etc. Instead, we can rigorously reduce the Lindblad equation to a classical Markov chain on "last-detected-jump(s)" space.

- The approximation resides in how we interpret the results of this Markov chain towards deducing an evolution of $\rho(t)$, in particular its fidelity to GHZ. Indeed, a particular output-signal configuration can correspond to many states $\rho(t)$ and those are in general not all orthogonal to $|GHZ_+\rangle$. Nevertheless, in a simplifying and pessimistic approximation, we will count as successful only the output-signal sequences after which we are certain to be on $|GHZ_+\rangle$, and these are summarized by configuration μ_{n+1}. In particular, after an error jump detection (configuration E), we will assume that successful overlap with $|GHZ_+\rangle$ is obtained only after applying a full reset and stabilizing sequence, although in reality this should not be necessary for any errors on any qutrits. Refinements of this approximation should be possible, but it appears to capture the dominant effect and compares reasonably well to simulations.

The definition of Markov chain configurations is somewhat different in the two analyses. It will built on an output signal $q(t)$ like in Section 3.1.2, which are a succession of detection events taken from

> $\{k\,L\}$: jump with L_k or $\tilde{L}_k$, for $k = 1, 2, ..., n-1$ (rate κ_c)

$\{k+\}$: jump with any of the $N_{k,...}$ indistinguishably for $k = 1, 2, ..., n$ (rate κ_{st})

$\{U\}$: jump with any of the $M_{0,...}$ indistinguishably (rate κ_u)

$\{k\,E\}$: jump with any of the error operators on qutrit k indistinguishably (rate κ_p)

3.2.2 Details of the qutrit-wave analysis, first method

This method considers that, in order to reach $|GHZ_+\rangle$, the system must undergo first a sequence of resets through level $|2\rangle$ *irrespectively of the occurrence of any* L_k *jumps* (see main text describing this advantage of the wave), then a sequence of jumps with L_k exclusively and containing the ordered sub-sequence $L_1, L_2, ...L_{n-1}$.

A benign but somewhat tedious task in the modeling, is that jumps at rate κ_p (errors) can in principle bring the system into any states. For instance, it could happen that while qutrits $1, 2, ..., k$ have just reset, another reset wave suddenly starts at e.g. $k + 3$ because an error much earlier had brought qutrit $k + 3$ onto level $|2\rangle$. This is benign because every κ_p effect on qutrits $1, 2, ..., k$ has been erased when the reset wave has reached k, while any event on qutrits $k + 1, k + 2, ...$ has no importance as the reset wave is going to wipe it out. More formally, we thus define the following classical Markov chain configurations, where each configuration aggregates a set of detection signals:

- U: any $q(t)$ ending with $\{U\}$, followed by an arbitrary sequence of $\{k+\}$ or $\{k\,L\}$ all with $k > 1$;
- R_k for $k = 1, 2, ..., n-1$: any $q(t)$ ending with $\{U\}$, followed by an arbitrary sequence of $\{k+\}$ or $\{k\,L\}$ containing the sub-sequence $\{1+\}, \{2+\}, ..., \{k+\}$ but not the sub-sequence $\{1+\}, \{2+\}, ..., \{k+1+\}$;
- R_n: any $q(t)$ ending with $\{U\}$, followed by an arbitrary sequence of $\{k+\}$ or $\{k\,L\}$ containing the sub-sequence $\{1+\}, \{2+\}, ..., \{n+\}$ but not the sub-sequence $\{1+\}, \{2+\}, ..., \{n+\}, \{1\,L\}$;
- G_k for $k = 1, 2, ..., n-2$: any $q(t)$ any with a sequence like R_n, followed by an arbitrary sequence of $\{k\,L\}$ containing the sub-sequence $\{1\,L\}, \{2\,L\}, ..., \{k\,L\}$ but not the sub-sequence $\{1\,L\}, \{2\,L\}, ..., \{k+1\,L\}$;
- $G_{n-1} =: G_{HZ}$: same as G_k, except the last condition is dropped since $\{n, L\}$ does not exist;
- E: any other $q(t)$, i.e. not containing $\{U\}$ or ending with $\{k\,E\}$ for some k not followed by $\{U\}$.

All signals $q(t)$ should take one of these forms. More precisely, an initial transient may yield arbitrary detections until $\{U\}$ is detected once; these are covered by configuration E. After that, we cannot have $\{1\,L\}$ before having seen either $\{1+\}$ or $\{1\,E\}$, i.e. we are in configuration U until switching either to R_1 or back to E. This reasoning can be pursued to show that all possible configurations are covered. The Markov chain with its corresponding transition rates is shown on Figure 3.7 left.

The attentive reader will have noticed that we have been pessimistic on several points in this aggregation of output signals.

First, we have required for reaching G_{HZ} that we follow first a full reset wave, then a full L_k wave. In principle, the two could propagate together, and an analysis in this way is carried out in the next section.

Second, starting from $|++...+\rangle$, it is not strictly necessary to have $\{1\,L\}, \{2\,L\}, ..., \{n-1\,L\}$ in order to end up on $|GHZ_+\rangle$. However, the possible alternatives see to be few, at the cost of a more complicated analysis, which we will not carry out.

Third, we have considered that, from any configuration, any error brings us into a "completely useless" configuration E from which the whole reset-then-L_k wave must be reapplied. This is of course pessimistic, since e.g. in the output sequence ending with $\{U\}, \{1+\}, \{2+\}, \{4\,E\}$, the error detection has no lasting effect and will be just erased by pursuing the reset wave.

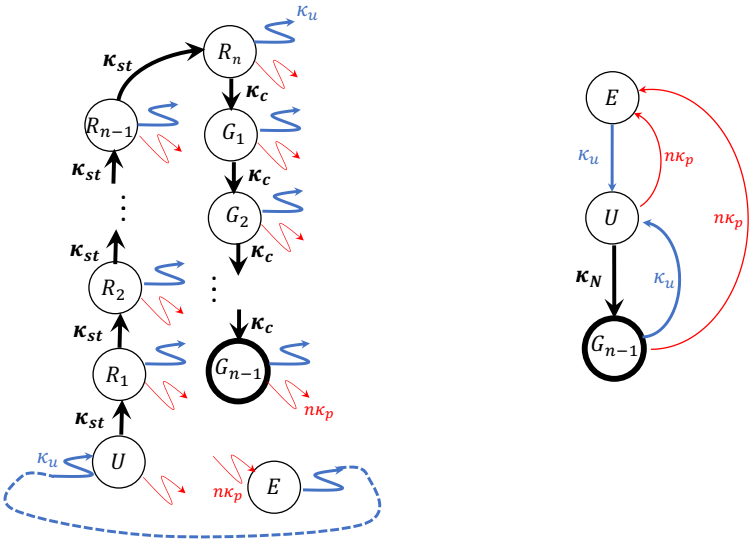

Figure 3.7: Left: The Markov chain used for the analysis of Section 3.2.2. Wiggly arrows indicate that all outflows connect to the inflow of the same color and shape. Right: reduced Markov chain where $1/\kappa_N$ is the expected time to cross the chain on the left from U to G_{n-1}, and yielding the same steady state $p_{G_HZ} = p_{G_{n-1}}$ at first order in $\epsilon,\ \epsilon_2$.

The grouping made above allows us to significantly simplify the analysis, by having a uniform rate $n\kappa_p$ of flowing towards E. Moreover, a more precise modeling can make no difference on the leading order. Indeed, we are targeting $p_{GHZ} = 1 - O(\epsilon, \epsilon_2)$; with this, just taking into account a flow at rate $n\kappa_p$ from G_{HZ} towards E, together with a rate κ_U for leaving E by launching a reset wave, we would already obtain $p_E > n\kappa_p(1 - O(\epsilon)) \ / \ \kappa_u = n\epsilon_2 + o(\epsilon, \epsilon_2)$. The result reported in Proposition 13, thus with the Markov chain of Figure 3.7 left, says no worse in terms of ϵ_2 error.

The result reported in Proposition 13, first part, is obtained rather directly by writing the steady state condition of the Markov chain depicted on Figure 3.7left, in a sequential way starting at configuration U:

$$\begin{aligned}
(\kappa_{st} + n\kappa_p)\, p_U &= \kappa_u(1 - p_U) \quad \Rightarrow \quad p_U = \tfrac{\kappa_u}{\kappa_p+\kappa_u+\kappa_{st}} \\
(\kappa_{st} + n\kappa_p + \kappa_u)\, p_{R_1} &= \kappa_{st} p_U \\
(\kappa_{st} + n\kappa_p + \kappa_u)\, p_{R_k} &= \kappa_{st} p_{R_k} \quad \Rightarrow \quad p_{R_k} = \left(\tfrac{\kappa_s t}{\kappa_p+\kappa_u+\kappa_{st}}\right)^k p_U \\
(\kappa_c + n\kappa_p + \kappa_u)\, p_{R_n} &= \kappa_{st} p_{R_{n-1}} \quad \Rightarrow \quad p_{R_n} = \tfrac{\kappa_s t}{\kappa_p+\kappa_u+\kappa_c}\, p_{R_{n-1}}
\end{aligned}$$

and similarly

$$p_{G_k} = \left(\tfrac{\kappa_c}{\kappa_p+\kappa_u+\kappa_c}\right)^k p_{R_n} \quad , \quad p_{G_HZ} = \tfrac{\kappa_c}{\kappa_p+\kappa_u}\, p_{G_{n-2}} \ .$$

Multiplying this out, we get

$$p_{G_HZ} = \left(\tfrac{\kappa_s t}{\kappa_p+\kappa_u+\kappa_{st}}\right)^n \left(\tfrac{\kappa_c}{\kappa_p+\kappa_u+\kappa_c}\right)^{n-1} \tfrac{\kappa_u}{\kappa_p+\kappa_u} \ .$$

Introducing the notation $\epsilon, \epsilon_2, \gamma$ and keeping only the first order terms in ϵ, ϵ_2 yields the reported result.

Note that the same result would be obtained, at first order, as a steady state of the Markov chain represented on Figure 3.7 right, where we have summarized the whole chain of dominating events, i.e. with κ_{st} and κ_c, by a single transition at an effective rate κ_N. This effective rate is

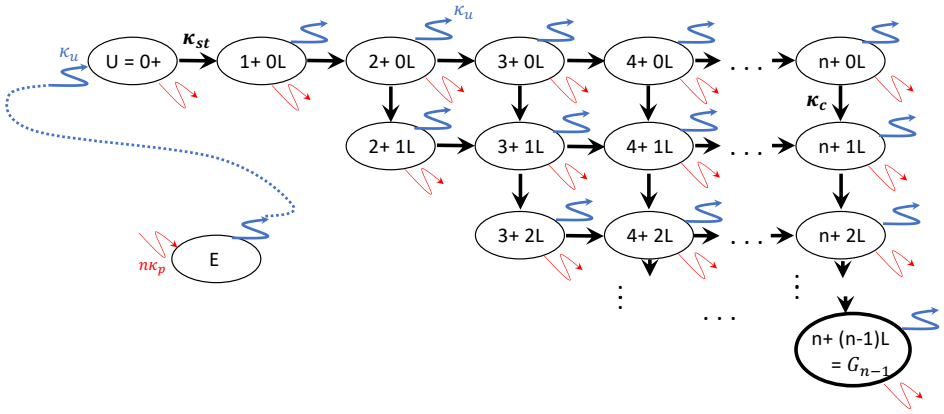

Figure 3.8: Markov chain defined for the "wave-propagation" analysis of Section 3.2.3. Like on other figures, outgoing wiggly arrows represent a flow towards the wiggly arrow of the same color and shape.

computed such that $1/\kappa_N$ corresponds to the expected time for crossing the chain of Figure 3.7 left from U to G_{n-1}, thus

$$\frac{1}{\kappa_N} = \frac{n}{\kappa_{st}} + \frac{n-1}{\kappa_c} \,.$$

This reduction is possible because jumps out of this chain happen at the same rates κ_p and κ_u irrespectively of the precise configuration. Our second analysis will hence directly aim at such characteristic times.

3.2.3 Details of the qutrit-wave analysis, second method

In the previous section, we consider that the wave of resets, propagating through level $|2\rangle$, has to finish first before a wave of L_k (or $\tilde{L}_k$) would be launched and reach the GHZ state. Since κ_c and κ_{st} are of the same order, there is no reason for the reset wave to finish before the L_k wave starts. We can thus try another analysis to take into account this concomitant propagation, instead of capturing only the success rate of two consecutive waves.

We hence define a Markov chain based on the following configurations. See Section 3.2.2 for possible remarks and explanations, and Figure 3.8 for a more visual explanation.

- U: any $q(t)$ ending with $\{U\}$, followed by an arbitrary sequence of $\{k+\}$ or $\{k\,L\}$ all with $k > 1$;
- $\{j_1 + j_2\,L\}$ for $j_2 < j_1$ and : any $q(t)$ ending with $\{U\}$, followed by an arbitrary sequence of $\{k+\}$ or $\{k\,L\}$ containing two sub-sequences $s_{+,j_1} := \{1+\},\{2+\},...,\{j_1+\}$ and $s_{L,j_2} := \{1\,L\},\{2\,L\},...,\{j_2\,L\}$; those sequences are interleaved such that $\{j\,L\}$ of sub-sequence s_{L,j_2} comes after $\{j+1+\}$ of sub-sequence s_{+,j_1}, for all $j = 1, 2, ..., j_2$. Furthermore, $q(t)$ contains no corresponding sub-sequences for $j_1' > j_1$ or $j_2' > j_2$.

  In particular, we have $\{n + (n-1)\,L\} =: G_{HZ}$.
- E: any other $q(t)$, i.e. not containing $\{U\}$ or ending with $\{k\,E\}$ for some k not followed by $\{U\}$.

All signals $q(t)$ should take one of these forms. More precisely, an initial transient may yield arbitrary detections until $\{U\}$ is detected once; these are covered by configuration E. After that, we cannot have $\{1\,L\}$ before having seen either $\{1+\}$ or $\{1\,E\}$, i.e. we are in configuration U until switching either to $\{1+0L\}$ or back to E. The states $\{j_1 + j_2\,L\}$ cover all possible combinations. Note that after having detected a sub-sequence $\{U\}\{1+\},\{2+\},...,\{j+\}$, it is impossible to re-detect any of the $\{k+\}$ with $k \leq j$, without re-encountering $\{U\}$ or some $\{k\,E\}$ before. Therefore,

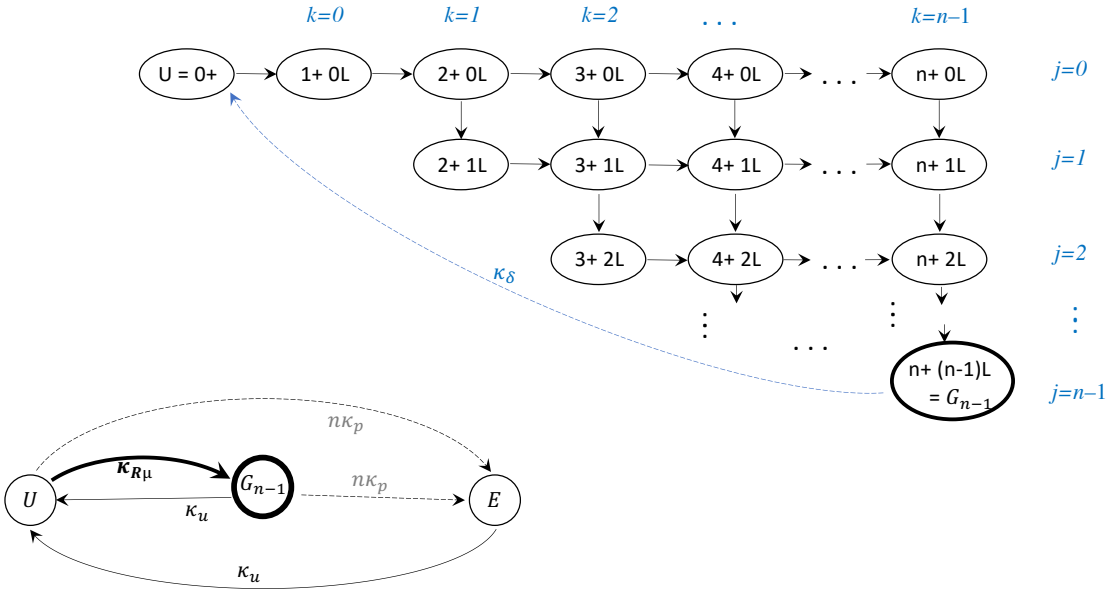

Figure 3.9: Simplified analysis for the Markov chain of Figure 3.8. Bottom left: reduced Markov chain where the fast transitions of Figure 3.8, i.e. those involving κ_c and κ_{st}, have all been aggregated into a single jump at effective rate $\kappa_{R\mu}$. Top right: The rate $\kappa_{R\mu}$ is computed such that $1/\kappa_{R\mu}$ is the expected time to cross this lattice from $|U\rangle$ to $|G_{n-1}\rangle$. All transitions here are at rate $\kappa_c = \kappa_{st}$. The coordinates labeled in blue, as well as the transition back from $|G_{n-1}\rangle$ to $|U\rangle$ at rate κ_δ, are used in the analysis leading to the value of $\kappa_{R\mu}$.

the effect of the $\{k\,L\}$ in the sub-sequence s_{L,j_2} defining $\{j_1 + j_2\,L\}$, will indeed be preserved, hence progressing towards $|GHZ_+\rangle$, unless we re-encounter $\{U\}$ or some $\{k\,E\}$ and thus switch to configuration U or E.

Like in Section 3.2.2, this Markov chain aggregates some output signals in a pessimistic way, e.g. assuming that a full stabilization chain has to be re-applied after any $\{k\,E\}$ has occurred on any starting configuration. However, at first order this has no effect, and it greatly simplifies the analysis. Our goal is to compute and maximize the steady state population on $\{n + (n-1)\,L\} =: G_{HZ}$, which we identify as the sole configuration contributing to $|GHZ_+\rangle$. We readily take $\kappa_c = \kappa_{st}$ at the maximal achievable reservoir rate.

The Markov chain represented on Figure 3.8 is harder to analyze exactly. Instead, we directly resort to the technique of characteristic times mentioned at the end of Section 3.2.2. Namely, we compute the steady state of the Markov chain shown on the bottom left of Figure 3.9, which has summarized all the "fast" transitions (i.e. those with κ_c and $\kappa_s t$) as a single jump with effective rate $\kappa_{R\mu}$, where $1/\kappa_{R\mu}$ is the expected time to cross the "fast transition lattice" represented on the top right of Figure 3.9.

The main analysis work is to properly estimate the transition rate $\kappa_{R\mu}$. Once this is fixed, a simple calculation gives

$$p_{G_{n-1}} = \frac{1}{(1+n\epsilon_2)(1+\tilde{\epsilon}+n\epsilon_2\tilde{\epsilon})} \simeq 1 - n\epsilon_2 - \tilde{\epsilon} + n^2\epsilon_2^2 + \tilde{\epsilon}^2 \tag{3.34}$$

where $\epsilon_2 = \kappa_p/\kappa_u$ and $\tilde{\epsilon} = \kappa_u/\kappa_{R\mu}$.

The *expected time* to cross the lattice on the top right of Figure 3.9 can be obtained as

$$1/\kappa_{R\mu} = 1/\kappa_\delta \left(\frac{1}{\bar{p}_{G_{n-1}}} - 1 \right) ,$$

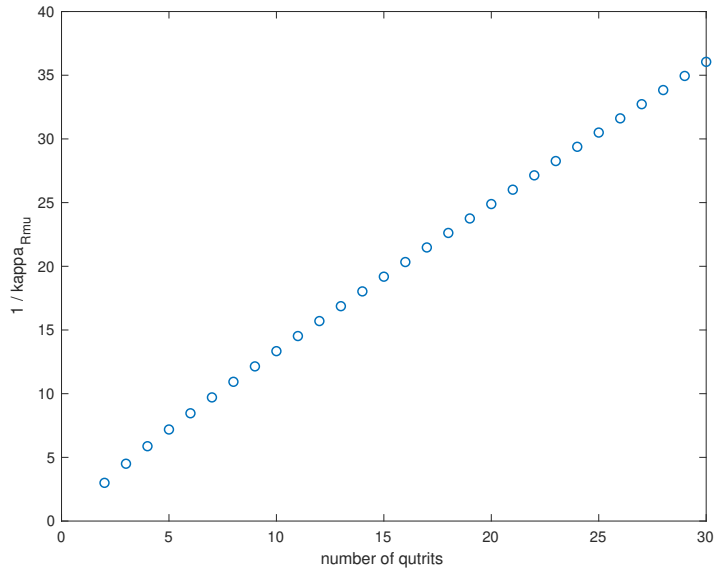

Figure 3.10: Rate $\kappa_{R\mu}$ computed as the inverse of the expected time to cross the lattice of Figure 3.9 from $|U\rangle$ to $|n+(n-1)L\rangle$, as a function of the lattice size n.

where $\bar{p}_{G_{n-1}}$ is the population on $|G_{n-1}\rangle$ in the steady state of the Markov chain associated to the lattice with an additional transition at rate κ_δ back from $|G_{n-1}\rangle$ to $|U\rangle$ (blue arrow on Figure 3.9). The following properties are easy to show recursively.

Proposition 12 *Denote by $\bar{p}_{j,k}$ the steady state population on the node depicted at coordinates j,k in the lattice of Figure Figure 3.9.*

- *(Steady-state relative population) For $j=0,1,...,n-2$ and $k=j,j+1,...,n-2$, we have*

$$\bar{p}_{j,k} = \bar{p}_{0,0}\; C^j_{j+k} \;/\; 2^{k+j}\;.$$

For $k=n-1$, we can compute recursively with

$$\begin{array}{rcl} \bar{p}_{0,n-1} & = & \bar{p}_{0,n-1} \quad , \quad \bar{p}_{n-1,n-1} = \bar{p}_{0,0}\,\frac{\kappa_{st}}{\kappa_\delta} \\ \bar{p}_{j,n-1} & = & \bar{p}_{j-1,n-1} + \bar{p}_{j,n-2} \quad \textit{for } j=1,2,...,n-2\;. \end{array}$$

One can double-check the recursion with the formula $\bar{p}_{n-2,n-1} = \bar{p}_{0,0}$.

Finally, $\bar{p}_U = \bar{p}_{0,0}$.

- *(Total and explicit population) The total population on row j of the lattice is*

$$\begin{array}{rcl} \textit{For } j=0: & \bar{p}_U + \sum_{k=0}^{n-1}\bar{p}_{0,k} \;=\; 3\,\bar{p}_{0,0} \\ \textit{For } j=1,2,...,n-2: & \sum_{k=j}^{n-1}\bar{p}_{0,k} \;=\; \bar{p}_{0,0}\left(1 + C^{j-1}_{2j-1} \;/\; 2^{(2j-1)}\right)\;. \\ \textit{For } j=n-1: & \bar{p}_{n-1,n-1} = \bar{p}_{0,0}\,\frac{\kappa_{st}}{\kappa_\delta}\;. \end{array}$$

From this, one deduces

$$\bar{p}_{\mu_{n-1}} = \frac{\kappa_{st}}{\kappa_\delta}\,\bar{p}_{0,0} = \frac{\frac{\kappa_{st}}{\kappa_\delta}}{(n-1)+2+\frac{\kappa_{st}}{\kappa_\delta}+\sum_{j=1}^{n-2}\frac{C^{j-1}_{2j-1}}{2^{(2j-1)}}}$$

and thus finally the rate

$$\kappa_{R\mu} = \kappa_{st}\;\frac{1}{n+1+\sum_{j=1}^{n-2}\frac{C^{j-1}_{2j-1}}{2^{(2j-1)}}} \tag{3.35}$$

The first iterations yield:

$$n=2:\ \kappa_{R\mu}=\tfrac{\kappa_{st}}{3}\quad,\quad n=3:\ \kappa_{R\mu}=\tfrac{\kappa_{st}}{4.5}\ ,$$
$$n=4:\ \kappa_{R\mu}=\tfrac{\kappa_{st}}{5+7/8}\quad,\quad n=5:\ \kappa_{R\mu}=\tfrac{\kappa_{st}}{6+19/16}\ .$$

The rate is graphically represented on Figure 3.10. For large n it roughly scales as

$$\kappa_{R\mu}\simeq\frac{\kappa_{st}}{n}\ .$$

Plugging this into the formula (3.34), we obtain the result announced in Proposition 13, part 2.

3.2.4 Results of approximate analysis

Proposition 13 *Denote $\kappa_u/\kappa_{st}=\epsilon\ll 1$, $\kappa_c/\kappa_{st}=\gamma=O(1)$ and $\kappa_p/\kappa_u=\epsilon_2\ll 1$.*

- *The Markov chain analysis described in 3.2.2 estimates a $|GHZ_+\rangle$ state population*

$$p_{GHZ+}\geq 1-n\epsilon_2-n\epsilon-\tfrac{(n-1)\epsilon}{\gamma}+o(\epsilon,\epsilon_2)\ . \tag{3.36}$$

- *The Markov chain analysis described in 3.2.3 estimates a $|GHZ_+\rangle$ state population*

$$p_{GHZ+}\simeq 1-n\epsilon_2-n\epsilon+o(\epsilon,\epsilon_2)\ , \tag{3.37}$$

  where we have assumed $\gamma=1$.

A realistic design constraint would be an upper bound $\bar{B}\gg 1$ on the ratio $\max(\kappa_{st},\kappa_c)/\kappa_p$ between maximally achievable reservoir rates and perturbation rate, which translates into

$$\frac{\max(1,\gamma)}{\epsilon\epsilon_2}\leq\bar{B}\ . \tag{3.38}$$

Thanks to having less timescales compared to the ancilla-based architectures of Section 3.1, an improvement by a factor c on $\bar{B}$ now enables an improvement by $\sqrt{c}$ on both ϵ and ϵ_2 and thus on the dominant error. In fact, we can compute the optimal tuning according to the estimates of Proposition 13.

- In (3.36), for ϵ,ϵ_2 fixed it is beneficial to increase γ, hence $\gamma<1$ cannot be optimal. Once $\gamma\geq 1$, the constraint (3.38) requires to modify ϵ,ϵ_2 if we further increase γ, and it turns out that the overall effect is disadvantageous; thus, we should take $\gamma=1$. This makes sense intuitively, as there seems to be no reason in our wave reservoir to slow down either κ_c or κ_{st} below the maximally achievable rate $\bar{B}\,\kappa_p$.

  The optimal value of κ_u, which determines the optimal values of $\epsilon^{(*)},\epsilon_2^{(*)}$, can then be computed with a Lagrangian involving the constraint $\epsilon\epsilon_2-1/\bar{B}=0$. Standard computations lead to

$$\epsilon^{(*)}=\sqrt{\frac{n}{\bar{B}(2n-1)}}\quad,\quad\epsilon_2^{(*)}=\sqrt{\frac{2n-1}{n\bar{B}}}\ .$$

  The corresponding performance is

$$p_{GHZ+}\simeq 1-2\sqrt{n\frac{2n-1}{\bar{B}}}\ .$$

  As anticipated, the error scales as $\sqrt{\cdot}$ in $\kappa_p/\kappa_{\text{reservoir}}$. It scales essentially linearly in n.

- In (3.37), we observe a somewhat better scaling with n. The optimal setting is (by symmetry) to take

$$\epsilon^{(*)}=\epsilon_2^{(*)}=\sqrt{\tfrac{1}{\bar{B}}}$$

  with a corresponding performance

$$p_{GHZ+}\simeq 1-2n\sqrt{\tfrac{1}{\bar{B}}}\ . \tag{3.39}$$

  The suggested optimal setting for κ_u is thus independent of n, the error estimate still linear in n and winning a factor $\sqrt{2}$.

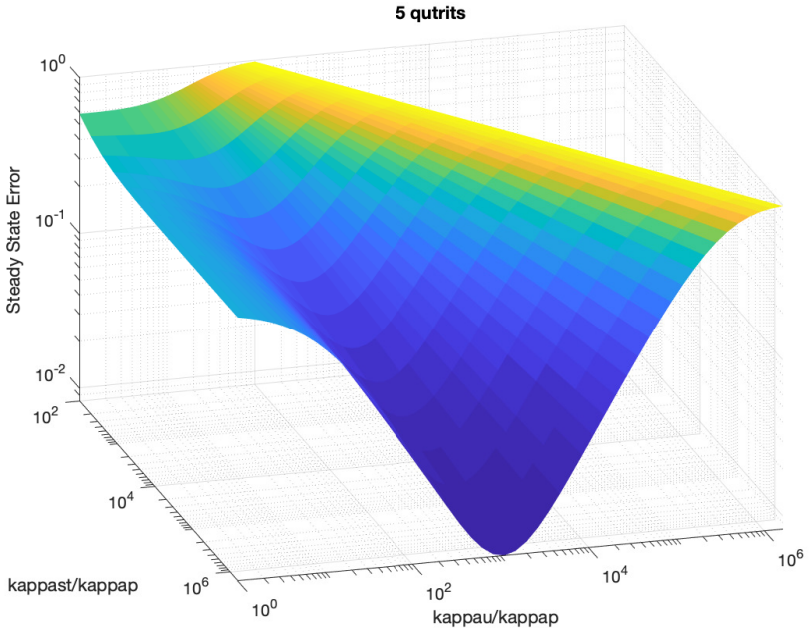

Figure 3.11: Simulation results of the steady state error with respect to the target state $|GHZ_+\rangle$, for the qutrit wave reservoir architecture and error channels $P_{k,j}$ with $k = 1, ..., 6$ and $j = 1, ..., n$ described at the beginning of Section 3.2.5. We here vary κ_u and κ_{st} (in units of the perturbation rate κ_p) for an illustratively fixed $n = 5$.

3.2.5 Simulations of the qutrit-based scheme

The simulation results consider the reservoir model (2.23) with $\kappa_c = \kappa_{st}$, since taking both at the maximal achievable jump rate seems beneficial. In particular, we do not assume the presence of some $\tilde{L}_k$ as we did for the analysis. As an error model, we wanted on each qutrit independently a channel drawing it towards the fully mixed state $\rho = \frac{|0\rangle\langle 0|+|1\rangle\langle 1|+|2\rangle\langle 2|}{3}$. For simplicity and in absence of any concrete physical model in mind, we implement this with the $6n$ jump operators:

$$P_{k,1} = \sqrt{\kappa_p}|0\rangle\langle 1| \ , \quad P_{k,2} = \sqrt{\kappa_p}|0\rangle\langle 2| \ , \quad P_{k,3} = \sqrt{\kappa_p}|1\rangle\langle 2| \ ,$$
$$P_{k,4} = \sqrt{\kappa_p}|1\rangle\langle 0| \ , \quad P_{k,5} = \sqrt{\kappa_p}|2\rangle\langle 0| \ , \quad P_{k,6} = \sqrt{\kappa_p}|2\rangle\langle 1| \ .$$

We then set up the full Lindblad equation and compute its steady-state, evaluating its fidelity to $|GHZ_+\rangle$ in presence of the perturbation.

We have performed simulations varying the parameter $\bar{B} = \kappa_{st}/\kappa_p$ and exploring values of the intermediate rate κ_u, for $n = 3, 4, 5, 6$. Beyond this number, the exponential scaling in n lead to too expensive simulations on a laptop. Figure 3.11 illustrates how the steady state error scales with κ_u and κ_{st} for fixed κ_u, and here for $n = 5$. Other numbers of qutrits show essentially the same behavior. A valley of optimal κ_u, leading to minimal error, is clearly visible.

Figure 3.12 shows the optimal value of κ_u, leading to this minimal error, as a function of n and κ_{st} (in units of κ_p). The simulation values (colored full lines) indicate a below-sampling-step dependence on n over these few values. They are in good agreement with the theoretically computed optimal setting, shown as a black dotted line (analysis of Section 3.2.2) and as black dots (analysis of Section 3.2.3). Figure 3.13 shows the corresponding steady state error. It confirms that our analytical formulas are close to the true error, overestimating it for lower values of κ_{st}/κ_p. The analysis of Section 3.2.3 appears to be quite close to the "truth" (i.e. full simulation values).

Before concluding, we must recall that a still better dependence on n is probably possible, if one considers the fidelity obtained by using the $|GHZ_+\rangle$ state progressively, from $k = 1$ up to $k = n$, at the same rate as the propagation of the "stabilization wave" along the qutrit chain; see

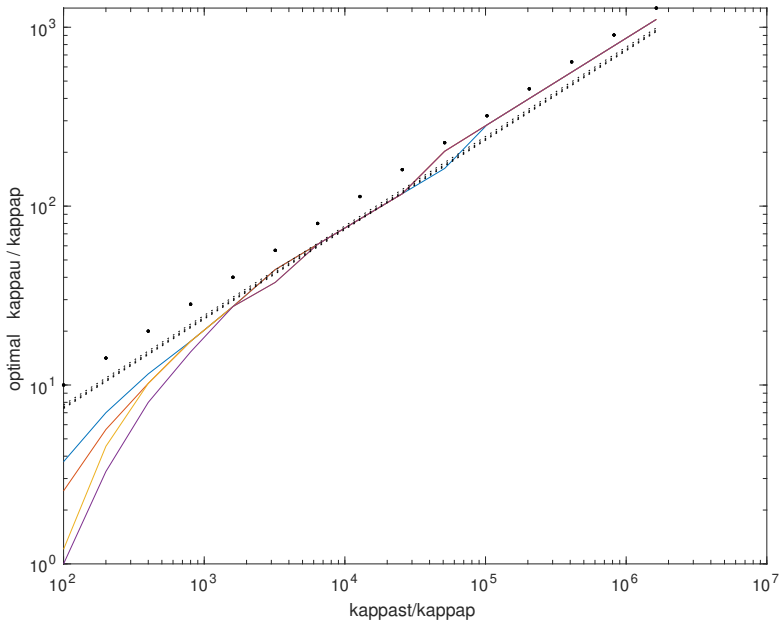

Figure 3.12: Optimal value of κ_u (in units of κ_p), leading to the smallest steady state error with respect to $|GHZ_+\rangle$ under the same conditions as Figure 3.11, as a function of n (colors) and of maximal reservoir power κ_{st} (in units of κ_p). Full colored lines are simulation results, dotted black lines represent the analysis of Section 3.2.2, black dots represent the analysis of Section 3.2.3. The number of qutrits is $n = 3, 4, 5, 6$.

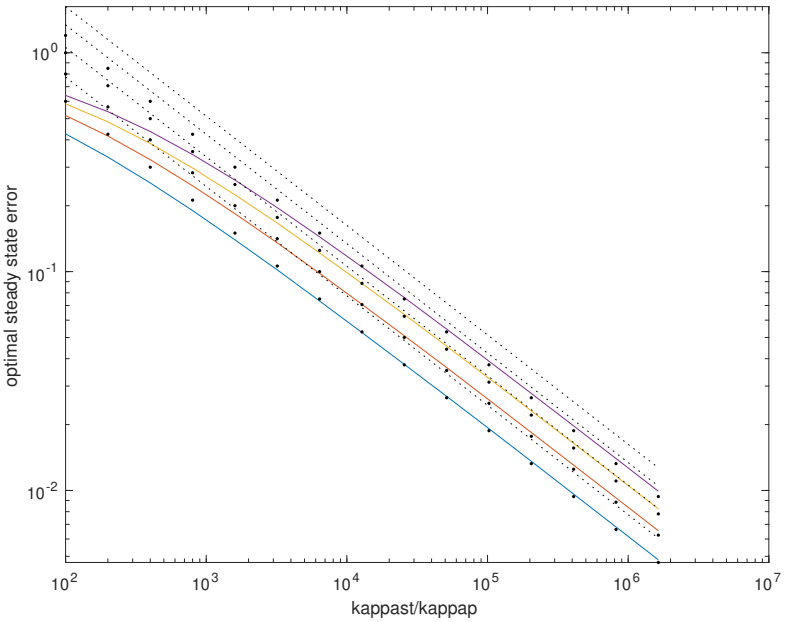

Figure 3.13: Steady state error corresponding to the setting of Figure 3.12. The number of qutrits is $n = 3, 4, 5, 6$ from bottom (lowest error) to top (largest error).

Section 2.2.3. We leave this open for future work since (i) it would only be relevant if a proper application using $|GHZ_+\rangle$ in this "wave-manner" is identified and (ii) the benefits for larger n would be hardly noticeable in our small-scale simulations anyways.

In this chapter we have analyzed two examples of set-ups stabilizing GHZ states by local couplings. We have given optimal parameters for the different rates of our systems in order to have a steady state as close to GHZ as possible. The main result was to give the scaling of the error in both set-up as a function of the number of qubits n and the ratio between the smallest and biggest rate of the system, backed by numerical simulations.

The analysis was performed using Markov chains, which required some simplifications in the model to allow this method. A potential improvement of this work would be to use adiabatic eliminations techniques to study the full Lindbladian chain without using the Markov simplifications. We note that this protocol could be applied to the stabilization of other entangled states, provided we have other conditional stabilization procedures for this state similar to 2.7.

Chapter 4

Quantum error correction set-ups with reservoir engineering

In this chapter, we will analyze two different set-ups performing error correction thanks to reservoir engineering. Throughout this chapter, we are focusing on the biased noise context (e.g. cat-qubits [21]), where one type of error is already suppressed in hardware and only a bias-preserving classical error correction scheme is needed in order to correct the other type of error. We hence consider two schemes for classical error correction of bit flips, yet implemented in a quantum-dissipative (Lindblad-type) setup. Both interlink qubits on a 2D-network and follow the constraint to use only local interactions. In section 4.1, we propose a simple way to scale the already existing three qubits code from [9], with a focus on keeping the local couplings and finding efficient parameters. In section 4.2, we consider the classical error correction protocol imagined by Toom in [31], where (qu)bits are disposed on the vertices of an $N \times N$ square lattice. Toom's update rule matches well with the 3-qubit correction proposal of [9]. We use adiabatic elimination formulas from the work of [1] to analyze precisely its error-correction capabilities in a Lindblad-dissipative implementation.

4.1 Triangle-based polyhedra to scale up the three qubit repetition code

We start from the work of [9], which aims to stabilize a logical qubit composed of 3 physical qubits in order to increase the memory fidelity under perturbations inducing physical bit flip errors. Repetition codes are recalled in our Section 1.3.1.

We first describe briefly the associated physical system and the resulting error correction protocol, before showing how it can be improved, scaling up the order of information protection, by coupling locally several of these systems into a network of 6, 12, and 30 physical qubits. The new method and pattern proposed here is modular and can be used to further extend the code.

4.1.1 The three qubit repetition code: description and tuning of the system

This subsection is entirely reformulated from the work of [9].

We work on a system composed of 3 qubits (basis states $|0\rangle$ or $|1\rangle$) and of 3 harmonic oscillators (cavities) that can practically be considered as also only living on the two first energy levels, as they will be strongly dissipative. Indeed, their role is to evacuate entropy from the system. The qubits in contrast contain the logical information, encoded on the two basis states $|000\rangle$ and $|111\rangle$ of their joint state space. We will note $\mathbf{a_i}$ the annihilation operator on i-th cavity, $\boldsymbol{\sigma}_i^x$, $\boldsymbol{\sigma}_i^z$, $\boldsymbol{\sigma}_i^-$ and $\boldsymbol{\sigma}_i^+$ the Pauli operator on i-th qubit, which are defined in Section 1.2.3. We will use the definition

of the Lindblad superoperator expression defined in (1.14), and h.c. will stand for hermitian conjugate of the preceding terms.

The goal, as mentioned in Section 1.2.2, is to obtain a particular coupling between the three qubits (the system of interest we want to stabilize) and the three dissipating cavities (auxiliary system), such that the resulting effect is countering the happening of logical bit flips. As physical bit flips will make the qubits leave the code space $C = span(|000\rangle, |111\rangle)$, we want our countering effect to do the opposite, i.e. bring back the qubits into the code space while preserving the coherence of the state. We thus want the following equation to govern our system:

$$\frac{d\rho}{dt} = \sum_{i=1}^{3} \Gamma_c \mathcal{L}_{\mathbf{c_i}}(\rho) + \gamma \mathcal{L}_{\boldsymbol{\sigma}_i^x}(\rho) \, . \tag{4.1}$$

The second Lindblad terms formulate the unavoidable bit flip errors, with γ the bit flip rate; the first ones represent the effective error correction, at a rate Γ_c, and should ideally be induced by the operators

$$\mathbf{c}_1 = |000\rangle\langle 100| + |111\rangle\langle 011|, \quad \mathbf{c}_2 = |000\rangle\langle 010| + |111\rangle\langle 010| \quad \text{and} \quad \mathbf{c}_3 = |000\rangle\langle 001| + |111\rangle\langle 110| \, ,$$

or an equal number of their independent linear combinations. Note that each $\mathbf{c}_i$ operator simultaneously changes the i-th qubit from $|0\rangle$ to $|1\rangle$ and from $|1\rangle$ to $|0\rangle$, depending on the two other qubits' state: this preserves the coherence, which would not be the case if there were two different operators doing each of these tasks. The construction of [9] proposes a system whose equations of motion closely approximate the target equation (4.1) in some regime we will now make more precise.

The initial system is described by the Lindblad equation:

$$\frac{d\rho}{dt} = -i[\mathbf{H}(t), \rho] + \sum_{i=1}^{3} \kappa \mathcal{L}_{\mathbf{a_i}}(\rho) + \sum_{i=1}^{3} \gamma \mathcal{L}_{\boldsymbol{\sigma}_i^x}(\rho) \tag{4.2}$$

where ρ is the state of the whole system (3 qubits and 3 cavities), $\kappa \mathcal{L}_{\mathbf{a_i}}$ represents the strong dissipation of the i-th cavity, and $\gamma \mathcal{L}_{\boldsymbol{\sigma}_i^x}$ is the weak bit flip process on the i-th qubit, which we have to counter. Towards achieving this, a particular coupling of the qubits to the cavities is achieved via the Hamiltonian, $\mathbf{H}(t)$

$$\begin{aligned} = \quad & \sum_{i=1}^{3} \omega_{a_i} \mathbf{a_i}^\dagger \mathbf{a_i} + \sum_{i=1}^{3} \frac{\omega_{b_i}}{2} \boldsymbol{\sigma}_i^z + \sum_{i=1}^{3} \epsilon_i^a(t)(\mathbf{a_i}^\dagger + \mathbf{a_i}) \\ & + \sum_{i=1}^{3} \epsilon_i^b(t)(\boldsymbol{\sigma}_i^+ + \boldsymbol{\sigma}_i^-) - \sum_{i=1}^{3} \frac{E_i}{\bar{h}} (\cos(\tfrac{\mathbf{\Phi}_i}{\Phi_0}) + \frac{1}{2}(\tfrac{\mathbf{\Phi}_i^2}{\Phi_0^2})) \, . \end{aligned} \tag{4.3}$$

with

$$\mathbf{\Phi}_i = \sum_{i'=1}^{3} \phi_{i,i'}^a (\mathbf{a_{i'}} + \mathbf{a_{i'}}^\dagger) + \sum_{i'=1}^{3} \phi_{i,i'}^b (\boldsymbol{\sigma}_{i'}^+ + \boldsymbol{\sigma}_{i'}^-) \tag{4.4}$$

Here in (4.3) the first two terms describe the dynamics of isolated cavities and qubits; the last one describes their nonlinear coupling as typically encountered in superconducting circuits with Josephson junctions with E_i the Josephson energy of qubit and Φ_0 the superconducting flux quantum; and the time dependent terms are drives on the cavities and the qubits (the pumps), which we take of the form $\epsilon_1^a(t) = \epsilon_1^{a,1}(e^{i\omega_{p_1}t} + e^{-i\omega_{p_1}t}) + \epsilon_1^{a,2}(e^{i\omega_{p_2}t} + e^{-i\omega_{p_2}t})$. The reservoir is engineered by selecting particular $\omega_{p_i}, \epsilon_1^{a,i}$, described later; the $\epsilon_i^b(t)$ are optional but would be of the same form, see below. Note that these are all fixed sinusoidal drives, without any precise feedback signals nor control logic to be timed.

The whole system is built to limit the effects of bit flips at rate γ: the cavities dissipating at rate κ serve to evacuate the associated entropy and stabilize the system; the Hamiltonian construction must ensure the stabilization of the wanted subspace, closely matching (4.1). The scheme differs

from the standard one based on pairwise parity measurement. Indeed, each dissipative cavity is coupled to all the qubits and stabilizes the system as a whole.

As $\Phi_0^2 \gg 1$, we can simplify the last term by expanding the cosine to 4th order which gives

$$\sum_{i=1}^{3} \mathbf{a_i}^\dagger \mathbf{a_i} \left(\frac{\chi_{a_i b_1}}{2}\boldsymbol{\sigma}_1^z + \frac{\chi_{a_i b_2}}{2}\boldsymbol{\sigma}_2^z + \frac{\chi_{a_i b_3}}{2}\boldsymbol{\sigma}_3^z\right)$$
$$+ \sum_{i=1}^{3} K_{a_i a_i} {\mathbf{a}_i^\dagger}^2 \mathbf{a}_i^2 + \sum_{i\neq j}^{3} K_{a_i a_j} \mathbf{a}_i^\dagger \mathbf{a}_i \mathbf{a}_j^\dagger \mathbf{a}_j + \sum_{i\neq j}^{3} K_{b_i b_j} \boldsymbol{\sigma}_i^z \boldsymbol{\sigma}_j^z \,.$$

The reservoir is tuned by taking $\sum_{i=1}^{3} \chi_{a_k b_i} = 0$ for all k, and $\omega_{p_1} = \frac{|\omega_{a_1} - \omega_{b_1}|}{2}$, $\omega_{p_2} = \frac{|\omega_{a_1} + \omega_{b_1}|}{2}$. The first condition ensures that the logical states ($|000\rangle$ and $|111\rangle$) of the qubit undergo the same phase evolution, whatever the cavities' state. The second condition favors the conversion of a single qubit excitation into a decaying photon of the cavity, thanks to 2 pump photons at frequency ω_{p_1}; and the re-excitation of a single decayed qubit simultaneously with the creation of a decaying photon in the cavity, by conversion of 2 pump photons at ω_{p_2} (see details below). In both processes, the fast decay of the cavity photon inhibits the reverse process, which a pure Hamiltonian coupling would induce at equivalent rate. Finally, we also fix the $\epsilon_1^{a,j}$ to satisfy

$$\Omega_{p_j} := \sqrt{K_{a_1 a_1} \chi_{a_1 b_1}} \mid \frac{\epsilon_1^{a,j}}{\omega_{a_1} - \omega_{p_j}} \mid^2 = \Omega_p \tag{4.5}$$

independently of j. The first and last conditions are necessary for preserving any superposition $\alpha|000\rangle + \beta|111\rangle$, $\alpha|100\rangle + \beta|011\rangle$, ... while converging back to the code space. In a first approach, we will keep the $\epsilon_i^b(t) = 0$.

Regarding the conversion of bit-flips into decaying cavity photons, the idea is to turn conversion couplings on or off by parametric resonance effects: the pumps at ω_{p_1} and ω_{p_2} will be on resonance only for a qubit which is in mismatch with its two agreeing neighbors; otherwise, i.e. when all three qubits agree or when the qubit sees two neighbors with each a different logical value, it should not move. For this resonance selection to work, we assume the following timescale separation: $\gamma \ll \kappa \ll \chi \ll \omega$. This is realistic in typical quantum superconducting circuits. Since cavity excitations are created through $\omega_{p_1}, \omega_{p_2}$ after bit-flip errors, the probability of having n excitations in the cavities is proportional to $(\gamma/\kappa)^n$; this becomes negligible for $n > 1$ in the regime $\gamma \ll \kappa$, and then the terms ${\mathbf{a}_i^\dagger}^2 \mathbf{a}_i^2$ and $\mathbf{a}_i^\dagger \mathbf{a}_i \mathbf{a}_j^\dagger \mathbf{a}_j$ vanish. The terms in $\boldsymbol{\sigma}_i^z \boldsymbol{\sigma}_j^z$ can be rigorously ignored by slightly modifying the pump frequencies.

The scheme can be analyzed as follows. A change of frame removes all the components of order ω, the dominating rate. Then by performing a Rotating Wave Approximation (RWA), which is roughly an averaging approximation, on the basis of $\chi \ll \omega$, we obtain a simpler form of the Hamiltonian. We then do a new change of rotational frame to remove the dominant terms now of order χ, and a new RWA on the basis of $\Omega_p \ll \chi$. Finally, choosing $\Omega_p < \kappa$, we use a last timescale separation to do adiabatic elimination: considering that the components in κ quickly converge towards their stationary values, we eliminate the variables associated to the cavities and only study their effect on the slow dynamics, i.e. the qubits. This then indeed gives the effective master equation (4.1), describing how the engineered reservoir affects the three qubits composing the coding space. Γ_c represents the effective correction rate and is well approximated by $\Gamma_c = \frac{\Omega_p^2}{\kappa}$.

Note that instead of having one cavity per qubit to counter the associated bit-flip, one can design an effective Hamiltonian which circulates the values of the three qubits and thus their potential errors, associated to a bit-flip correction mechanism only on the first qubit. This possibility may be easier to implement. More precisely, this circulation is obtained by applying two extra drives $\epsilon_i^b(t)$ of fixed amplitudes and of frequencies $\omega_{p_{12}} = \frac{|\omega_{b_1} - \omega_{b_2}|}{2}$ and $\omega_{p_{23}} = \frac{|\omega_{b_2} - \omega_{b_3}|}{2}$, together with the terms in $\boldsymbol{\sigma}_i^z \boldsymbol{\sigma}_j^z$. This effectively implements Hamiltonians $H_{\text{exch}(i,j)}$ inducing a Rabi oscillation between $|01\rangle_{ij}$ and $|10\rangle_{ij}$, which corresponds to a swap of the qubits i, j. In addition to [9], we observe that when $H_{\text{exch}(i,j)}$ is significantly slower than the remaining cavity

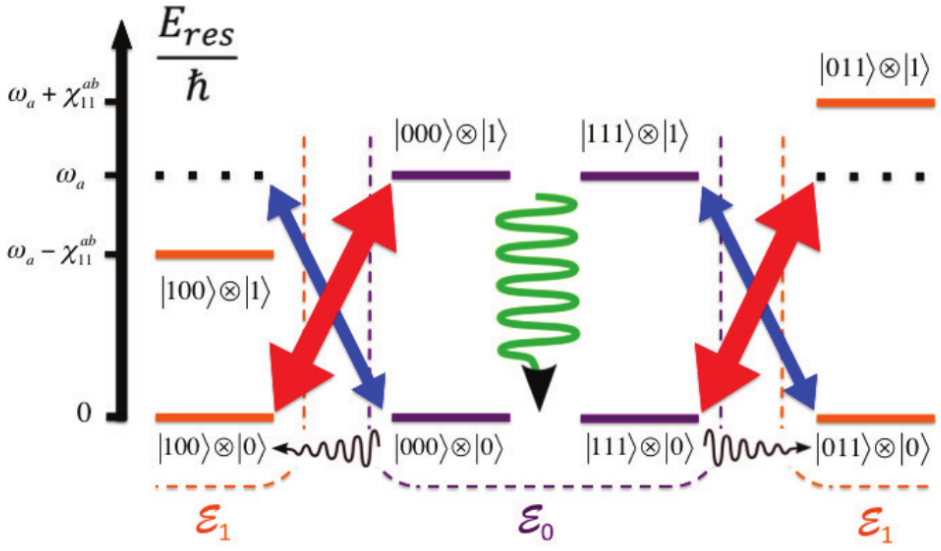

Figure 4.1: [taken from [9]] Energy-level diagram of the resonator only (qubits energies not represented here) as a function of the joint-state of the qubits-cavity system ($\mathcal{E}_0$ is the code space, $\mathcal{E}_1$ one of the error space). Thick red (resp. thin blue) straight-line arrows indicate couplings between two states induced by the pump at frequency ω_{p1} (resp. ω_{p2}). Green wavy arrow indicates the decay channel due to the decay of the single photon in the ancillary resonator. Black wavy arrow represents the bit flip channel.

reset Γ_{c_2}, an adiabatic elimination translates its effect into a Lindbladian like (4.1), but where $\Gamma_{c_1} = \Gamma_{c_3} = g^2/\Gamma_{c_2}$ with g the magnitude of $H_{\text{exch}(i,j)}$.

4.1.2 Scaling up: concept and first layer (the tetrahedron design)

The reservoir engineering technique presented in the last paragraph works in a fundamentally different way from the syndrome measurement technique described in Section 1.3.1. Its scaling up to larger codes also needs to be significantly different, since error-correction based on syndrome measurements in a repetition code requires non local decoding; the latter cannot be engineered into a simple dissipative autonomous system. Directly extending a setup as in last subsection 4.1.1 to n qubits, would be even less scalable, as it would require direct physical coupling of n qubits to each cavity. The challenge is thus to keep the error correction local, and to be able to scale it by increasing the number of physical qubits it is encoded in, to better protect the information.

We here propose a design allowing to scale up the number of qubits but without having to couple a cavity to an increasing number of qubits. It is based on using section 4.1.1 on triangles of interconnected qubits, and combining these triangles into a larger geometric figure. For simplicity of discussion, we here take for these figures the triangle-based regular polyhedra.

The first scaled-up version of our error correction design thus consists of four instances of the system described in section 4.1.1, organized in a tetrahedral shape, see Figure 4.2. In this representation, there is a qubit on each edge and three cavities on each face, for a total of four "locally correcting subsystems" (one for each face). Each qubit belongs to two different subsystems. We will note $\mathbf{a_{ij}}$ the annihilation operator in the i-th system on j-th cavity. Qubits will be numbered according to the systems they belong to: we will note $\mathbf{b_{ij}}$ the annihilation operator of the qubit belonging to the i-th and the j-th subsystem (which implies $\mathbf{b_{ij}} = \mathbf{b_{ji}}$). The tetrahedron features a total of 6 physical qubits.

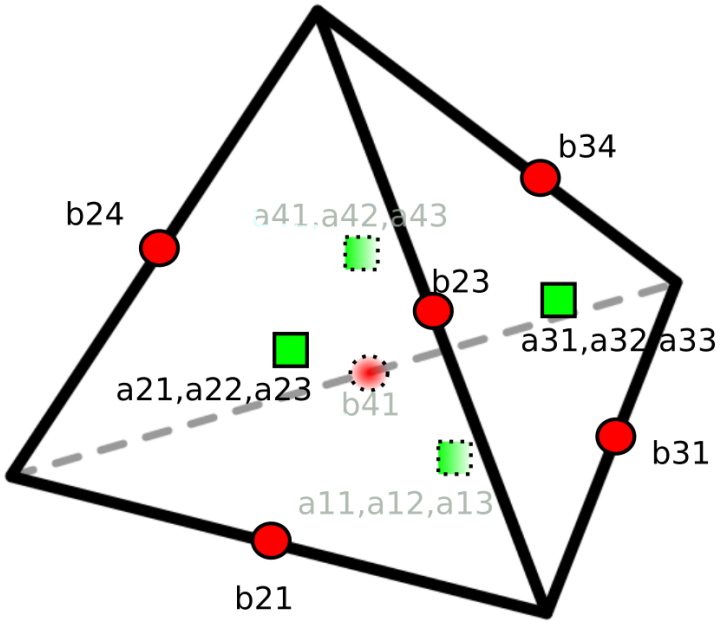

Figure 4.2: Regular tetrahedron with one qubit on each edge (red) and three cavities on each face (green). Dotted elements are on the back of the tetrahedron. Subsystem 1 is at the bottom of the volume, subsystem 2 on the left front face, subsystem 3 on the right front face, and subsystem 4 on the back face. Subsystem number 1 thus comprises the qubits b_{21}, b_{31} and b_{41}, and the cavities a_{11}, a_{12} and a_{13}; and so on. The full system features a total of 6 qubits, and we will show that it allows to correct bit-flip errors on any 2 of these qubits.

The system is described by the Lindblad equation:

$$\frac{d\rho}{dt} = -i[\mathbf{H}(t), \rho] + \sum_{i=1}^{4}\sum_{j=1}^{3} \kappa \mathcal{L}_{\mathbf{a_{ij}}}(\rho) + \sum_{i,j=1}^{3} \gamma \mathcal{L}_{\boldsymbol{\sigma}^x_{ij}}(\rho) \tag{4.6}$$

where the Hamiltonian is described similarly to (4.3). We do the first same simplifications: no drive $\epsilon_i^b(t)$ (optionnal), we Taylor expand the terms in $(\cos(\frac{\mathbf{\Phi}_i}{\Phi_0}) + \frac{1}{2}(\frac{\mathbf{\Phi}_i^2}{\Phi_0^2}))$, we do the same tuning for the χ ($\sum_{j=1}^{3} \chi_{a_{ik}b_{ij}} = 0$ for all $k = 1, 2, 3$ wich means each cavity in a subsytem, and for all $i = 1, 2, 3$ which means all subsystems) and the Ω_p decribed as in (4.5), and we neglect terms in K as they are of order 4.

This gives us a Hamiltonian $\mathbf{H}(t) = \sum_{i=1}^{4} \mathbf{H}_i(t)$ with $\mathbf{H}_i(t)$

$$= \sum_{j=1}^{3} \Big[\omega_{a_{ij}} \mathbf{a_{ij}^\dagger a_{ij}} + \frac{\omega_{b_{ij}}}{2} \boldsymbol{\sigma}^z_{ij} - \mathbf{a_{ij}^\dagger a_{ij}} (\frac{\chi_{a_{ij}b_{i1}}}{2} \boldsymbol{\sigma}^z_{i1} + \frac{\chi_{a_{ij}b_{i2}}}{2} \boldsymbol{\sigma}^z_{i2} + \frac{\chi_{a_{ij}b_{i3}}}{2} \boldsymbol{\sigma}^z_{i3}) \Big]$$
$$+ \sum_{j=1}^{3} \epsilon^a_{ij}(t) \Big(\mathbf{a_{ij}} (1 + \sum_{k=1, k\neq i}^{4} e^{i\chi_{a_{kj}b_{ik}t}} + e^{-i\chi_{a_{kj}b_{ik}t}}) + h.c. \Big)$$

The new terms, involving drives of the form,

$$\sum_{j=1}^{3} \epsilon^a_{ij}(t) \Big(\mathbf{a_{ij}} (\sum_{k=1, k\neq i}^{4} e^{i\chi_{a_{kj}b_{ik}t}} + e^{-i\chi_{a_{kj}b_{ik}t}}) + h.c. \Big) , \tag{4.7}$$

are added to deal with the effects of overlapping subsystems, and the objective of obtaining second-order error correction. Hence, for example, if the cavity a_{11} needs to correct the qubit b_{11}, it needs

to do so both when the cavities a_{41}, a_{42} and a_{43} are populated or not. These possibilities lead to more energy levels for which we want the correction to take place, and thus more transition frequencies to be activated. Choosing two coupling strengths equal in each subsystem, for example $\chi_{a_{ij}b_{k1}} = \chi_{a_{ij}b_{k2}} = -\frac{\chi_{a_{ij}b_{k3}}}{2}$, allows to only add 2 extra drives instead of 3. Towards further scaling, it is important to note that these extra drives only come from two subsystems meeting at each qubit, regardless of the number of triangles assembled in this way.

The parameters in each subsystem are tuned similarly to the building block presented in the previous section. The only new requirement is that adjacent subsystems must have different coupling values (χ), in order to ensure that integer combinations of various couplings do not lead to dark states. Here this leads to 4 different sets of parameters. We will see later that this number does not incrase when scaling up the number of triangles.

To analyze this architecture, similarly to subsection 4.1.1, we perform a first change of frame to remove all the components of order ω:

$$U(t) = e^{iH_0 t} \prod_{i=1}^{4} \prod_{j=1}^{3} D_{-\xi_{p_{ij}}} \tag{4.8}$$

where $\mathbf{D}_\alpha = e^{\alpha \mathbf{a}^\dagger - \alpha^* \mathbf{a}}$ is the displacement operator, and with

$$\begin{cases} H_0 = \sum_{i=1}^{4} \sum_{j=1}^{3} \omega_{a_{ij}} \mathbf{a_{ij}^\dagger a_{ij}} + \sum_{i,j=1}^{3} \frac{\omega_{b_{ij}}}{2} \boldsymbol{\sigma}_{ij}^z \\ \frac{d\xi_{p_{ij}}}{dt} = -i\omega_{a_1} \xi_{p_{ij}} - i\epsilon_{ij}^a(t) - \frac{\kappa}{2} \xi_{p_{ij}} \end{cases} \tag{4.9}$$

This allows us to perform the standard RWA in the $\chi \ll \omega$ regime, and gives the effective hamiltonian

$$\mathbf{H_{eff}} = \sum_{i=1}^{4} [\sum_{j=1}^{3} -\mathbf{a_{ij}^\dagger a_{ij}} (\frac{\chi_{a_{ij}b_{i1}}}{2} \boldsymbol{\sigma}_{i1}^z + \frac{\chi_{a_{ij}b_{i2}}}{2} \boldsymbol{\sigma}_{i2}^z + \frac{\chi_{a_{ij}b_{i3}}}{2} \boldsymbol{\sigma}_{i3}^z) + \frac{\Omega_p}{2} \sum_{j=1}^{3} (\boldsymbol{\sigma}_{ij}^+ \mathbf{a_{ij}} + \boldsymbol{\sigma}_{ij}^- \mathbf{a_{ij}} + h.c.)]$$

We then do a second change of frame

$$U_{new}(t) = e^{i\mathbf{H_1}t}$$

$$\mathbf{H_1} = -\sum_{i=1}^{4} \sum_{j=1}^{3} \mathbf{a_{ij}^\dagger a_{ij}} (\frac{\chi_{a_{ij}b_{i1}}}{2} \boldsymbol{\sigma}_{i1}^z + \frac{\chi_{a_{ij}b_{i2}}}{2} \boldsymbol{\sigma}_{i2}^z + \frac{\chi_{a_{ij}b_{i3}}}{2} \boldsymbol{\sigma}_{i3}^z)$$

and a new RWA in $\Omega_p \ll \chi$ regime, giving the resulting system

$$\frac{d\rho}{dt} = -i[\mathbf{H_{new}}, \rho] + \sum_{i=1}^{4} \sum_{j=1}^{3} \kappa \mathcal{L}_{\mathbf{a_{ij}}}(\rho) + \sum_{i,j=1}^{3} \gamma \mathcal{L}_{\boldsymbol{\sigma}_{ij}^x}(\rho)$$

$$\mathbf{H_{new}} = \frac{\Omega_p}{2} \sum_{i=1}^{4} \sum_{j=1}^{3} \mathbf{a_{ij}} \otimes c_{ij}^\dagger + \mathbf{a_{ij}^\dagger} \otimes c_{ij}$$

where $c_{i1} = |000\rangle_i\langle 100|_i + |111\rangle_i\langle 011|_i$, acting on the qubits of the i-th system and acting as the identity on the other qubits. The operators c_{i2} and c_{i3} are defined in the same way, but the qubits they flip in the i-th system is the second and third respectively.

The last model reduction is an adiabatic elimination of the cavities, based on the fact of their decaying much faster than the Hamiltonian Ω_p, to obtain the final equation approximating the dynamics for large time-scale separations:

$$\frac{d\rho}{dt} = \sum_{i=1}^{4} \sum_{j=1}^{3} \Gamma_c^i \mathcal{L}_{\mathbf{c_{ij}}}(\rho) + \sum_{i=1}^{3} \sum_{j=1}^{3} \gamma \mathcal{L}_{\boldsymbol{\sigma}_{ij}^x}(\rho) \, . \tag{4.10}$$

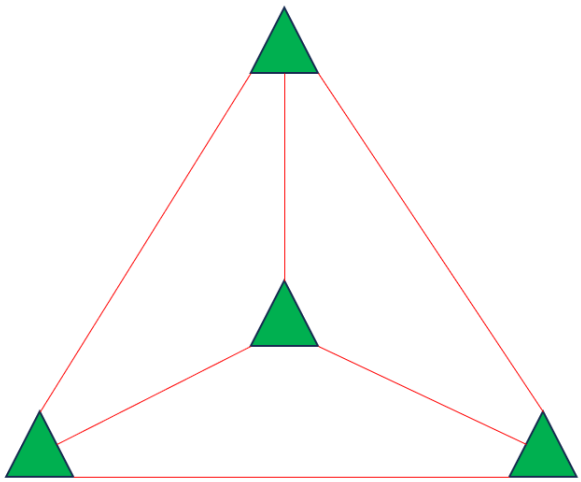

Figure 4.3: Connection Graph associated to the tetrahedral subsystem. Here the faces of the tetrahedron are the graph nodes, represented by the green triangles, and the qubits are graph edges, represented by the red lines joining them. By construction of a graph each qubit (edge) belongs to two faces (nodes), and two faces (nodes) have at most one qubit (edge) in common. Furthermore, for geometric figures based on triangles, each node is of degree 3 i.e. connected to 3 edges (since each triangular face has 3 edges). Flipping a bit thus corresponds to flipping the logical value associated to a graph edge. The majority-correction rule works in the following way on this graph: if two edges around one node differ from the third one, then this third edge can flip.

Here $\mathbf{c_{ij}} = (\boldsymbol{\sigma}_{ij}^{-}\Pi_{i_{|00\rangle}}^{\neq j} + \boldsymbol{\sigma}_{ij}^{+}\Pi_{i_{11\rangle}}^{\neq j}) \otimes \boldsymbol{I}_{\neq \boldsymbol{i}}$ for $i = 1, 2, 3$, where $\Pi_{i_{|00\rangle}}^{\neq j}$ is the projection on $|00\rangle$ for the two qubits different from j in the i-th subsystem and $\boldsymbol{I}_{\neq \boldsymbol{i}}$ is the identity operator on the qubits not belonging to the i-th system. This final equation shows the two competing phenomena taking place: the correction protocol at a rate Γ_c, which tends at each interval of time to apply a rule of majority inside a face/subsystem, and the bit flips at a rate γ, which tend at each interval of time to flip any qubits.

Performance analysis: In this section, we analyze the performance of scaling up, first from the 3-qubit code to the tetrahedron, but introducing tools which can be useful for further scaling. We carry out the analysis in the same standard way as most error-correction code papers. Namely, we set $\gamma = 0$ but start with a number of initial errors, and show how many of them, on any qubits, this system can correct. For the tetrahedron code, this will be any 2 qubits, as compared to 1 qubit in the 3-qubits code of Section 4.1.1. This is an improvement since for a low, independent bit-flip probability p_l on each qubit, the probability to corrupt more than 3 qubits out of 6 is of order p_l^3 and hence much lower than the probability $O(p_l^2)$ to have corrupted any two qubits in the three-qubit system. Further scaling, with more precise constants, will be discussed below. This analysis uses the Connection Graph associated to the triangle-based polyhedron, see Figure 4.3. For simplicity of notation, we will assume all Γ_c^i equal, and we will assume the initial codeword to have all qubits on $|0\rangle$, so "corrupted qubits" are the qubits on $|1\rangle$.

We first enunciate some principles on which we will build our proof:

- *Markov chain:* We adopt a classical Markov chain formalism. Indeed, similarly to Chapter 3, the Lindblad system can be reduced (exactly) to the evolution of the diagonal of ρ. Each basis state is then considered a configuration of the Markov chain, and the Lindblad equation becomes a Master equation describing the evolution of probabilities in this Markov chain. A reader needing more details on this point is invited to check Chapter 3, especially the treatment of clock ancillas evolution done there.
- *Flip rule*: a qubit can flip, with rate Γ_c, if one of the faces it belongs to has two qubits in the

other state. This rule and the Connection Graph fully define the Markov chain transition matrix.

- *Max-set* $\Omega(S)$: Given an initial configuration c_S in which all qubits are on $|0\rangle$ except the qubits $i \in S$ which are on $|1\rangle$, the set $\Omega(S)$ is the support of all qubits that could possibly switch to $|1\rangle$ when applying (4.10) with $\gamma = 0$ from this initial state. We call c_Ω the configuration where all the qubits of $\Omega(S)$ are set to $|1\rangle$, and all other qubits to $|0\rangle$.

Lemma 1 *Assume that $\Omega(S)$ features no closed loop in the Connection Graph (see Fig. 4.3). Then, when applying (4.10) with $\gamma = 0$, the initial configuration c_S asymptotically converges towards all qubits on $|0\rangle$.*

Proof: By definition of $\Omega(S)$, the dynamics is reduced to the subspace of configurations where subsets $S' \subseteq \Omega(S)$ feature qubits on $|1\rangle$. The configuration with all qubits on $|0\rangle$ is an absorbing one, which will never be left. It is then easy to see, for instance from the Markov chain steady state equations, that convergence towards this configuration is ensured as soon as we show that any configuration with k qubits on $|1\rangle$ has a nonzero probability to jump towards a configuration with $k-1$ qubits on $|1\rangle$. The latter is indeed the case for any $S' \subseteq \Omega(S)$. Namely, if the Connection Graph associated to $\Omega(S)$ features no closed loops, then this is also true for any of its subsets S', and hence the Connection Graph associated to S' consists of a set of trees. The leaves of these trees correspond to triangles with a single flipped edge, meaning a single qubit on $|1\rangle$; hence, there is a nonzero probability that this qubit gets corrected to $|0\rangle$. □

From this Lemma, the remaining task to show error correction is to characterize the sets $\Omega(S)$ for any configurations with few qubits switched to $|1\rangle$. The following properties may help formalize this characterization.

Lemma 2 *(i) (Principle of delayed choice): Consider a sequence where we progressively switch the qubits of S from $|0\rangle$ to $|1\rangle$, while applying the switching rule not only afterwards but also in between in order to corrupt from $|0\rangle$ to $|1\rangle$ some other qubits. Then we also reach $\Omega(S)$.*
(ii) Two qubits belonging to the same triangle T_A cannot both belong to another triangle T_B.
(iii) Consider S' any subset of $\Omega(S)$. Then $\Omega(S') \subseteq \Omega(S)$.
(iv) The sets $\Omega(S)$ are the sets containing no triangle with only 2 qubits on $|1\rangle$, i.e. no node on Fig.4.3 with only two edges switched.
(Note that a closed loop on Fig.4.3 must be composed of a sequence of triangles with at least 2 selected edges each, hence at least 2 corrupted qubits each.)

Proof: (i) This just follows from the observation that, if a qubit can switch from $|0\rangle$ to $|1\rangle$ when qubits in some set S_0 are on $|1\rangle$, then it can also switch from $|0\rangle$ to $|1\rangle$ when any more qubits than S_0 are on $|1\rangle$. This applies in both direction. First, if the switching rule has corrupted more qubits than just S once all qubits of S are corrupted, then this can afterwards only lead to a possibly larger set $\Omega'(S) \supseteq \Omega(S)$. Second, any qubit that could switch from $|0\rangle$ to $|1\rangle$ at an intermediate stage, can also switch once all of S is corrupted; hence, $\Omega'(S) = \Omega(S)$.

(ii) This property just recalls how the code is built: qubits are on edges of the polyhedron, and two polyhedron faces cannot share more than one edge.

(iii) The main argument hinges on the same observation as for point (i). We then proceed by contradiction. Consider a state with qubits of $\Omega(S')$ being on $|1\rangle$, where $\Omega(S') \not\subseteq \Omega(S)$. The Markov chain switches qubits one by one, so at some point on its way to $\Omega(S')$ it must transition from a configuration with $S_1 \subseteq \Omega(S)$ to a configuration with S_2 containing a single qubit outside $\Omega(S)$. But if this qubit can flip from $S_1 \subset \Omega(S)$, then by our initial observation it can also flip from $\Omega(S)$. Assuming that this qubit is outside of $\Omega(S)$ is in contradiction with the definition of $\Omega(S)$. Hence, we reach a contradiction when claim (iii) is not true, meaning that claim (iii) must be true.

(iv) By the *Flip rule*, the only opportunity to switch a qubit from $|0\rangle$ to $|1\rangle$ is to have a triangle with 2 qubits already on $|1\rangle$. Conversely, if any set S' contains a triangle with 2 qubits on $|1\rangle$,

then the 3rd qubit can flip. Thus S' cannot be the max-set $\Omega(S)$ of any initial configuration S. □

For the tetrahedral code, the characterization is simple.

Proposition 14 *Consider S a set with $|S| \leq 2$ qubits on $|1\rangle$ on the tetrahedral code. Then $\Omega(S)$ features no closed loop in the graph of Fig. 4.3.*

Proof: By the Flip rule, only a triangle already containing two qubits on $|1\rangle$ can switch another qubit to $|1\rangle$. Hence, no further qubit can be corrupted for $|S| < 2$, nor when $|S| = 2$ but no triangle contains both corrupted qubits (e.g. let those qubits be the horizontal and vertical edges on Fig. 4.3). Those cases can thus generate no closed loop.
If $|S| = 2$ and both corrupted qubits belong to one triangle T_r, then the third qubit of T_r can get corrupted. By Lemma 2 (ii), since each pair of corrupted qubits now belong to T_r, none of those pairs can belong to another triangle, hence no other triangle can contain two corrupted qubits; there is thus no opportunity for any more corrupting switches. By the observation at the end of Lemma 2, this single triangle implies no closed loop. □

Together with Lemma 1, this demonstrates that the tetrahedral system improves the error protection, correcting all situations with up to 2 corrupted qubits out ot 6, instead of just 1 out of 3.

4.1.3 Scaling up the scheme

We can extend the system of the last subsection to correct up to 3 and 4 errors, by creating bigger 3-D polyhedra from our triangle-error-correction building block. The implementation is similar and would result in a similar equation to 4.10.

Octahedral code We can correct up to 3 errors by building the code on the basis of a regular octahedron, composed of a qubit on each edge to form a subsystem on each triangular face. This would result in a system composed of 12 qubits and 8 subsystems (faces). The resulting connection graph is represented on Figure 4.4. An important observation is that *closed loops on this graph have a length of at least 4 edges.*

To prove that the octahedral code corrects up to 3 errors, we apply the exact same reasoning as for the tetrahedron. The only thing we have to adapt is the last Proposition, ensuring no closed loops in $\Omega(S)$.

Proposition 15 *Consider S a set with $|S| \leq 3$ qubits on $|1\rangle$ on the octahedral code. Then $\Omega(S)$ features no closed loop in the graph of Fig. 4.4.*

Proof: If no triangle contains more than one corrupted qubit, then $\Omega(S) = S$. If one triangle contains all the corrupted qubits, then $\Omega(S) = S$ as well, by the same reasoning as for Proposition 14. In both these situations, by the observation at the end of Lemma 2, there can be no closed loops.
We finally use Lemma 2(i) and graph symmetry to address the cases where some triangle(s) initially contain errors. By the principle of delayed choice thus, first place these two errors. By the flip rule, we corrupt the third qubit of the corresponding triangle. Then we place the last error. If it comes in a triangle that had no error, then after corruption no triangles have 2 errors, so we have reached $\Omega(S)$; having a single triangle with ≥ 2 corrupted edges, we can have no closed loop on Fig. 4.4. If the last error comes in a triangle that had one error already, then the third qubit of this triangle can switch, resulting in two connected triangles with all edges corrupted. If two of those edges where touching another triangle, then together they would form a closed loop of length 3, in contradiction with the octahedron graph property. Hence, no more triangle can have two corrupted edges, meaning that we have reached $\Omega(S)$ with 2 corrupted triangles, i.e. no closed loop. □

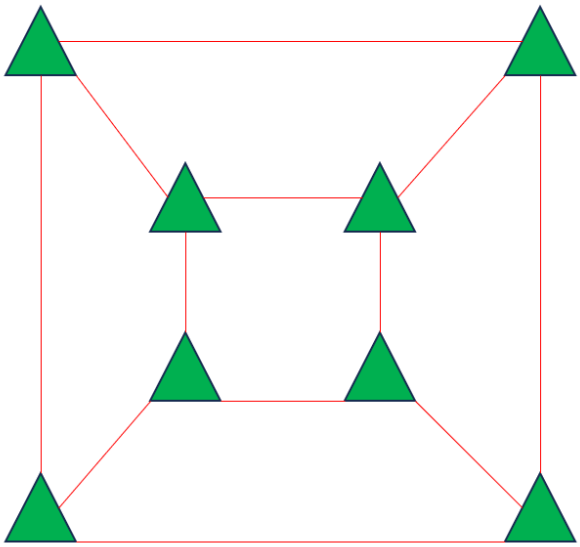

Figure 4.4: Connection Graph associated to the octahedral code. Like for the tetrahedron, the faces of the polyhedron, representing a majority-vote correction operator, here correspond to nodes (green triangles); the edges of the polyhedron, representing a physical qubit of the code, are also edges of the graph (red lines). In this Connection Graph, closed loops are constituted of at least 4 edges.

Icosahedron code Along the same line, we can scale up further by assembling our triangular building blocks into a regular icosahedron, with 30 qubits (edges) and 20 faces (triangles = graph nodes). The resulting connection graph is represented on Figure 4.4 and its *closed loops have a length of at least 5 edges.* From this, we can prove protection against up to 4 initial errors among the 30 qubits. Again the only novelty is the search for closed loops in $\Omega(S)$.

Proposition 16 *Consider S a set with $|S| \leq 4$ qubits on $|1\rangle$ on the icosahedral code. Then $\Omega(S)$ features no closed loop in the graph of Fig. 4.4.*

Proof: Like in the other cases, if no triangle contains 2 errors, then $\Omega(S) = S$. With 4 edges corrupted, this cannot form a closed loop.
Otherwise, we again use the principle of delayed choice, Lemma 2(i). Start by placing 2 errors in the same triangle T_A. The flip rule can then corrupt the 3rd qubit of T_A while leaving 2 initialization errors to place. There are now 3 triangles with one error around T_A. Call them T_1, T_2,

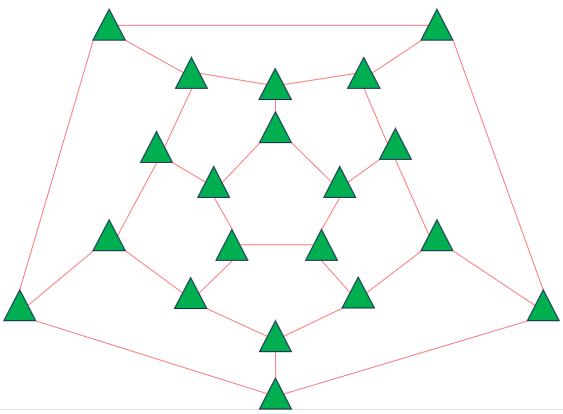

Figure 4.5: Connection Graph associated to the icosahedric code, same symbols as in previous figures. The shortest closed loop on this graph has a length of at least 5 edges.

T_3. We can consider 3 options for the remaining 2 errors.
- If we place the two remaining errors in two different triangles that are not T_1, T_2, T_3, then we have reached $\Omega(S)$.
- If we place the two remaining errors in the same triangle T_B outside T_1, T_2, T_3, then the flip rule can corrupt the third qubit of T_B. If this third qubit does not belog to T_1, T_2, T_3 either, then we have reached $\Omega(S)$. Otherwise, i.e. if say the third qubit of T_B belongs to T_1, then the flip rule can now corrupt the third qubit of T_1. This yields a chain of 3 fully corrupted triangles, with corresponding chains of ≤ 4 corrupted edges. The ends of these chains cannot meet at any further triangle to corrupt, since otherwise we would have a closed loop of length ≤ 4. Hence, we must have reached $\Omega(S)$.
- Finally, if we place one error in S_1, then the flip rule can corrupt the third qubit of T_1, while leaving one initial error to place. There are thus 4 triangles around T_A,T_1 with one corrupted qubit each. At worst, we can place the remaining initial error in one of those triangles, leading the flip rule to corrupt its third qubit. Then we are back to the situation of the previous item. □

General scaling observations The essential ingredient in our approach seems to be Connection Graphs with minimal cycles of increasing length.

Conversely to the above propositions, indeed, *once a closed loop of the Connection Graph is corrupted, the system cannot recover* while using the flip rule. In fact, to flip back an edge of this closed loop, one of its two connected nodes should have no other corrupted edge, but by definition of a closed loop each of its nodes has at least two corrupted edges.

Further scaling the error-correction capability to k errors thus seems to amount to creating Connection Graphs where each node has degree 3 and every closed loop has length at least $k+1$. Beyond being not too exotic to implement with physical couplings in a 2D or 3D environment, they do not have to correspond to any regular shapes. For instance, a hexagonal lattice folded in torus shape (periodic boundary conditions, for sufficient lattice size) has cycle length 6 and seems to correct up to 5 erroneous qubits. With a fixed lattice type, the number of qubits would scale quadratically with the lattice length, which bounds the number of errors that can be corrected. With this procedure further requiring larger cycles, we expect a number of qubits which grows somewhat faster than quadratic in the number of correctable errors. A deeper study is left for future work.

4.2 The Toom's rule set-up

Toom's rule is a 2-dimensional cellular automaton model created by Andrei Toom [31]. It consists in a 2D code, where qubits (in our application) are disposed on the vertices of a n×n square. In a discrete time approach, at each round of correction, the protocol is: if one qubit is different from both its bottom and right neighbours, then flip it. There are finally boundary conditions for the square. This automaton has already been used in order to realize fault tolerance in quantum systems [19]. It has the particularity to treat the 3 qubits involved in one operation in an asymmetric way, as only one qubit can be flipped. The goal of this subsection is to observer how this setup fits the reservoir engineering capabilities, only using local interactions coupled with the 3-qubits scheme developed in [9], and to analyze quantitatively how this is diminishing the rate of logical bit flip in a continuous-time reservoir implementation. To analyze this setup in continuous time, we reduce the uncertain evolution of bit-information to a classical Markov chain and describe its dynamics as

$$\frac{dr}{dt} = \Gamma L_0 r + \gamma L_1 r \ ,$$

where L_0 and L_1 are matrices representing respectively the effect of the correction process and the effect of the local spurious bit flips, and r is a probability distribution vector over all the possible bit strings of the system. The parameter $\frac{\gamma}{\Gamma}$ is supposed to be small, representing the relative rate of error processes compared to correction processes. We will use the method developed in

[1], called "adiabatic elimination" and which computes via series expansion the slow eigenspace of the full system and its associated dynamics. Indeed, logical error processes should be identified with the information lost at the slowest rate, at most comparable to γ. The method of [1] was developed for Lindblad-type equations, and we here specialize it to classical Markov chains; this is of course a special case, but it is worth mentioning that this approach seems to be absent from the much more far-reaching standalone literature on classical Markov chains.

We will start by describing a way of implementing the Toom's rule set up with the 3-qubits reservoir of [9]. Then we will give an understanding of the analysis method for simple repetition codes before exploring more precisely the Toom's rule set-up. The particular protocol of Toom's rule allows us to directly connect it to the basic set-up seen in last section.

4.2.1 Implementation

As seen on Figure 4.6, the elementary cell of Toom's automaton is composed of 3 elements, with two of them correcting the third one. Assuming qubits are only subject to bit flips, this can be modeled just as in last subsection. It is in fact simpler, as we only need to correct one of the three qubits inside one subsystem, thus only needing one cavity. On one such cell, we thus have

$$\frac{d\rho}{dt} = -i[\mathbf{H}(t), \rho] + \kappa\mathcal{L}_{\mathbf{a}}(\rho) + \gamma\sum_{j=1}^{3}\mathcal{L}_{\boldsymbol{\sigma}_j^x}(\rho) \tag{4.11}$$

with

$$\mathbf{H}(t) = \sum_{j=1}^{3}(\frac{\omega_{b_j}}{2}) + \omega_a\mathbf{a}^\dagger\mathbf{a} - \mathbf{a}_{\mathbf{ij}}^\dagger\mathbf{a}(\frac{\chi_{ab_1}}{2}\boldsymbol{\sigma}_1^z + \frac{\chi_{ab_2}}{2}\boldsymbol{\sigma}_2^z + \frac{\chi_{ab_3}}{2}\boldsymbol{\sigma}_3^z) + (\epsilon^a(t)\mathbf{a} + h.c.)$$

The coefficients used are the same as last subsection, and with similar calculations we can arrive at the simplified model for one elementary cell

$$\frac{d\rho}{dt} = \Gamma_c^1\mathcal{L}_{\mathbf{c_1}}(\rho) + \sum_{i=1}^{3}\gamma\mathcal{L}_{\boldsymbol{\sigma}_i^x}(\rho)\ . \tag{4.12}$$

with the qubit numbered 1 being the one at the angle of the cell, and $\mathbf{c}_1 = |000\rangle\langle 100| + |111\rangle\langle 011|$. We can then group all the elementary cells together, which gives the complete reduced model, e.g. for the 3*3 grid:

$$\frac{d\rho}{dt} = \sum_{i=1}^{9}\Gamma_c^i\mathcal{L}_{\mathbf{c_i}}(\rho) + \sum_{i=1}^{9}\gamma\mathcal{L}_{\boldsymbol{\sigma}_i^x}(\rho)\ . \tag{4.13}$$

The only requirement is that the neighbouring subsystems must have different coupling values (χ), in order to ensure that integer combinations of various couplings do not lead to dark states. The Toom's rule, although asymmetric, thus very naturally links to the three-qubits operation of [9] which was also conceived without inherent symmetry.

4.2.2 Analysis method description

We begin by giving an idea of how we will use the work of [1].

We will work in the same setup as previous subsection, which means we will only consider bit flip errors. This allows us to consider our system in a classical way, modeling jumps from one configuration to another with a classical Markov chain. Indeed, when discarding phase values and hence starting with a diagonal ρ in the bit-basis, the density matrix ρ describing the state of this quantum system remains diagonal throughout its evolution; a simple way to verify this, is to write the differential equation on each non diagonal coefficient with the assumption that all of them start equal to zero, and note that their derivative is also zero in that case. The technique described in [1] is much simplified by this fact, as we will do model reduction only on the diagonal of our system; or in other words, we do adiabatic elimination on a classical Markov chain.

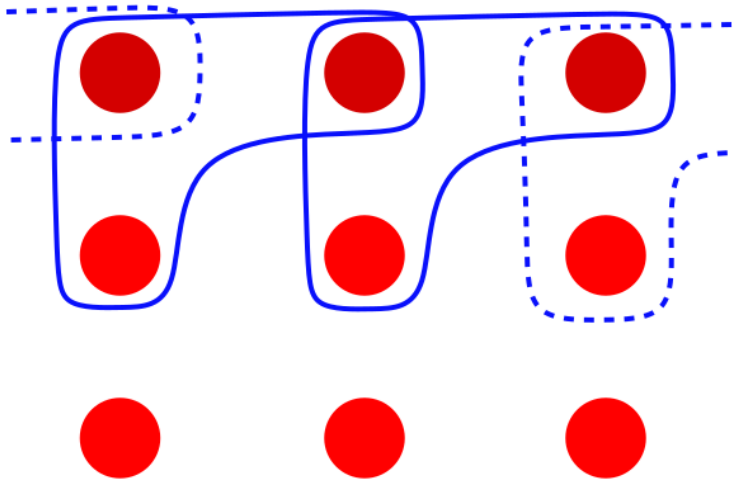

Figure 4.6: Toom's setup for a 3*3 grid: qubits are represented by red dots. The blue lines show the shape of subsystems, as described in last subsection. The corrected qubit is the one at the angle of the subsystem.

We want to study in this section systems of the form

$$\frac{dr}{dt} = L_0 r + \epsilon L_1 r \tag{4.14}$$

with r a vector of size 2^N, N the number of qubits, and L_0, L_1 matrices of size $2^N * 2^N$. The r represents the probability distribution over system levels (diagonal of ρ) in the canonical basis. The ϵ parameter is small, the L_0 dynamics rapidly converges towards a definite "code subspace", and thus by perturbation theory the $L_0 + \epsilon L_1$ dynamics should feature slow dynamics on an invariant subspace of same dimensions as the code subspace. We want to craft a reduced model trying to approach this subspace (section 2 in [1]), parameterized by r_s which follows reduced dynamics in linear form $\frac{dr_s}{dt} = L_s r_s$, associated to a linear relation between the reduced parameter set and the slow invariant eigenspace of the complete model $r = M r_s$. Similarly to [1], we want to satisfy some conditions on the matrices M and L_s. To preserve total probability, the sum of each column must equal 1 for M and equal 0 for L_s. Furthermore, we want M and L_s to preserve the positivity of probability distributions.

To build those matrices M and L_s, we are going to make a decomposition in orders of ϵ: $L_s = \sum_k \epsilon^k L_{s,k}$ and $M = \sum_k \epsilon^k M_k$. Then, we develop the relation

$$\frac{dr}{dt} = (L_0 + \epsilon L_1) M r_s = M \frac{dr_s}{dt} = M L_s r_s \tag{4.15}$$

and identify the terms at different orders of ϵ to progressively find the M_k and $L_{s,k}$ for increasing values of k.

The goal of the next subsections will be to explicitly compute those matrices at different orders, and to witness that the more we add qubits the more we have to push the development to higher orders to see nonzero dynamics in L_s, meaning that we have a better protection against the logical bit flip rate.

4.2.3 Three qubits code

To illustrate the method, let us consider the system composed of 3 qubits described in [9], on which two phenomena happen: the bit flips at a rate γ and the correction protocol at a rate Γ. In the absence of phase flip, the dynamics of the system is (4.14) where r is the state vector with 8 components, ordered e.g. such that r_1 describes the population on $|000\rangle$, r_2 on $|111\rangle$, r_3 on $|100\rangle$,

etc.. . Note that in this ordering, we have grouped each bitstring with its opposite. In this basis, the 8×8 correction matrix L_0 writes

$$L_0 = \begin{pmatrix} 0 & 0 & 1 & 0 & 1 & 0 & 1 & 0 \\ 0 & 0 & 0 & 1 & 0 & 1 & 0 & 1 \\ 0 & 0 & -1 & 0 & 0 & 0 & 0 & 0 \\ 0 & 0 & 0 & -1 & 0 & 0 & 0 & 0 \\ 0 & 0 & 0 & 0 & -1 & 0 & 0 & 0 \\ 0 & 0 & 0 & 0 & 0 & -1 & 0 & 0 \\ 0 & 0 & 0 & 0 & 0 & 0 & -1 & 0 \\ 0 & 0 & 0 & 0 & 0 & 0 & 0 & -1 \end{pmatrix}.$$

This operator leaves untouched the spaces $|000\rangle$ and $|111\rangle$, and brings the other spaces to the closest one of the two: for example it brings $|100\rangle$ to $|000\rangle$ (first line, third column). The 8×8 bit flip matrix writes

$$\epsilon L_1 = \frac{\gamma}{\Gamma} \begin{pmatrix} -3 & 0 & 1 & 0 & 1 & 0 & 1 & 0 \\ 0 & -3 & 0 & 1 & 0 & 1 & 0 & 1 \\ 1 & 0 & -3 & 0 & 0 & 1 & 0 & 1 \\ 0 & 1 & 0 & -3 & 1 & 0 & 0 & 0 \\ 1 & 0 & 0 & 1 & -3 & 0 & 0 & 1 \\ 0 & 1 & 1 & 0 & 0 & -3 & 1 & 0 \\ 1 & 0 & 0 & 1 & 0 & 1 & -3 & 0 \\ 0 & 1 & 1 & 0 & 1 & 0 & 0 & -3 \end{pmatrix}$$

This operator represents the possibility to have a bit flip on either of the three qubits: for example the first column represents the possibility to go from $|000\rangle$ to either $|001\rangle$, $|010\rangle$ or $|100\rangle$.

Since L_0 brings all states towards $\text{span}(|000\rangle, |111\rangle)$ at a fast rate, we are going to craft a reduced model of dimension 2, representing the perturbation of this perfect codespace by ϵL_1.

We want to build the matrices M and L described in the previous subsection for this example. We begin at order 0: by definition, the dynamics on the reduced manifold at the zero-th order is $L_{s,0} = 0$. Then, writing the condition (4.15) at zero-th order, we observe that the 8×2 matrix of transition M_0 between the full space and the reduced space has to satisfy the simple condition $L_0 M_0 = 0$, which leads to $M_0 = \begin{pmatrix} 1 & 0 \\ 0 & 1 \\ 0 & 0 \\ \vdots & \vdots \\ 0 & 0 \end{pmatrix}$ as we have to have the sum of each column equal to 1.

To facilitate computation of the next order, we introduce the operator $\bar{R}$, defined as $\lim_{t\to+\infty} e^{L_0 * t}$, giving:

$$\bar{R} = \begin{pmatrix} 1 & 0 & 1 & 0 & 1 & 0 & 1 & 0 \\ 0 & 1 & 0 & 1 & 0 & 1 & 0 & 1 \\ 0 & 0 & 0 & 0 & 0 & 0 & 0 & 0 \\ 0 & 0 & 0 & 0 & 0 & 0 & 0 & 0 \\ 0 & 0 & 0 & 0 & 0 & 0 & 0 & 0 \\ 0 & 0 & 0 & 0 & 0 & 0 & 0 & 0 \\ 0 & 0 & 0 & 0 & 0 & 0 & 0 & 0 \\ 0 & 0 & 0 & 0 & 0 & 0 & 0 & 0 \end{pmatrix} \tag{4.16}$$

This corresponds to the projection onto the code space, according to the dynamics imposed by L_0.

We now focus on the terms of ϵ^1 in the relation (4.15). This yields the equation $L_0 M_1 + L_1 M_0 = M_0 L_{s,1}$. Similarly to [1], we apply $\bar{R}$ to this equation, taking advantage of the fact that $\bar{R} L_0 = 0$ (since L_0 commutes with its own exponential and $L_0 \bar{R} = 0$ obviously) and $\bar{R} M_0 = M_0$ (since $\bar{R}$

acts as the identity on the codespace). Further pre-multiplying by $M_0^\dagger$, we obtain the explicit form ${M_0}^\dagger \bar{R} L_1 M_0 = L_{s,1}$. Calculating the left part for the particular case at hand gives us $L_{s,1} = 0$, meaning the dynamics up to the first order in γ/Γ is still 0 on this eigenspace.

To finish the first order, we now have to find M_1, thus the mapping of r_s to a subspace ϵ-close to the codespace. Taking back the expression $L_0 M_1 + L_1 M_0 = M_0 L_{s,1} = 0$, the solution is $M_1 = \begin{pmatrix} a & b \\ c & d \\ 1 & 0 \\ 0 & 1 \\ 1 & 0 \\ 0 & 1 \\ 1 & 0 \\ 0 & 1 \end{pmatrix}$ with the condition $a + c = -3$ and $b + d = -3$, to respect the condition that $M = M_0 + M_1$ has all its columns of sum 1. There is thus a gauge degree of freedom in choosing the parameterization with a, b, c, d, for instance take $b = c = 0$ and $a = d = -3$, or $a = b = c = d = -3/2$. At this stage, this is just a choice on how to parameterize the slow eigenspace. In higher-order developments, we have observed that this choice can make it easier or harder to ensure positivity of the reduced model, see also the discussion in [1].

For the second order, we have to solve the equation corresponding to the ϵ^2 terms of (4.15), which yields $L_0 M_2 + L_1 M_1 = M_0 L_{s,2} + M_1 L_{s,1}$. Here we can plug in the known first-order components $L_{s,1}$ and M_1. Then, similarly to the first-order procedure, applying $\bar{R}$ to this equation yields an explicit expression for $L_{s,2}$, namely

$$L_{s,2} = \begin{pmatrix} -6 & 6 \\ 6 & -6 \end{pmatrix} ,$$

here independently of the gauge choice for M_1. This represents the dominating dynamics in the reduced space, i.e. the dominant contribution to the slowest information loss, in other words the logical bit-flip rate from a state close to $|000\rangle$ to a state close to $|111\rangle$. The adiabatic elimination approach has thus allowed us to precisely quantify this bit-flip rate while a reservoir is applying error-correction. We could go on with higher orders in this series expansion in order to quantify this rate more accurately, just along the same lines. Instead, let us illustrate how this approach also yields the code scaling to higher orders.

4.2.4 Five qubits code

We consider a similar system as previously, except that it is now composed of 5 physical qubits instead of 3, in a standard repetition code layout. The state vector of the system now describes a 32-dimensional space where r_1 describes the population on $|00000\rangle$, r_2 on $|11111\rangle$ spanning the nominal code space, r_3 on $|10000\rangle$ up to r_{12} on $|11110\rangle$ spanning the one-bit-flip subspace, and r_{13} on $|11000\rangle$, r_{14} on $|00111\rangle$, r_{15} on $|10100\rangle$... the two-bit-flip subspace. For further reference, and in agreement with a "majority vote" conclusion if this was the situation at the very end of some processing, we say that all configurations with a majority of ones correspond to the same logical value, and all configurations with a majority of zeros correspond to the other logical value.

The full system is still described by

$$\frac{dr}{dt} = \Gamma L_0 r + \gamma L_1 r$$

where L_0 and L_1 are now 32×32 matrices. Even if it is still possible to write them down to understand precisely the calculations, this is not necessary for what we aim to do. It is sufficient to know that the bit flip matrix L_1 is of the form

$$\begin{bmatrix} \begin{bmatrix} -5 & 0 \\ 0 & -5 \end{bmatrix} & A_1 & \mathbf{0} \\ {A_1}^\dagger & -5I_{10} & A_2 \\ \mathbf{0} & {A_2}^\dagger & -5I_{20} + B \end{bmatrix}$$

where B is symmetric, and more importantly A_k are matrices with ones only on spots with columns and lines corresponding to the same logical value and zero elsewhere; and B on the opposite has ones only on spots where columns and lines correspond to different logical values. This is understandable by the fact that, thanks to the way we have ordered our states, the A_k matrices represent transitions between states with a large majorities of 0 (or 1) and states with a smaller majority of 0 (or 1), whereas B represents transitions between states at the boarder of the two logical classes, i.e. where one more 0s than 1s becomes one more 1s than 0s or vice versa. For the correction matrix L_0, assuming a decoding and correction scheme where a configuration with k erroneous qubits is set back to a configuration with $k-1$ erroneous qubits in some way[1], we have the form:

$$L_0 = \begin{bmatrix} \begin{bmatrix} 0 & 0 \\ 0 & 0 \end{bmatrix} & C_1 & \mathbf{0} \\ \mathbf{0} & -I_{10} & C_2 \\ \mathbf{0} & \mathbf{0} & -I_{20} \end{bmatrix},$$

with C_k matrices having ones only on spots with columns and lines of same logical state and zeros elsewhere. Computing $\bar{R}$ is very simple, as it represents the result of full correction without any bit flips, thus

$$\bar{R} = \begin{pmatrix} 1 & 0 & 1 & 0 & ... & 1 & 0 \\ 0 & 1 & 0 & 1 & ... & 0 & 1 \\ 0 & 0 & 0 & 0 & ... & 0 & 0 \\ \vdots & \vdots & \vdots & \vdots & ... & \vdots & \vdots \\ 0 & 0 & 0 & 0 & ... & 0 & 0 \end{pmatrix}.$$

Finally, we will still craft a reduced space of dimension 2, as any initial state is still asymptotically converging to the two-dimensional space span$(|00...0\rangle, |11...1\rangle)$ under the fast dynamics L_0. Just as previously, the zeroth order gives by definition $L_{s,0} = 0$, and it immediately follows

$$M_0 = \begin{pmatrix} 1 & 0 \\ 0 & 1 \\ 0 & 0 \\ \vdots & \vdots \\ 0 & 0 \end{pmatrix}.$$

For the first order, with the same reasoning as for the 3-qubit case, we get ${M_0}^\dagger \bar{R} L_1 M_0 = L_{s,1}$. With only what we have said of $\bar{R}$ and L_1, and adding that there are five ones on each column of B (because there are five possibilities to go from a majority of zeros to a majority of ones) we have that

$$\bar{R}L_1 = \begin{bmatrix} \begin{bmatrix} 0 & 0 & ... & 0 \\ 0 & 0 & ... & 0 \end{bmatrix} A \\ \mathbf{0} \qquad\qquad \mathbf{0} \end{bmatrix} \tag{4.17}$$

with A a 2×20 matrix of the form $\begin{pmatrix} -3 & -3 & ... & -3 \\ -3 & -3 & ... & -3 \end{pmatrix}$. It also helps to know that the sums of each column of L_1 is 0, as it represents transitions between the populations of different states. It follows that ${M_0}^\dagger \bar{R} L_1 = 0$, and thus $L_{s,1} = 0$.

[1] We are here discussing the five-qubit repetition code for illustration of the analysis method, yet we have not discussed how a local reservoir engineering setup would implement this 1D error correction proposal. Our local reservoir engineering, analyzed below, instead relies on a 2D error correction lattice where each operator corrects one error at a time. We hence assume this arbitrary model by similarity.

Along similar lines as in the previous section, M_1 is now found to take the form

$$M_1 = \begin{bmatrix} \begin{bmatrix} a & b \\ c & d \end{bmatrix} \\ I_2 \\ I_2 \\ I_2 \\ I_2 \\ I_2 \\ \mathbf{0} \\ \vdots \\ \mathbf{0} \end{bmatrix}$$

with $a + c = -5$ and $b + d = -5$.

For the second order, proceeding exactly as before, we have $L_{s,2} = {M_0}^\dagger \bar{R} L_1 M_1$. With the form (4.17), this directly yields $L_{s,2} = 0$, implying that with this code the dynamics on the reduced (code) space vanishes also at the second order. This implies that the correction protocol is better by one order of ϵ than with 3 qubits, as the slow loss of information occurs at worst at a rate of order ϵ^3.

We note that it is not too difficult to extend this result to a $2i + 1$ qubits repetition code: the principle is always the same, we use the particular form of the matrices $\bar{R}$ and L_1, and the fact that the M_k matrices have ones on all their lines only at the i-th order.

What is missing though in this picture, is a specification of how to implement the correction protocol, from i errors to the correct codeword, with local operators. Indeed, we have here just assumed that our reservoir L_0 somehow features a mechanism such that any corrupted state reduces its number of errors by 1. However, in the repetition code, such mechanism *cannot* be done just locally on the basis of measurements involving a few qubits only; instead, taking a decision in the correct direction sometimes requires to combine information from the whole chain. This makes it unrealistic to assume ever building such a reservoir. It has been shown that it is not impossible to stabilize a chain of bits with a local rule only [12], but this construction is incredibly complicated. Toom's rule, by going from a 1D chain to a 2D lattice, allows to circumvent this obstacle and proposes a simple local process to correct an increasingly large number of possible errors.

4.2.5 Toom's code

We now analyze the correction protocol imagined by Toom in [31] with the same method. As said, this discrete algorithm can quite easily be implemented as a continuous-time reservoir engineering scheme, with the 3-qubit interaction strategy developed in [9]. We will consider a Toom's scheme of 3×3 qubits in this section and assume periodic boundary conditions. The dynamics of such a system is still

$$\frac{dr}{dt} = \Gamma L_0 r + \gamma L_1 r$$

where L_0 and L_1 are respectively the correction and bit flip matrices, of size 512×512. It is thus out of the question to write them down completely. Instead, with the same way of numbering the different states as previously (first the code space, then the order one errors,... , up to the order four errors, always associating the symmetric states side by side, for example $|100000000\rangle$ and $|011111111\rangle$), we can manage to describe the global shape of those matrices.

To begin with, the matrix of bit flips L_1 is the same as the one we would have for the repetition code, since it only describes the possible transition from a state to another by flipping one qubit, independently of the geometry of the correcting reservoir system. With a similar way of thinking

as in the last section, we can see that

$$L_1 = \begin{bmatrix} \begin{bmatrix} -9 & 0 \\ 0 & -9 \end{bmatrix} & A_1 & \mathbf{0} & \mathbf{0} & \mathbf{0} \\ {A_1}^t & -9I_{18} & A_2 & \mathbf{0} & \mathbf{0} \\ \mathbf{0} & {A_2}^t & -9I_{72} & A_3 & \mathbf{0} \\ \mathbf{0} & \mathbf{0} & {A_3}^t & -9I_{168} & A_4 \\ \mathbf{0} & \mathbf{0} & \mathbf{0} & {A_4}^t & -9I_{252} + B \end{bmatrix}$$

where the size of k-th error space is $2\binom{9}{k}$, where B is symmetric, and A_k are matrices with ones only on spots with columns and lines corresponding to the same logical value, and B on the opposite has ones only on spots corresponding to different logical values. Their respective sizes can be found by looking at the neighbouring matrices (for example A_1 is of size $2 * 18$).

The correction matrix L_0, on the other hand, is different from the one of a 9 qubit repetition code, as it represents the correction protocol. It is sufficient to know that it is an upper-triangular matrix, with the first 92 columns exactly similar to what a 9-qubit repetition code would look like. There remains to analyze the form of $\bar{R}$, which still represents the convergence of a state when $\epsilon = 0$ (thus $\bar{R} = \lim_{t\to+\infty} e^{L_0 * t}$). Unfortunately, the Toom's rule scheme does not correct perfectly all errors up to k for 2k+1 qubits as in a repetition code, but only up to $k-1$ errors in a k^2 code. For example, a column of errors cannot be corrected and is in fact another invariant state under L_0. In other words, some error states are not projected onto the code state by the correction protocol and $\bar{R}$ is of the form

$$\begin{bmatrix} I_2 C_1 C_2 B_1 B_2 \\ \mathbf{0}\ \mathbf{0}\ \mathbf{0}\ \mathbf{0}\ \mathbf{0} \\ \mathbf{0}\ \mathbf{0}\ \mathbf{0}\ \mathbf{0}\ \mathbf{0} \\ \mathbf{0}\ \mathbf{0}\ \mathbf{0}\ B_3 B_4 \\ \mathbf{0}\ \mathbf{0}\ \mathbf{0}\ B_5 B_6 \end{bmatrix}$$

with C_1 a 2×18 and C_2 a 2×72 matrix of the form $\begin{pmatrix} I_2 & I_2 & \dots & I_2 \end{pmatrix}$. The reason the second and third line are all zeros is because all one and two errors states are corrected back to the codespace, and thus all the population tends to disappear from those states. For $> k-1$ initial errors, the Toom's rule correction process can increase the number of errors over time. For example, a situation with four qubits wrong can be brought by Toom's rule into 6 wrong. Mathematically, this translates into the fact that $B1, B_2$ matrices have some ones on spots corresponding to different logical values on column and line.

The partial correction property however has a bigger consequence: in this setup, it is not justified to directly focus on a reduced space of dimension 2 only, since under L_0 it is not true that all degrees of freedom except 2 will quickly vanish. We will thus build a reduced space of dimension $2+m$, where $2+m$ is number of eigenvalues of L_0 whose real part is zero — in principle this can include steady states, but also undamped periodic oscillations. For the present purpose, we do not care so much about identifying m and the associated behavior, as we will show instead that *all our conclusions can be drawn by focusing only on general properties of L_0 and L_1 on few-error subspaces.*

We still want to build the matrices M and L_s as in the last subsections, which will be of size $512 * (2+m)$ and $(2+m) * (2+m)$ respectively. The difference in this setup is what we ultimately want: in the previous sections we wanted the full matrices L_s to understand the logical bit flip rate, as the entire reduced space was only of the same dimension as the code space. Here we are still only interested in the logical bit flip rate, but in principle we must build an L_s of dimension $(2+m)$, matching the perturbed slow eigenspace. Luckily, at low orders, it is possible to compute a 2-dimensional part of L_s identified as the logical bit flip while leaving its other parts unspecified/symbolic, as we don't need them for deducing the bit-flip result. In other words, we compute what happens (approximately) when starting on a 2-dimensional subspace of the slow eigenspace, which we identify with the codespace under perturbation, but we do not explicitly work out what is the rest of the slow dynamics under perturbation; this is just about partially

working out the algebra, while the general perturbation theory is applied to the full eigenspace of L_0 corresponding to zero-real-part eigenvalues (thus non-vanishing on the long run).

We begin at order 0: the first difficulty arises here, as $L_{s,0}$ is not necessarily the null matrix: there could be moving parts in the stationary regime. We can only write $L_{s,0} = \begin{pmatrix} \mathbf{0}_{2*2} & \mathbf{0}_{2*m} \\ \mathbf{0}_{m*2} & * \end{pmatrix}$ as we know nothing comes in or out of our code space in steady state at order 0.

Thus our order 0 equation is $L_0 M_0 = L_{s,0}$. We obtain that the first two columns of M_0 must be, as done for the two previous subsections, $\begin{pmatrix} 1 & 0 \\ 0 & 1 \\ 0 & 0 \\ \vdots & \vdots \\ 0 & 0 \end{pmatrix}$. Since the first two columns of L_0 are only zeros, the first two lines of M_0 must be in the kernel of L_0, we can choose it to be zeros (gauge choice in parameterizing the slow eigenspace). We thus have our matrix $M_0 = \begin{pmatrix} 1 & 0 & 0 & ... & 0 \\ 0 & 1 & 0 & ... & 0 \\ 0 & 0 & * & ... & * \\ \vdots & \vdots & & & \\ 0 & 0 & * & ... & * \end{pmatrix}$ where we leave the lower-right diagonal block unspecified.

For the first order, and the second after, the key once again resides in the computation of $\bar{R}L_1$. Thanks to the different matrices whose form we have explicited (and recalling that the sums of each column of L_1 is 0), the first two entire columns of $\bar{R}L_1$ and the next 18 columns up until the 20th line are all zeroes. For the first 2 columns the calculations are straightforward for all the lines except the two first, where we have to use the particular concordance in the spots with value 1 between C_1 and ${A_1}^t$ to have $C_1 * {A_1}^t = -9I_2$. For the first 20 lines of next 18 columns, it is in fact similar calculations as in (4.17), as it would be the exact same process as in finding these columns in the 9-qubits repetition code (similar L_1, similar first 92 columns of $\bar{R}$). We thus obtain $\bar{R}L_1 = \begin{pmatrix} \mathbf{0_{2*2}} & \mathbf{0_{2*18}} & * \\ \mathbf{0_{18*2}} & \mathbf{0_{18*18}} & * \\ \mathbf{0_{492*2}} & * & * \end{pmatrix}$

We now look at the first order terms in (4.15) which gives $L_0 M_1 + L_1 M_0 = M_0 L_{s,1}$. As before we first apply $\bar{R}$ to obtain the equation $\bar{R}L_1 M_0 = M_0 L_{s,1}$ (as $\bar{R}L_0 = 0$ and $\bar{R}M_0 = M_0$ for similar reasons as before), then we apply ${M_0}^\dagger$. The difference here is that ${M_0}^\dagger M_0$ is not the identity, but only the $(2+m)*(2+m)$ matrix $\begin{pmatrix} 1 & 0 & 0 & ... & 0 \\ 0 & 1 & 0 & ... & 0 \\ 0 & 0 & * & ... & * \\ \vdots & \vdots & & & \\ 0 & 0 & * & ... & * \end{pmatrix}$.

The calculations of ${M_0}^\dagger \bar{R} L_1 M_0$ gives the $(2+m)*(2+m)$ matrix $\begin{pmatrix} \mathbf{0_{(2+m)*2}} & * \end{pmatrix}$

This result, combined with the form of ${M_0}^\dagger M_0$, lets us know that $L_{s,1} = \begin{pmatrix} \mathbf{0_{(2+m)*2}} & * \end{pmatrix}$. To end the work on the first order we just have to find the $512*(2+m)$ matrix M_1. This is done in the same manner as previously, and gives

$$M_1 = \begin{bmatrix} \begin{bmatrix} a & b \\ c & d \end{bmatrix} & * \\ I_2 & * \\ \vdots & \\ I_2 & * \\ \mathbf{0} & * \\ \vdots & \\ \mathbf{0} & * \end{bmatrix}$$

with nine I_2 in total, and $a + c = -9$ and $b + d = -9$.

Finally for order 2, we take the corresponding condition in (4.15) which is $L_0 M_2 + L_1 M_1 = M_0 L_{s,2} + M_1 L_{s,1}$. We once again multiply this equation by ${M_0}^\dagger \bar{R}$ which gives ${M_0}^\dagger \bar{R} L_1 M_1 - {M_0}^\dagger \bar{R} M_1 L_{s,1} = {M_0}^\dagger M_0 L_{s,2}$. The $512 * (2 + m)$ matrix $\bar{R} L_1 M_1$ trivially has its first two columns composed of zeros, which is transferred to the $(2 + m) * (2 + m)$ matrix ${M_0}^\dagger \bar{R} L_1 M_1$. The matrix $\bar{R} M_1 L_{s,1}$ has also immediately its first 2 columns equal to zero, which is thus true for ${M_0}^\dagger \bar{R} M_1 L_{s,1}$. These calculations, coupled with the form of ${M_0}^\dagger M_0$, give us that $L_{s,2} = \begin{pmatrix} \mathbf{0}_{(\mathbf{2+m})*\mathbf{2}} & * \end{pmatrix}$.

We have thus showed that up to the second order included, the L_s matrix has its first two columns equal to zero. This proves that the logical bit flip rate is only of order 3 or higher, which is a similar level of protection as the five qubits repetition code, but achieved with only local interactions. It should be possible to attain better error correction by simply taking bigger Toom's rule lattices (i.e. with a square of size N*N instead of 3*3), which should lead with similar calculations to a logical bit flip rate of zero until the N-th order. This would lead to a quadratic growth of the number of qubits in the order of logical bit flip rate, but in-depth calculations would be required to confirm it.

To conclude this chapter, we have shown two methods to scale up the design of the 3-qubit scheme developed in [9] while still keeping local interactions, in order to have realistic setups to protect information at higer orders. The main difference between the two is that the method of section 4.1 only uses a majority vote, while the one in section 4.2 uses directionality in its correction protocol. The set up of section 4.1, which is a personal contribution, was analyzed in a very standard manner of finding its code distance, whereas the Toom's rule approach of section 4.2, which is an already known method with the additional twist to use [9], was analyzed thanks to the more novel method of adiabatic elimination. The analysis seems to confirm mathematically that an error correction scheme which perfectly corrects "up to k errors in the initial state", can be identified with an error rate in fully continuous-time that scales as the $k + 1^{th}$ power of the local bit-flip rate. The adiabatic elimination computation, with associated simplifications naturally popping up, thus seems to be a successful tool to evaluate error correction performance. It further gives the corresponding prefactors and may be pushed to higher orders in principle, which may help identify settings where "bad" combinations of $> k$ errors are in fact rare.

Concerning the two schemes, our idea in section 4.1 was to investigate an alternative to Toom's rule where each operator would treat its associated qubits symmetrically. This is just one idea and we are not sure to have hit the optimal design. Nevertheless, the more than quadratic scaling of the number of necessary qubits with the intended code distance, suggests that the directionnality may be an essential ingredient in the efficiency of the Toom's rule set up. It may be noteworthy that the reservoir engineering implementation of Toom's rule leads to an asynchronous application of its automaton rules across local sites. This does not preclude its error-correction capabilities, and in fact it can be beneficial in leaving some undesired situations which would be stationary regimes under synchronous working.

Chapter 5

Conclusion

This thesis' main focus was to use reservoir engineering techniques in order to stabilize quantum systems composed of qubits, and do it with only local interactions to have realistic set ups while the number of qubits in the system increases. Its first part developed several propositions to stabilize approximately GHZ states, by combining dynamics that periodically resets the whole system to the particular state $|+ + ...+\rangle$ with an existing conditional stabilization scheme, where the system converges towards the GHZ state if each qubit is initialized in the particular state $|+ + ...+\rangle$. This was done with two different approaches, the first one being the addition of an auxiliary chain of ancilla qubits to our data qubits where the information of the GHZ state is stored, acting as a clock determining when to apply each of the schemes. The second one instead replaces the data qubits by qutrits, where the third level takes over the role of the clock. After presenting those different setups, we did a theoretical analysis to estimate the performance and understand the optimal tuning of each parameter in order to have the best protection rate of the GHZ state against local perturbations. The results are backed up by simulations, confirming that the approximations lead to sufficiently accurate conclusions. The method used in the analysis was to build classical Markov chains in order to avoid to deal with the full Lindbladian. What stood out was the clear superiority of using qutrits resetting as a wave instead of using data qubits and ancillas qubits, as the former gives a much better scaling in terms of the ratio of the different parameters (error scaling in $\epsilon^{\frac{1}{2}}$) than the latter (error scaling in $\epsilon^{\frac{1}{3}}$). An interesting note is that this protocol could be applied to the stabilization of other entangled states.

The second part focused on applying reservoir engineering methods with local couplings to quantum error correction to protect against one type of error. We developed two setups protecting errors from happening by redundantly encoding information on interlinked qubits in a 2-D network, and only using local interactions to have a practical setting that can be applied for realistic experiments. Both setups used a pre-existing three qubits bit flip protection protocol as the basic building block. The first one, which was a personal contribution, aimed to arrange the qubits in various shaped graphs with a simple majority vote correction protocol on local trhee-qubit sets, while the second one used the Toom's rule set up, which takes advantage of directionnality in an automaton-like error correction protocol; its reservoir engineering implementation leads to an asynchronous application of the automaton, which does not preclude its proper operation (unlike for GHZ state stabilization). The analysis we performed on the two setups showed a quadratic scaling in the number of error it corrects for the latter, and somewhat worse than quadratic for the former.

Three major points stand out as unanticipated observations in this thesis.

- First, we have observed a considerable gain by going from qubits+ancillas to qutrits in the GHZ stabilization schemes. This suggests that further engineering of automata (reservoirs) on quantum information, should seriously consider the options opened up by working with such multilevel quantum systems. A quite direct application could be to try this in error-correction protocols, improving upon the Toom's rule setup of Chapter 4.

- Second, in both parts of this thesis, the directionality of protocols appeared to play an important role. Both for GHZ stabilization (wave) and for error correction (Toom's rule), the scheme with directionality, which is enabled by dissipative Lindbladian operation rather than reciprocal Hamiltonian operation, apparently leads to better scaling.
- Third, we have successfully proposed approximation methods for performance analysis. The adiabatic elimination expansion to higher orders and on classical probabilities, appears to characterize error protection in an accurate way, once continuous-time error-correction dynamics have been formulated. For GHZ state stabilization, the main contribution was to approximate the problem with a classical Markov chain, by replacing the quantum state by hypothetical measurement sequences.

From a general perspective, we worked on automata implemented by reservoir engineering, and we showed that with quite simple setups (constant or resonant drive), we could already have interesting effects in order to stabilize systems in nontrivial states. This shows how natural phenomena can stabilize themselves without the need for complicated designs and how complexity can emerge from simple basic building blocks in an open quantum systems context.

Bibliography

[1] Rémi Azouit. Adiabatic elimination for open quantum systems. *HAL*, 2017, 2017.

[2] Jean-Louis Basdevant, Jean Dalibard, and Manuel Joffre. *Mécanique quantique*. Editions Ecole Polytechnique, 2002.

[3] Charles H Bennett, Gilles Brassard, Sandu Popescu, Benjamin Schumacher, John A Smolin, and William K Wootters. Purification of noisy entanglement and faithful teleportation via noisy channels. *Physical review letters*, 76(5):722, 1996.

[4] Charles H Bennett, David P DiVincenzo, John A Smolin, and William K Wootters. Mixed-state entanglement and quantum error correction. *Physical Review A*, 54(5):3824, 1996.

[5] Héctor Bombín and Miguel A Martin-Delgado. Optimal resources for topological two-dimensional stabilizer codes: Comparative study. *Physical Review A*, 76(1):012305, 2007.

[6] Heinz-Peter Breuer, Francesco Petruccione, et al. *The theory of open quantum systems*. Oxford University Press on Demand, 2002.

[7] Hans J Briegel, David E Browne, Wolfgang Dür, Robert Raussendorf, and Maarten Van den Nest. Measurement-based quantum computation. *Nature Physics*, 5(1):19–26, 2009.

[8] Alba Cervera-Lierta, Mario Krenn, Alán Aspuru-Guzik, and Alexey Galda. Experimental high-dimensional greenberger-horne-zeilinger entanglement with superconducting transmon qutrits. *Physical Review Applied*, 17(2):024062, 2022.

[9] Joachim Cohen. *Autonomous quantum error correction with superconducting qubits*. PhD thesis, Université Paris sciences et lettres, 2017.

[10] BM Escher, Ruynet Lima de Matos Filho, and Luiz Davidovich. General framework for estimating the ultimate precision limit in noisy quantum-enhanced metrology. *Nature Physics*, 7(5):406–411, 2011.

[11] Tianfeng Feng, Xiaoqian Zhang, Yuling Tian, and Qin Feng. On-chip multiphoton entangled states by path identity. *International Journal of Theoretical Physics*, 58(11):3726–3733, 2019.

[12] Peter Gács. Reliable cellular automata with self-organization. *Journal of Statistical Physics*, 103:45–267, 2001.

[13] Crispin Gardiner, Peter Zoller, and Peter Zoller. *Quantum noise: a handbook of Markovian and non-Markovian quantum stochastic methods with applications to quantum optics*. Springer Science & Business Media, 2004.

[14] Kurtis Geerlings, Zaki Leghtas, Ioan M Pop, Shyam Shankar, Luigi Frunzio, Robert J Schoelkopf, Mazyar Mirrahimi, and Michel H Devoret. Demonstrating a driven reset protocol for a superconducting qubit. *Physical review letters*, 110(12):120501, 2013.

[15] Israel Gohberg, Peter Lancaster, and Leiba Rodman. *Matrix polynomials*. Springer, 2005.

[16] Daniel Gottesman. Fault-tolerant quantum computation with constant overhead. *arXiv preprint arXiv:1310.2984*, 2013.

[17] Daniel M Greenberger, Michael A Horne, Abner Shimony, and Anton Zeilinger. Bell's theorem without inequalities. *American Journal of Physics*, 58(12):1131–1143, 1990.

[18] Serge Haroche and J-M Raimond. *Exploring the quantum: atoms, cavities, and photons*. Oxford university press, 2006.

[19] Michael Herold, Michael J Kastoryano, Earl T Campbell, and Jens Eisert. Cellular automaton decoders of topological quantum memories in the fault tolerant setting. *New Journal of Physics*, 19(6):063012, 2017.

[20] Peter D Johnson, Francesco Ticozzi, and Lorenza Viola. General fixed points of quasi-local frustration-free quantum semigroups: from invariance to stabilization. *Quantum Information & Computation*, 16(7-8):657–699, 2016.

[21] Mazyar Mirrahimi, Zaki Leghtas, Victor V Albert, Steven Touzard, Robert J Schoelkopf, Liang Jiang, and Michel H Devoret. Dynamically protected cat-qubits: a new paradigm for universal quantum computation. *New Journal of Physics*, 16(4):045014, 2014.

[22] Mazyar Mirrahimi and Pierre Rouchon. Dynamics and control of open quantum systems. *Lecture notes*, 2015.

[23] Naomi H Nickerson, Joseph F Fitzsimons, and Simon C Benjamin. Freely scalable quantum technologies using cells of 5-to-50 qubits with very lossy and noisy photonic links. *Physical Review X*, 4(4):041041, 2014.

[24] Michael A Nielsen and Isaac Chuang. Quantum computation and quantum information, 2002.

[25] Joe O'Gorman, Naomi H Nickerson, Philipp Ross, John JL Morton, and Simon C Benjamin. A silicon-based surface code quantum computer. *npj Quantum Information*, 2(1):1–14, 2016.

[26] JF Poyatos, J Ignacio Cirac, and P Zoller. Quantum reservoir engineering with laser cooled trapped ions. *Physical review letters*, 77(23):4728, 1996.

[27] Peter W Shor. Algorithms for quantum computation: discrete logarithms and factoring. In *Proceedings 35th annual symposium on foundations of computer science*, pages 124–134. Ieee, 1994.

[28] Peter W Shor. Scheme for reducing decoherence in quantum computer memory. *Physical review A*, 52(4):R2493, 1995.

[29] Francesco Ticozzi and Lorenza Viola. Steady-state entanglement by engineered quasi-local markovian dissipation: Hamiltonian-assisted and conditional stabilization. *Quantum Information & Computation*, 14(3-4):265–294, 2014.

[30] Jean-Pierre Tillich and Gilles Zémor. Quantum ldpc codes with positive rate and minimum distance proportional to the square root of the blocklength. *IEEE Transactions on Information Theory*, 60(2):1193–1202, 2013.

[31] Andrei L Toom. Stable and attractive trajectories in multicomponent systems. *Multicomponent random systems*, 6:549–575, 1980.

[32] Rupert Ursin, F Tiefenbacher, T Schmitt-Manderbach, H Weier, Thomas Scheidl, M Lindenthal, B Blauensteiner, T Jennewein, J Perdigues, P Trojek, et al. Entanglement-based quantum communication over 144 km. *Nature physics*, 3(7):481–486, 2007.

[33] Frank Verstraete, Michael M Wolf, and J Ignacio Cirac. Quantum computation and quantum-state engineering driven by dissipation. *Nature physics*, 5(9):633–636, 2009.

[34] Tao Yu, Ai-Dong Zhu, Shou Zhang, Kyu-Hwang Yeon, and Seong-Cho Yu. Deterministic controlled-phase gate and preparation of cluster states via singly charged quantum dots in cavity quantum electrodynamics. *Physica Scripta*, 84(2):025001, 2011.

[35] Petr Zapletal, Andreas Nunnenkamp, and Matteo Brunelli. Stabilization of multimode schrödinger cat states via normal-mode dissipation engineering. *PRX Quantum*, 3(1):010301, 2022.

[36] Shi-biao Zheng and Guang-can Guo. Generation of multi-atom entangled states via the raman atom-cavity-field interaction. *Chinese physics letters*, 14(7):485–487, 1997.